A STUDY ON THE DURABILITY AND PERFORMANCE OF PHOTOVOLTAIC MODULES IN THE TROPICS

XIONG ZHENGPENG

NATIONAL UNIVERSITY OF SINGAPORE

2015

A STUDY ON THE DURABILITY AND PERFORMANCE OF PHOTOVOLTAIC MODULES IN THE TROPICS

XIONG ZHENGPENG

M.Eng., National University of Singapore

B.Eng., Huazhong University of Science & Technology

A THESIS SUBMITTED

FOR THE DEGREE OF DOCTOR OF PHILOSOPHY
DEPARTMENT OF MECHANICAL ENGINEERING
NATIONAL UNIVERSITY OF SINGAPORE

2015

DECLARATION

DECLARATION

I hereby declare that this thesis is my original work and it has been written by me in its entirety. I have duly acknowledged all the sources of information which have been used in the thesis.

This thesis has also not been submitted for any degree in any university previously.

XIONG ZHENGPENG

Jun 26, 2015

ACKNOWLEDGEMENTS

I would like to thank my supervisor Professor Andrew A.O. Tay, co-supervisor Professor Armin G. Aberle, and scientific advisor Dr. Timothy M. Walsh for their guidance in my PhD study. Their support greatly helped me in exploring durability, characteristics, and simulations of PV modules. It was my great pleasure to work with them in this work.

Also, I would like to thank my lab fellows of the PV Module Performance Analysis Unit of the Solar Energy Research Institute of Singapore for their support on performing various tests. Without them it would have been impossible to finish the test tasks for the study.

Thanks to my colleagues in the Solar Energy Research Institute of Singapore and the Department of Mechanical Engineering for their help and discussions.

And to my family, Yanqiong, Yuyang, and Yicheng, thank you for supporting me in the journey.

TABLE OF CONTENTS

SUMMARY

Photovoltaic module degradation causes significant impact on PV system lifetime. The degradation is demonstrated to be caused by various factors such as photo-degradation by UV photons in sunlight, corrosion by moisture ingress, thermal degradation in field service, and thermo-mechanical stress due to thermal cycling, wind/snow/hail, etc. This thesis describes a study on the durability of different types of PV modules for terrestrial applications.

In the study, stressing and characterization tests were conducted on 10 types of commercially available thin-film PV modules (Amorphous silicon, micro-morph silicon, amorphous silicon tandem, CdTe, and CIGS) and silicon-wafer based PV modules (Monocrystalline silicon, multicrystalline silicon, monocrystalline silicon BIPV, Back-contact monocrystalline silicon, and Hetero-junction monocrystalline silicon with amorphous silicon thin layer). The PV modules were tested with different stressing conditions (moisture, UV, thermal, mechanical, electrical, outdoor, etc.). Several tightened stress test conditions, e.g. Damp heat 90°C/90%R.H., Damp Heat 85°C/85%R.H. with 1000 V DC bias, etc, further differentiated degradation rates of the modules. Moisture ingress simulations were performed with Finite Element Analysis (FEA) software ABAQUS-CAE® to reveal moisture concentration distributions under different test conditions and different materials/structure. Other PV module characteristics (e.g. temperature coefficient, nominal operating cell temperature, low irradiance performance, etc) for different PV module technologies were also obtained in order to predict electricity generation in Singapore's outdoor conditions. Outdoor performance results of

the modules for eight months were summarized in order to correlate the results from accelerated stressing tests with actual performance under Singapore weather conditions.

Degradation rates of each PV module technology were obtained in thermo-mechanical stressing, moisture induced corrosion, UV induced degradation, etc to reveal the acceleration factors in order to better predict lifetime of PV modules. From the different behaviours of the modules, certain solutions were derived to reduce the effects of such stressing on PV module performance. The interactions of IV curve parameters with module power were analysed. The open-circuit voltage V_{oc} was found as the most important factor that resulted in power degradation from the stressing tests.

FEA simulations demonstrated the effect of moisture dose in accelerated damp heat and outdoor test, which revealed uneven distribution of moisture concentration in silicon wafer PV modules. Other explorations were conducted on structures and materials of PV module for design improvement against moisture ingress.

Various characteristic tests were performed to obtain performance parameters ($NOCT_{sg}$, temperature coefficient, performance at $NOCT_{sg}$) for better estimation of PV module's performance in Singapore outdoor test condition. The instability issue of thin-film modules, particularly for amorphous silicon-based modules, were studied through light soaking and thermal annealing which revealed strong thermal annealing effects for a-Si based modules at as low as 65°C and 85°C.

A module power prediction was developed by including the effects from degradation and characteristics of PV modules. The predicted power output was compared with outdoor test results in Singapore for each type of module. The CdTe module selected in this study seems to be a good choice in terms of module energy yield for Singapore weather.

LIST OF TABLES

LIST OF FIGURES

ABBREVIATIONS

A-Si	Amorphous Silicon
BAPV	Building-Attached Photovoltaics
BIPV	Building-Integrated Photovoltaics
BSF	Back Surface Field
CdTe	Cadmium Telluride
CIGS	Copper Indium Gallium Selenide
CSF	Comprehensive Stress Factors
CTE	Coefficients of Thermal Expansion
CVD	Chemical Vapour Deposition
DC	Direct Current
DH	Damp Heat
EVA	Ethylene-Vinyl-Acetate
FEA	Finite Element Analysis
FF	Fill Factor
HF	Humidity Freeze
IEC	International Electrotechnical Commission
JPL	Jet Propulsion Laboratory
LID	Light-Induced Degradation
Mono-Si	Monocrystalline Silicon
MPP	Maximum Power Point
MPPT	Maximum Power Point Tracking
Multi-Si	Multicrystalline Silicon
NASA	National Aeronautics and Space Administration
NB	Negative Bias
NOCT	Nominal Operating Cell Temperature
NREL	National Renewable Energy Laboratory

PB	Positive Bias
PET	Poly-Ethylene-Terephthalate
PID	Potential-Induced Degradation
PR	Performance Ratio
PV	Photovoltaic
PVB	Poly-Vinyl-Butyral
PVF	Poly-Vinyl-Fluoride
RoHS	Restriction of Hazardous Substances
PVPA	PV Module Performance Analysis Unit
SERIS	Solar Energy Research Institute of Singapore
STC	Standard Test Condition
SWE	Staebler & Wronski Effect
TC	Thermal Cycling
TCO	Transparent Conductive Oxide
TPT	Tedlar-PET-Tedlar
UV	Ultraviolet
UVB	Ultraviolet B
WVTR	Water Vapour Transmission Rate

CHAPTER 1

INTRODUCTION

1.1 Solar photovoltaics

Various ever-evolving technologies utilizing solar energy exist nowadays, such as solar heating, solar photovoltaics (PV), solar thermal electricity, solar architecture and artificial photosynthesis, to harness solar energy and convert it into a useful resource for the world. There are many exciting projects such as solar architectures with harmonically designs for solar energy utilization, solar farms or solar parks [1] in transferring light into electricity on large land scale, as well as solar powered transportation vehicles [2] as shown in Fig. 1. Renewable energies are getting more attention as an important sustainable energy source in the world, including Singapore.

Fig. 1. NASA's "Helios" solar plane (Upper); Singapore's "solar park" (Lower) [1,2]

Solar photovoltaics is an important technology nowadays among solar energy technologies because of the vast need for electricity in the modern society. A PV system for terrestrial applications is often composed of PV module, mounting structure, cables, and/or electrical devices such as invertor, monitoring/metering, battery, etc. Photovoltaic module is the major device of the system to convert light in solar energy into electrical energy. A module usually contains a number of solar cells, protection materials (e.g. glass, backsheet, encapsulant), and connectors (e.g. wire, cable, junction-box). The solar cell is the essential component to absorb photons in sunlight and generate electrons/holes through photovoltaic effect, which was first experimentally demonstrated by Edmond Becquerel in 1839. In 1883 Charles Fritts built the first solid state photovoltaic cell by coating the semiconductor selenium with a thin layer of gold to form a heterojunction. The device was only around 1% efficient [3]. Research works subsequently carried out kept improving the solar cell efficiency and nowadays the best research cells reach over 40% efficiency for certain multi-junction cells under solar concentration and over 30% efficiency for a III-V tandem solar cell of Alta Devices tested in the National Renewable Energy Laboratory (NREL) as shown in Fig. 2.

Various PV modules have been developed to maintain or enhance the efficiency of solar cells for long-term field applications especially for terrestrial PV module, which is the subject of this study.

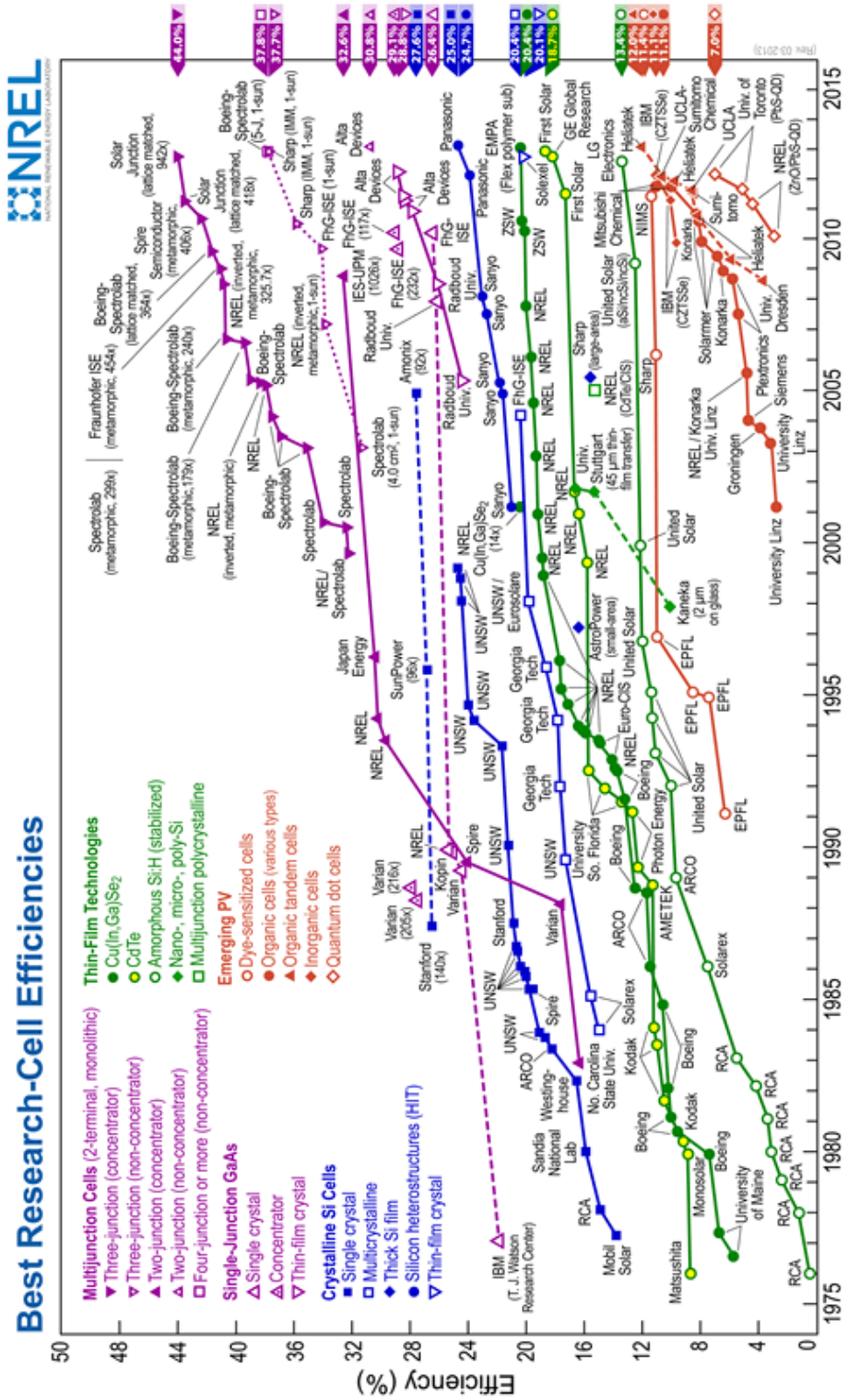

Fig. 2. NREL's efficiency map of the best research solar cells in the world [4].

1.2 Terrestrial PV modules

Terrestrial PV modules can be classified into different categories according to materials or applications. Si wafer PV module and thin-film PV modules are common PV module types nowadays. Silicon wafer PV modules can be further clarified as monocrystalline silicon PV module, multicrystalline silicon PV module, etc. A silicon solar cell is a photovoltaic diode with P-N junction fabricated in a silicon wafer. An antireflective coating (e.g. silicon nitride) is usually built on the surface of the solar cell for light trapping. To transfer photo-generated electrons into an external circuit, surface metallization (usually silver grids) is applied through a sintering process at the top and bottom of the solar cell. Cell to cell connection is achieved with copper strips soldered to the metallization layers on Si wafer. To improve efficiency, a thick-film aluminium layer is deposited at the bottom of the solar cell to generate a back-surface field (BSF) to enhance photo-generated electron diffusion through the P-N junction. For most thin-film solar modules, light absorption layer (e.g. Si, CdTe, CIGS) is deposited on a superstrate such as glass, using a chemical vapour deposition (CVD) process. The cell-to-cell interconnect is achieved by transparent conductive oxide (TCO) such as SiO_2, ZnO, etc as front and/or back contact layers or by silver as back contact layers. Various polymeric materials (e.g. encapsulant, backsheet, edge sealant, sealing tape, potting material, etc) are used to protect solar cells. In some cases, backsheet are replaced by back glass for better structural strength.

Figure 3 shows two common types of PV modules (silicon wafer PV module and thin-film PV module) with front glass, encapsulant (usually Ethylene-Vinyl-Acetate, EVA), silicon wafer solar cell or thin film solar cell, backsheet (usually a laminated film with Poly-Vinyl-Fluoride PVF and Poly-Ethylene-Terephthalate PET, etc) or back glass, metal string, junction box and cables. The front glass serves as a superstrate for thin-film solar cells and it also provides mechanical support and a

transparent optical medium for sunlight to pass through for both types of modules. The encapsulant protects solar cells and attaches glass/cell/backsheet or back glass together. EVA or PVB are commonly used as encapsulants as they possess good optical transparency, high adhesion strength, and low moisture absorption. Backsheet is usually a laminated film with good weatherability. PVF is stable against UV induced degradation from solar irradiation and PET/PVF are also good moisture barrier materials. An aluminium frame is usually employed to enhance overall mechanical strength of PV module against mechanical and thermo-mechanical stress caused by wind/snow load, thermal cycling, etc.

For thin-film PV modules, (e.g. CdTe, amorphous Si, CIGS) a light-absorption layer as well as TCO layers are applied on front glass or other types of medium. A laser scribing process is usually used to create interconnects between thin-film solar cells. Metal strips/strings with precoated solder (e.g. lead-free solder Sn96.5Ag3.5) are soldered or attached onto solar cells to conduct electricity to the junction box and output cables.

Certain PV module types are specially designed for integration into buildings or attached to buildings, known as Building Integrated PV module (BIPV) and Building Attached PV module (BAPV). The former is usually designed as an integrated part of the building (e.g. roof, window, wall) and is usually a Glass-Glass module structure. Si solar cells are sparsely located within the module to allow sunlight to pass through the gaps between Si wafers for natural lighting purposes. A thin-film type BIPV module is also available usually with amorphous silicon thin-film solar cells as it can be fabricated as a semi-transparent module so that parts of the spectrum can be transmitted through the a-Si thin film into the building for illumination purposes. BAPV is generally the same as the usual PV modules. With simple retrofitting, it can be attached onto the surfaces of the buildings.

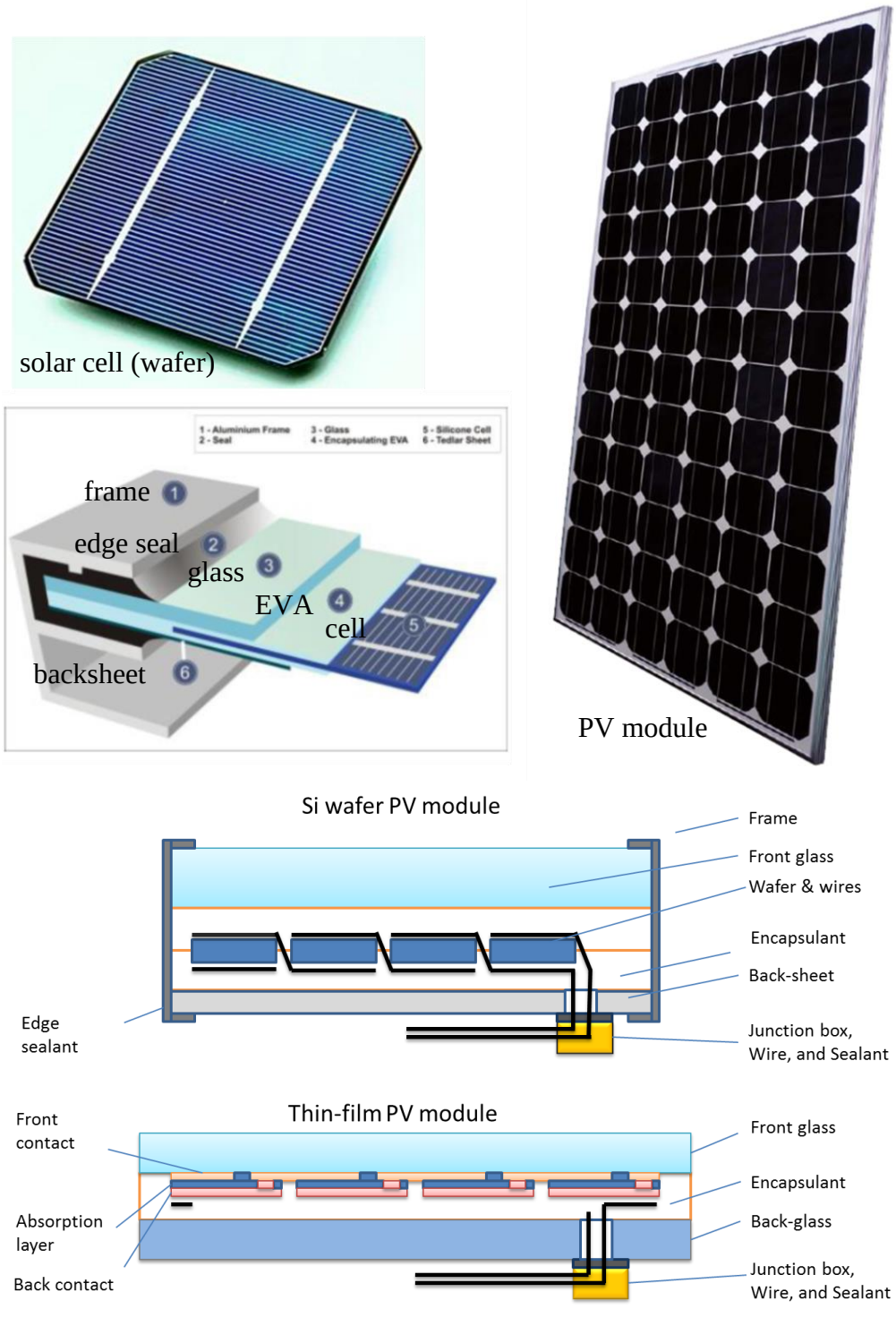

Fig. 3. Common structures of PV modules and solar cells [3,5].

1.3 Durability of PV modules

The performance of PV modules in field applications can be affected by external and internal factors. Nowadays different PV technologies compete with each other in terms of conversion efficiency, long-term durability, eco-friendliness of manufacturing process, abundance of raw materials, and even aesthetics of product design. Performance difference has direct effect on grid parity which aims to provide end customers with a clean while low-cost electricity. It is well known that PV module performance is influenced by various weathering factors (e.g. solar spectrum, ambient temperature, UV dose, humidity) and degradation mechanisms are moisture ingress, UV-induced photo/thermal-oxidation, thermo-mechanical stresses, electro-chemical corrosion, etc. [6-9]. PV modules must have a long field operating lifetime to ensure a good return on investment. Many leading PV module manufacturers now offer product warranties of 20-25 years with no more than 20% power degradation. The target is equivalent to a degradation rate 0.8%/year or 0.0022%/day or 0.0001%/hour on average. To meet this target, various tests and development activities have been conducted in the world on materials, structures, processes, and reliability to establish a better-efficiency PV system that lasts longer.

The required long-term stability of more than 20 years could represent an enormous challenge to Singapore [10], a tropical country located one degree north of the equator, because of its hot and humid weather (Relative humidity > 70% and ambient temperature 23-34^{0}C on average for the whole year) [11]. High operating temperatures of PV modules and serious corrosion issues are the major considerations for PV module durability. Other weather conditions in Singapore will influence performance of different PV modules. For example, considerable cloud cover brings "bluer" spectrum [12] and higher fraction of diffuse radiation [13]. High ambient temperature benefits amorphous silicon-based modules [14-15] and those PV modules

with higher bandgap [16]. Due to the low latitude of Singapore, PV modules installed at low angles of inclination (< 10°) to better harvest the solar irradiation face soiling issues and heat dissipation issues. Thus it is important to study the characteristics and durability of different PV modules for Singapore weather conditions.

1.4 Conclusions

In this chapter, an introduction of terrestrial PV modules and their structures was given. Thin-film modules and Si-wafer modules were compared in terms of their structure and materials. The main functions of the common materials used in PV modules, such as front glass, backsheet, encapsulant, etc, were elaborated. The challenges on the performance and durability of PV modules in a tropical climate were discussed.

CHAPTER 2

PV MODULE DEGRADATION MECHANISMS

2.1 Literature Survey

Over 40 years of research has been done on the performance degradation and failure mechanisms for terrestrial PV systems all over the world. Common problems can be attributed to thermo-mechanical stress (e.g. broken cell, solder joint failure, interconnection or junction box failures), moisture ingress (e.g. delamination, corrosion), UV photo-thermal ageing (e.g. EVA yellowing), hotspots, etc. For thin-film based module, the instability problems [14] exhibited more obviously than silicon wafer module. Thin film is a material inherently with defects (e.g. pin holes, micro-cracks, etc) from its fabrication process. Also thin-film modules are more susceptible to moisture induced corrosion in PV module as thin film is deposited on superstrate or substrate such that the packaging (encapsulation) is not as good as those wafer based PV module because the wafers are sandwiched by two layers of encapsulant film. Thin film solar cell is composed of a series of very thin materials thus the inter-diffusion cannot be neglected especially for modules in hot operating environment. Jordan and Kurtz [17] reported long-term degradation rates of PV modules in different countries in the world. They found a mean degradation rate of 0.8%/year and the majority, 78% of all data, reported a degradation rate of < 1%/year for PV systems/modules in field service. Osterwald *et al.* [19] found degradation rates for crystalline-Si (0.4%/year) and a-Si (1.25%/year) in field output. Wohlgemuth *et al.* [8,18] studied the failure of modules and found the top common failures were corrosion 45.3% and broken cells/interconnects 40.7%. Osterwald *et al.* [19] studied the mechanism of potential-induced degradation and showed that leakage current and the total charge transferred were closely related to power degradation. Czanderna and Pern, Kempe *et al.* [20-22] studied the EVA yellowing mechanism and highlighted

the EVA deacetylation which released acetic acid and the loss of UV absorber were the causes of yellowing and corrosion. Various reports from researchers all over the world reveal that durability relates to multiple factors [9, 20, 23-30], internal and external.

Durability deals with the assessment how PV modules perform in a stable way in long term within product life. As the electrical output of PV modules can be significantly affected by various environmental factors such as humidity, ultraviolet light, temperature, and also internal factors such as product design, installation, etc., many different tests have been developed to assess degradation of PV modules. Degradation is a common phenomenon observed for PV systems installed in different locations of the world. Power generation was found reducing with the years of outdoor service usually in a small degradation rate over long periods [6,8,17-18]. Serious degradation has a significant impact on the spreading of PV technology as it simply makes the electricity generated by PV system more costly. Common degradation mechanisms can be packaging-related issues [24-25] such as encapsulant yellowing, metal grid corrosion [29], solar cell cracking, hot spot at interconnect joints, delamination at different interfaces [20,27-30], etc. To enhance PV module durability, understanding degradation factors is critical.

UV light in solar spectrum is harmful to many polymeric materials used in PV modules. It causes photo-induced degradation through chain-scissoring (breaking molecules of polymers) and crosslinking (formation of free radicals). Scissoring reduces the molecular weight of polymers that results in loss of mechanical strength, such as elongation to break. Crosslinking makes polymers more brittle. Czanderna and Pern [21-22] reviewed EVA failures from the field. A serious failure mode observed on EVA was “yellowing” which affected light transmission and module power as EVA is subject to deacetylation of the vinyl acetate pendant group that

forms predominantly acetic acid and polyenes, which are the discolouring chromophores, and crosslinks with adjacent chains that increases the gel content. Also, the stability of UV absorber content in EVA film formulation is another cause of photo-thermal degradation for the encapsulant. Such ageing can affect adhesion of polymeric material of PV modules that causes delamination and other moisture-related problems. That is why PVF-based materials are commonly used as backsheets as fluoropolymers possess superior properties against photolysis [31-32]. In PV module with front glass as superstrate, the glass allows visible light to pass through but it is opaque to shorter wavelength UV light and reduces the transmission of longer wavelength UV light. The portion of UV light transmitted through the front glass still has a harmful effect to the encapsulant under the glass. To enhance module efficiency, low iron high transmission glass is commonly used for PV modules [33] which allows more UV light transmitting through the glass and hence the EVA used needs to be more UV-stable. Cerium-doped glass helps reduce UV light transmission in the glass and it was found as an effective solution for module stability [34].

Thermo-mechanical stress is another factor of PV module degradation. The coefficients of thermal expansion (CTE) of silicon, EVA, glass, and backsheet are different by one to two orders of magnitude. Thus the interfaces between the dissimilar materials experience thermo-mechanical stress with temperature changes as materials expand and shrink differently. It can cause significant degradation in the joints between copper string and solar cell connected by solder or epoxy conductive adhesive in fatigue failure mode as shown in Murphy *et al.* and Hsieh *et al.* and Su‘s studies [35-37]. Solder cells and copper strings are usually soldered using eutectic Sn-Pb solder (Sn63Pb37). With RoHS requirements, the solder material is changed to lead-free solders such as Sn-Ag solder, e.g. Sn96.5Ag3.5. The SnAg solder exhibits improved stability due to its low creep strain property under cyclic loading conditions caused by thermal-mechanical stress [38]. Solder fatigue causes an increase in

electrical resistance of the interconnects which affects conversion efficiency. The propagation of fatigue can also cause localized high current density that develops into hot spots due to the joule heating effect. For solar cells encapsulated by EVA, acetic acid generated in field application [20-22] can further deteriorate the joints by triggering corrosion fatigue phenomenon. When an electrical conductive adhesive is used to join copper strings with the back-contact layer in thin-film PV modules, the joint degradation due to inner mechanical stress can deteriorate degradation electrical conduction at the joints. Moisture absorption in the adhesive reduces Young's modulus of the epoxy matrix and degrades fracture toughness of the epoxy/silver interface, which accelerates debonding of silver flakes from the epoxy resin [37]. Interfacial delamination is a direct result of the stress that affects power output seriously [39-40]. Delamination can affect light transmission between solar cell and front glass or front encapsulant and result in severe moisture ingress issue due to the loss of protection.

Besides, a number of other factors can influence PV module stability and affect power output, such as the temperature induced power drop due to the effect of temperature on the bandgap of semiconductors, and the light-induced degradation significantly affecting amorphous silicon solar cells. Moisture ingress is one of the most significant factors that deserves an in-depth study as many failures from field service can be attributed to moisture ingress [38-43].

Moisture ingress is a significant factor of degradation. It causes corrosion in PV modules as well as degradation of bulk/interfacial properties. Moisture can attack solar cells and metals inside the PV module through electro-chemical corrosion and result in general corrosion as well as other types of corrosion (e.g. galvanic corrosion). When moisture is present in a polymeric material (e.g. encapsulant), electrical insulation is affected. It results in leakage current increasing between active

circuit and grounding (module frame) and affects module performance of PV array. The loss of electrical charge directly degrades efficiency [44,46]. Also, moisture absorption results in swelling of polymer material, which increases inner stress inside PV modules. Hygro-stress is caused by polymeric material swelling after absorbing moisture because water can penetrate into polymers by filling the "free volume" inside polymer material, form hydrogen bonds with polymer chain, and separate loose bonds [45]. Polymer swelling has been reported for a variety of polymer materials. Unfortunately, encapsulant materials (e.g. EVA) are prone to moisture permeation as with many other polymer materials. It needs additional barriers to minimize moisture ingress. Kempe [47] and Dhoot [48] studied moisture ingress for EVA, backsheet, PET materials and characterized moisture absorption and desorption process. Such data can also be found from manufacturer, e.g. DuPont [49]. For PV modules with a Glass-Glass structure, encapsulant and solar cells are sandwiched between front glass and back glass. Because of extremely low permeability of water in glass, the structure gives superior moisture protection as well as good mechanical strength. To minimize moisture ingress from the edge of the encapsulant, edge sealant can be applied along PV module peripherals. Such Glass-Glass structure is often adopted in thin-film modules, which are more sensitive to moisture ingress, and Building-Integrated PV module (BIPV) where mechanical strength is important. For another commonly-adopted PV module structure, Glass-Backsheet structure, encapsulants and solar cells are sandwiched between front glass and a backsheet. The backsheet (usually a multiple-layer film laminated with PVF and PET that possess low moisture permeability) acts as a barrier for the encapsulant material against moisture ingress and UV light.

Metal corrosion is one of the major defects found in PV modules after long-term service, usually found on solder joints, silver grids, or strings [29,35,50]. The corroded joints increase local electrical resistance that result in electrical opens. It

may also result in hot spots where the local temperature is very high due to concentrated current density, which speeds up module degradation as the localized heating often causes delamination, EVA yellowing or burns, etc. In field applications PV modules are exposed to outdoor conditions for a long period. Metallic materials inside PV modules suffer from general corrosion due to moisture. Galvanic corrosion can also occur even for those relatively noble materials such as Ag, Sn, etc as a result of dissimilar metals used for solar cells [35,38,51-54] because galvanic corrosion occurs when the overvoltage ($E_{cathodic} - E_{anodic}$) is greater than 0.

Table 1. Common cathodic and anodic reactions of galvanic corrosion [45].

Cathodic reactions	**$E_{cathodic}$**	**Remarks**
$O_2 + 4\ H^+ + 4\ e^- \rightarrow 2\ H_2O$	1.229 V	Oxygen reduction in acidic solution
$O_2 + 2\ H_2O + 4\ e^- \rightarrow 4\ OH^-$	0.401 V	Oxygen reduction in neutral/basic solution
$2\ H^+ + 2\ e^- \rightarrow H_2$	0.000 V	Hydrogen evolution in acidic solution
Anodic reactions	**E_{anodic}**	**Remarks**
$Ag \rightarrow Ag^+ + e^-$	0.800 V	Oxidation
$Cu \rightarrow Cu^{2+} + 2\ e^-$	0.340 V	Oxidation
$Sn \rightarrow Sn^{2+} + 2\ e^-$	-0.135 V	Oxidation
$Pb \rightarrow Pb^{2+} + 2\ e^-$	-0.126 V	Oxidation
$Al \rightarrow Al^{3+} + 3\ e^-$	-1.662 V	Oxidation

Table 1 lists relevant cathodic and anodic reactions with electrode potentials for metallic materials commonly used in Si-wafer PV modules [45]. Metals in acidic solution are the most susceptible to galvanic corrosion as the relevant reaction has the highest cathodic electrode voltage of 1.229 V, when oxygen and H^+ are present. Such conditions can happen inside PV modules as the EVA encapsulant releases acetic acid as a result of photo/thermal degradation and oxygen/water can diffuse into the EVA layer. So even for noble material such as silver, the corrosion can occur as overvoltage = 1.229 – 0.8 > 0. In neutral or basic solution, the risk of galvanic corrosion is reduced as the electrode potential of the relevant cathodic reaction is 0.401V. However, such condition can still result in the overvoltage > 0 for Cu, Sn, Pb, or Al. To prevent the occurrence of corrosion, eliminating the reactants is the

proven way in many corrosion improvement studies. For PV modules, one example besides minimizing moisture diffusion is avoiding EVA decomposition as much as possible because it releases acid.

When corrosion is involved, another important factor should be taken into consideration: the ion content inside PV modules. There are a lot of mobile ions inside a PV module due to impurities of PV packaging materials as a result of impurities in the raw materials or the assembly process. Sodium is known as a mobile ion in soda-lime glass [55] while may cause degradation as it reacts with transparent conductive oxide [19]. When soldering process is used in connecting solar cells with copper strips, flux residue usually contains Cl^- which is highly mobile and corrosive. Cl^- is well known as a corrosive ion which causes pit corrosion on metals as it attacks their protective metal oxide coating. In Integrated-Circuit semiconductor chips, the existence of Cl^- could cause serious electrolytic corrosion on Au-Al and Cu-Al joints when a bias current is present, and this could result in early failure in Temperature-Humidity-Bias (THB) and Highly-accelerated-stress-test (HAST) tests [52-53]. Moisture diffused into PV modules can serve as an electrolyte that is needed for galvanic and electrolytic corrosions.

Potential-induced degradation (PID) is another failure mechanism related to corrosion [56-58]. In actual field applications as illustrated in Fig. 4 the frame of the PV module is usually grounded for safety reasons. As PV modules are connected in series and parallel in PV arrays, the voltage potential of the active circuit of the last module in a series-connected PV module chain will be high. This may trigger electro-chemical corrosion especially when moisture is present as an electrolyte for the reactions. Accelerated tests can be conducted by applying a high DC bias voltage between module frame and active circuit of the PV module under damp heat (usually 85^0C/85%R.H.) conditions or outdoor conditions. In this test, anode/cathode will

experience different electrical-chemical reactions. The anode loses electrons and usually becomes corroded. The cathode gains electrons and attracts ions, which may trigger corrosion to the cathode material, e.g. TCO corrosion for thin-film PV modules [19,58]. IEC standard 62804 [59] specified test methods for studying PID degradation for crystalline silicon photovoltaic (PV) modules.

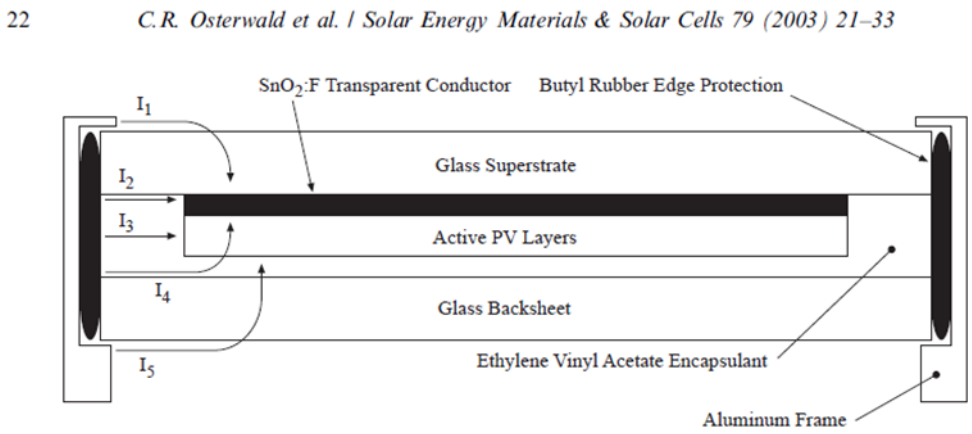

Fig. 4. Sketch of Potential-Induced Degradation (PID), showing ion moving paths when bias voltage is applied between active circuit and module frame [19]

2.2 Accelerated stress tests for PV modules

Obviously 20-25 years is a very long time for module performance assessment. Hence various accelerated stress tests have been developed to study failure mechanisms and design weakness of PV modules [60]. Accelerated stress methods have been widely applied in the semiconductor industry [51,61-66] as an important means of reliability engineering to assess product reliability in a shortened time by applying stresses (temperature, humidity, voltage, etc) in excess of those normally experienced by the product in service. Various life-stress models [67-69] have been developed to describe the relationship in the form of a mathematical formula. The Arrhenius life-stress model is the most common life-stress relationship utilized in accelerated life testing that was derived from chemical reactions stimulated by temperature. The ratio of product life or degradation rate between normal service level and a higher test

stress level is known as acceleration factor. For a thermal degradation [65], an acceleration factor can be described by equation (1).

$$A_T = \lambda_{T1}/\lambda_{T2} = \exp[(-E_a/k)(1/T_1 - 1/T_2)] \quad (1)$$

where

E_a is the activation energy (eV);

k is the Boltzmann constant (8.62×10^{-5} eV/K);

T_1 is the absolute temperature of test 1 (K);

T_2 is the absolute temperature of test 2 (K);

λ_{T1} is the observed failure rate at test temperature T_1 (h^{-1});

λ_{T2} is the observed failure rate at the test temperature T_2 (h^{-1}).

For PV products, Wohlgemuth [18], Osterwald and McMahon [60] reviewed the history of development of qualification test standards from JPL Blocks I-V (1975-1981) for crystalline Si to IEC 61215 (Ed 2-2005) for Crystalline Si and IEC 61646 (E2-2007) for Thin Films. The IEC qualification standards are living documents that are revised with new knowledge in PV durability. Currently IEC61215/61646 standards [70-71] are regarded as mandatory test standards that PV module manufacturers need to follow to qualify the performance of their PV modules for terrestrial applications. The standards define the test conditions of accelerated stress tests and performance characterization tests for silicon wafer modules and thin-film modules.

The Damp Heat test is an accelerated corrosion test. PV modules are tested in 85°C, 85% Relative Humidity (R.H.) conditions for 1000 hours that promotes rapid moisture diffusion into PV modules through polymeric materials such as backsheet, EVA, edge sealant, etc. The high temperature (85°C) not only increases moisture diffusion, and but also intensifies corrosion reactions. Tamizh Mani [23] studied the failure modes in stress tests and showed that it was the most stringent stressing test for crystalline and thin-film PV modules.

Thermal Cycling is another type of accelerated test to assess performance change due to thermo-mechanical stress. As a PV module is made of different materials that possess different CTEs, inner stress is built up when the PV module is subjected to a temperature change in field applications that can cause fatigue or cracking at inter-connects, interfaces, and bulk material of solar cells. IEC standards define test conditions in 200 cycles from 85^0C to -40^0C.

The Humidity Freeze test applies several degradation factors together to assess performance. It consists of a UV preconditioning for 15 kWh/m^2 followed by 50 cycles of thermal cycling, and then a humidity-freeze cycling for 10 cycles (one cycle consists of 24 hours staging at 85°C/85% R.H., 1 hour staging at -40°C, and ramp-up/ramp-down time). The combined stressing factors are used to assess the weakness of a PV module in that the UV and thermal-cycle precondition degrades the PV materials first for higher moisture ingress at the humidity freeze stage.

2.3 Objective of PV module testing in this study

In this study, 10 types of commercially available PV module/technology are subjected to various stress tests in the PV module performance analysis unit (PVPA) of the Solar Energy Research Institute of Singapore (SERIS). Standard test conditions are applied for performance measurement to determine degradation rates. Understanding degradation rate is important for the development of accelerated stress test for a particular PV module to estimate its lifetime in actual field applications at a specific location. For tropical countries such as Singapore, hot and humidity weather conditions promote corrosion and/or other moisture-ingress related issues. Thus moisture stress tests are the focus of PV module testing in this study. Module performance prediction is another focus in this study in order to select suitable PV modules fit for Singapore's weather conditions. The modules are subjected to the standard accelerated stress tests and characterization tests defined in IEC standards as

well as tightened stress tests in order to characterize the durability of different PV technologies.

The stress tests can be classified into moisture corrosion tests, UV degradation tests, thermal-cycling tests, outdoor tests and performance characterization tests. For moisture corrosion tests, different moisture stress test conditions are applied including Humidity Freeze -40^{0}C to 85^{0}C for 10 cycles, Damp Heat 85^{0}C/85%R.H. for 1000 hours, Damp Heat 90^{0}C/90%R.H. for 1000 hours, and bias Damp Heat test @ 85^{0}C/85%R.H. for 650 hours with 1000 V DC bias voltage applied between active circuit and module frame. For UV degradation tests, UV exposure is performed in a UV ageing chamber for 15 kWh/m^2 and 50 kWh/m^2. For the thermal cycling test, thermal cycling from -40^{0}C to 85^{0}C is applied for 200 cycles. For outdoor exposure tests, PV modules are placed on rooftops with resistive loads attached. For performance characterization tests (NOCT, temperature coefficient, low-irradiance performance, etc), PV modules are also assessed in PVPA of SERIS. Also, the same ten module types tested in PVPA are installed by SERIS on the rooftop of a building at the National University of Singapore for outdoor tests with maximum power point tracker attached for long term monitoring.

2.4 Conclusions

This chapter started with a literature survey on the various degradation mechanisms of PV modules, including metal corrosion, string fatigue, EVA deacetylation, potential-induced degradation, light-induced degradation, interfacial delamination, etc. Accelerated stressing test methods were discussed for assessing PV module durability. Finally the objective of the study, the general test plan and methodologies were shown in which various indoor accelerated stress tests and outdoor tests were described.

CHAPTER 3

SIMULATIONS OF MOISTURE DIFFUSION IN PV MODULES

3.1 Literature Survey

Moisture penetration in polymers has been widely studied using Finite Element Analysis (FEA). FEA has proven to be a powerful tool for simulating moisture diffusion. Xiong and Tay [72], Tay and Lin [73] studied moisture diffusion in electronic IC packaging and crack propagation influenced by hygro-stress which resulted from material expansion after absorbing moisture. Fan *et al*. [74] measured moisture diffusivity and solubility for epoxy mold compound with TGA and TMA equipment. Kempe [47] measured common materials used in PV modules with water vapour transmission rate (WVTR) test and also performed FEA simulations to reveal moisture concentration variation of PV modules in Florida, USA, which revealed moisture desorption/ absorption cycles in field service [75-76].

The Finite Element Method is a powerful numerical technique for solving engineering problems. One example is the calculation of π of a circle used by ancient mathematicians. In this method, the whole domain is divided into a number of subdomains with simple geometry (elements). By solving partial differential equations on the elements, one can obtain an approximate solution and the solution is examined by applying Newton-Raphson iteration technique to calculate residuals to minimize errors of the approximation.

A mass transfer problem can be described by Fick's laws [77]. The first Fick's law in a 1-dimensional study is described as

$$J = -D\left(\frac{\partial c}{\partial x}\right) \qquad (2)$$

J is the flux of mass flow. *D* is diffusivity. *c* is concentration and *x* is location.

The change of concentration *c* with time *t* is governed by the following differential equation obtained from the law of conservation of species:

$$\frac{\partial C}{\partial t} = D \cdot (\frac{\partial^2 C}{\partial x^2} + \frac{\partial^2 C}{\partial y^2} + \frac{\partial^2 C}{\partial z^2}) \qquad (3)$$

D is the diffusivity of moisture diffusion of material. *c* is concentration of moisture and *t* is the time of moisture diffusion. *x, y,* and *z* correspond to the coordinates in 3D space.

With sophisticated computational software such as ABAQUS-CAE®, moisture diffusion can be modelled for complex structures. After meshing the geometry, defining material properties, applying boundary conditions and initial condition to the problem, the software will calculate the solution for the whole model. The governing equations for mass diffusion are extensions of Fick's equations: they allow for non-uniform solubility of the diffusing substance in the base material and for mass diffusion driven by gradients of temperature and pressure. The basic solution variable (used as the degree of freedom at the nodes of the mesh) is the "normalized concentration" (often also referred to as the "activity" of the diffusing material), where *c* is the mass concentration of the diffusing material and *s* is its solubility in the base material. Therefore, when the mesh includes dissimilar materials that share nodes, the normalized concentration is continuous across the interface between the different materials.

$$\int_V \frac{dc}{dt}\, dV + \int_S \mathbf{n} \cdot \boldsymbol{J}\, dS = 0 \qquad (4)$$

where *V* is any volume whose surface is *S*; **n** is the outward normal to *S*; ***J*** is the flux of concentration of the diffusing phase leaving *S* [78].

3.2 Material properties in FEA simulation

In order to simulate moisture diffusion, two material properties need to be input into the FEA model: diffusivity *D* and solubility *S*. Diffusivity represents how fast moisture can move in a medium and solubility represents the amount of moisture the medium can hold when it is saturated with moisture. For moisture diffusion in a structure with dissimilar materials, moisture concentration needs to be "normalized" by solubility such that the solution obtained from FEA will be continuous over the interfaces of dissimilar materials. The normalized concentration is also called the "wetness" of a material. The material properties for this study are shown in Fig. 5.

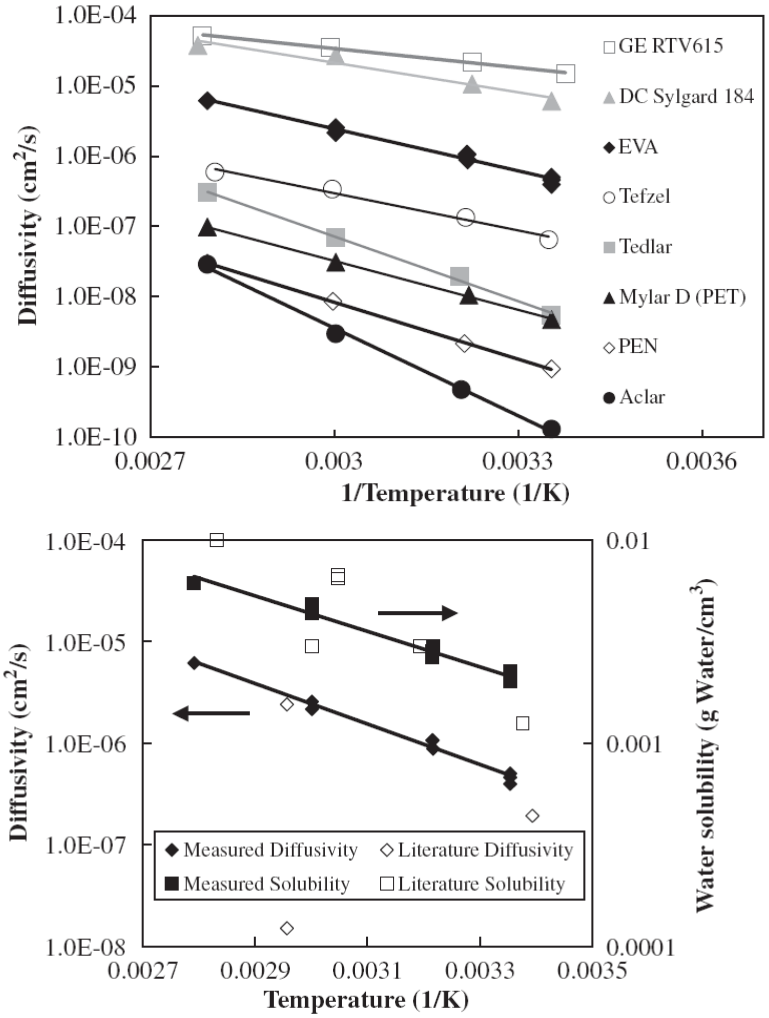

Fig. 5. Temperature dependent material properties of common PV packaging materials [47].

3.3 Moisture diffusion simulation: Theory verification

Understanding moisture diffusion in a film is the basis of understanding the moisture ingress phenomenon in PV modules. In the following section, moisture diffusion is solved numerically and the result is compared with an analytical solution for a film in moisture soaking condition. The analytical solution of the 1-D diffusion equation [77] is given in equation (5). C_1 is boundary condition – moisture concentrations at the surfaces of the film and C_o is initial condition – moisture concentration in the film just before moisture diffusion starts. l is a dimension (half film thickness) and t is time. x represents location.

$$\frac{C-C_o}{C_1-C_0} = 1 - \frac{4}{\pi}\sum_{n=0}^{\infty}\frac{(-1)^n}{(2n+1)}\exp\left[-\frac{(2n+1)^2\pi^2 D}{4l^2}t\right]\cos\frac{(2n+1)\pi x}{2l} \qquad (5)$$

The above formula can be used to reveal the moisture concentration field inside the object of study. As the moisture diffusion problem can also be solved by finite element analysis, comparing the results obtained from the two methods on an object with simple structure can verify whether there is any mistake in the simulation, which is very important before any further study on complex structures. Figure 6 plots the results of the analytical solution and FEA simulation for the normalized moisture concentrations at different times and different locations in a moisture soaking process for a film totally dried at the starting time and saturated at the ending time. Different curves represent the distribution of moisture concentrations from film surface (x/l = 1) to film centre (x/l = 0) at different normalized time (Dt/l^2), showing moisture concentration increasing with time. Both results match well with each other. This serves to demonstrate the accuracy of the subsequent simulations of moisture diffusion in actual PV modules.

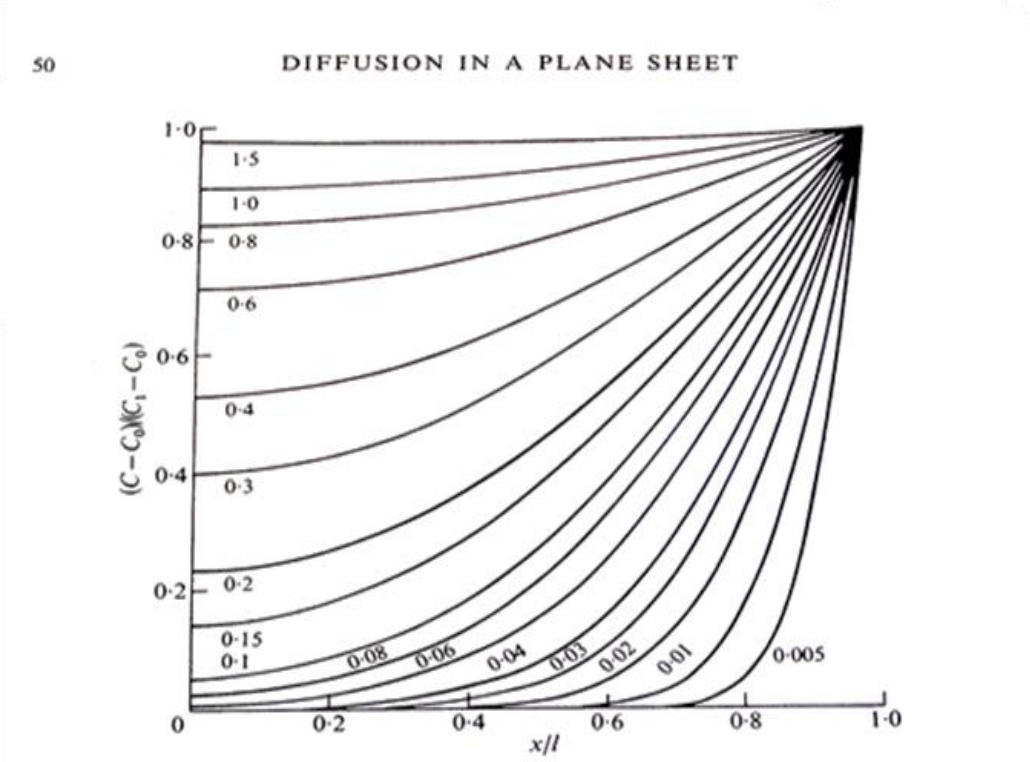

FIG. 4.1. Concentration distributions at various times in the sheet $-l < x < l$ with initial uniform concentration C_0 and surface concentration C_1. Numbers on curves are values of Dt/l^2.

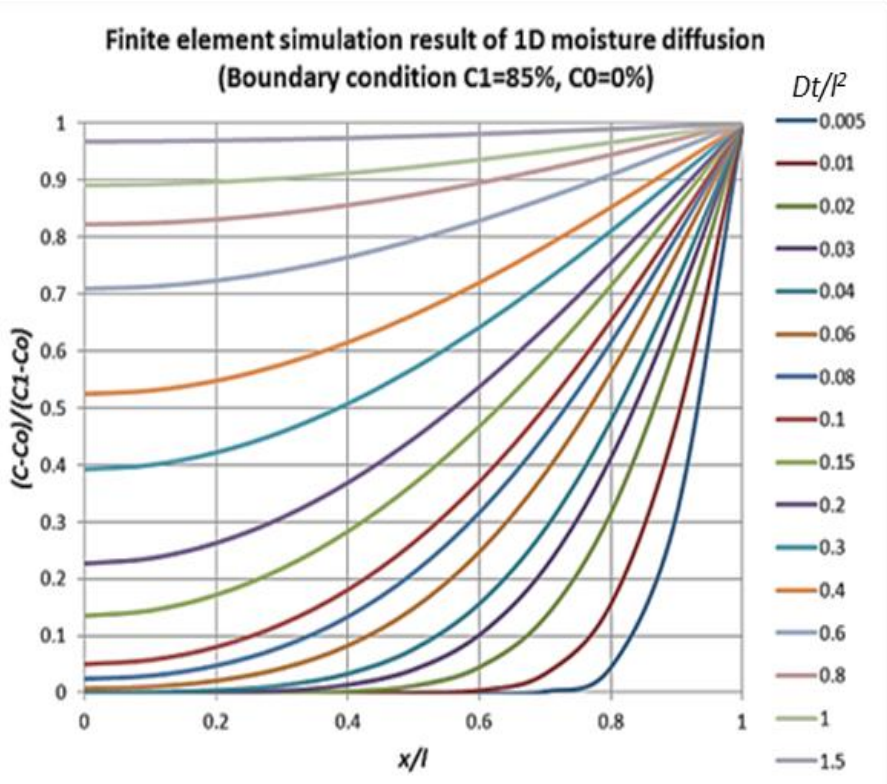

Fig. 6. Moisture distribution in a film. Moisture ingress from two sides of a totally dried film. (Upper) Analytical solution [77] vs. (Lower) FEA result. FEA result matches with that of the analytical solution.

3.4 Moisture diffusion simulation: Effect of testing conditions

The following study is for simulating moisture diffusion from the external environment into the PV module. In the 2-dimensional simulation, a PV module in Glass-Backsheet structure with silicon wafers as solar cells is used and the geometry information is listed in Table 2.

Table 2. Geometry and materials of the FEA model for moisture simulation

Geometry	Material	Thickness (μm)	Length (mm)
Encapsulant	EVA (2 layers)	500; 500	79.75
Backsheet	Tedlar	38	79.75
	PET	254 (Thick); 76 (Thin)	79.75
	Tedlar	38	79.75
Si wafer	Silicon	200	78.00

As commercial Glass-Backsheet PV modules are basically in large panel structure, and front glass is a moisture impermeable material with much larger thickness than encapsulants or backsheet, moisture ingress from the bottom of backsheet should be the main path of moisture ingress and the ingress from module edge is negligible for the whole PV module. To simplify the FEA model, a section of PV module is taken into the FEA model as the section represents other same sections in the PV module symmetrically. In the model, the symmetric planes are placed at the centre of the silicon wafer and the centre of the gap between Si wafers in the vertical direction such that the sections of the module at the two sides of the symmetric planes mirror against each other as shown in Fig. 7. The technique is commonly used in FEA modelling to greatly reduce the problem region and speed up the simulation.

The silicon wafers are 156 x 156 x 0.2 mm (L x W x T), sandwiched between top encapsulant and bottom encapsulant, and the gap between Si wafers in the lateral direction is 2.5 mm as measured on the mono-Si PV module for the study. Front glass and Si wafer are modelled as moisture-impermeable material thus they are neglected

in the geometric model. Boundary conditions (moisture concentration) are applied at the bottom surface of Tedlar-PET-Tedlar backsheet to simulate moisture ingress from the ambient towards the Si wafer solar cells. Initial condition (internal moisture concentration: 0%) is applied to the encapsulant and backsheet to simulate the totally dry status inside the PV module. Backsheet is a TPT type with a PET layer sandwiched by two Tedlar films. By altering the thickness of the PET layer, the moisture barrier ability can be changed for the backsheet. In Fig. 7, the zones of interest (1, 2, 3, 4) are indicated which represent the four regions of Si wafer: 1) The centre of the bottom surface, 2) the edge of the bottom surface, 3) the edge of the top surface, and 4) the centre of the top surface, respectively. Focus is given to these regions in order to understand how moisture moves in the top and bottom EVA encapsulant layers.

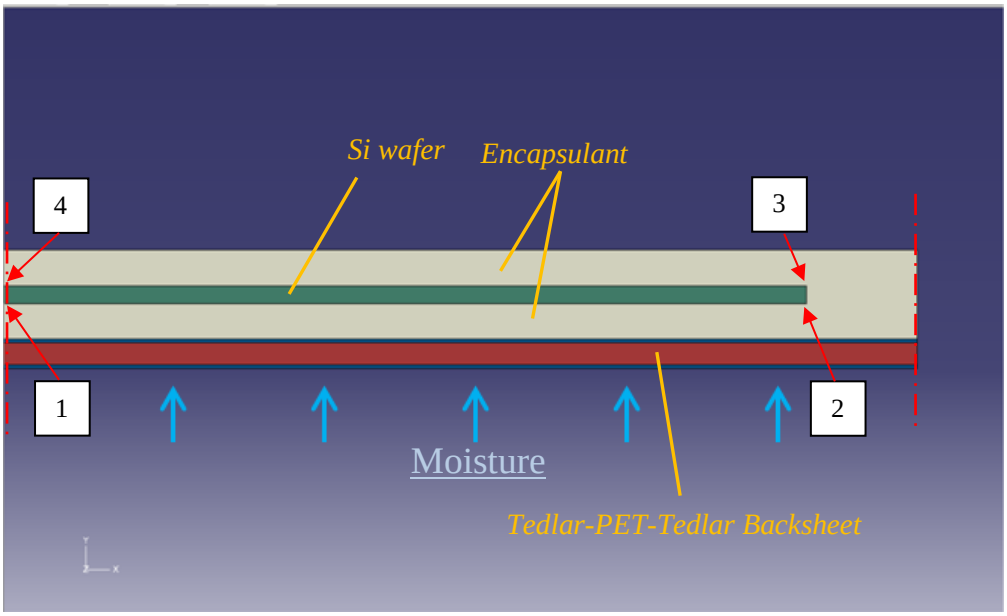

Fig. 7. Two-dimensional model for moisture diffusion in a Glass-Backsheet Si-wafer PV module. Symmetric planes are located at the centre of solar cell and the centre of the cell-to-cell gap.

Two simulations were run with the same geometry and material set but different boundary and initial conditions as shown in Table 3 to study moisture diffusion under damp heat test and outdoor test conditions. Boundary conditions are applied at the bottom surface of the backsheet and initial conditions are applied to the whole model

at the starting time. Temperature loading is applied to the whole model assuming that the temperature is uniform over the whole module.

Table 3. Boundary condition, initial condition and temperature loading of FEA models.

Simulation	Boundary condition	Initial condition	Temp. loading
Damp Heat	Concentration: 85%	Concentration: 0%	85°C
Outdoor	Ambient humidity	Concentration: 0%	Module temp.

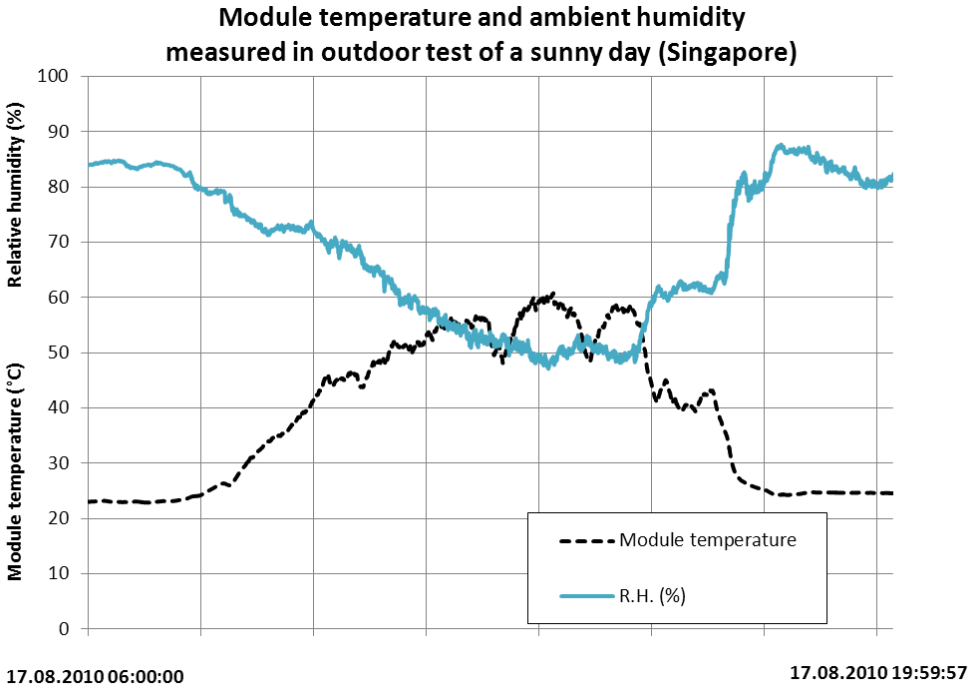

Fig. 8. Temperature of a Si wafer PV module and relative humidity of air measured in a typical sunny day in Singapore

In the simulation of the outdoor test, the measured data of ambient humidity and module temperature of a PV module in Singapore on a sunny day (Fig. 8) over 24 hours (reference day) was input into the simulation as boundary condition and temperature loading. The data was measured every 5 seconds in an outdoor test on the rooftop of PVPA on a sunny day. For simulations over 1000 hours, it was assumed that the variations of ambient humidity and module temperature throughout every subsequent day are identical to the reference day. As can be seen in Fig. 8, the module temperature varied between 23°C and 60°C and the ambient humidity varied

between 49% and 85% R.H. on the reference day. During the morning of the test day, the module temperature increased as it absorbed heat from sunlight. It reached a peak at around 2pm as solar insolation is typically the strongest at this time in Singapore. Module temperature decreased in the afternoon and stayed at around 23°C during the night. Ambient humidity varied inversely with temperature. During the day, it decreases to the lowest value at about 2pm in the afternoon and reaches the highest value during the night.

Figure 9 shows the normalized module concentration C/C_{sat} in the backsheet and encapsulant layers after 85°C/85%R.H. soaking for 1000 hours. The direction of moisture diffusion is clearly demonstrated in the moisture concentration field. Moisture concentration of the bottom encapsulant becomes saturated quickly in about 18 hours while the top encapsulant layer is far from saturation even after 1000 hours. The Si wafer acts as a "moisture barrier" that retards moisture diffusion from the bottom encapsulant layer to the top encapsulant layer. Moisture can only diffuse through the gap between the Si wafers to penetrate into the top encapsulant layer from the wafer edge towards the wafer centre.

Figures 10 and 11 shows the normalized moisture along the top and bottom surfaces of the Si wafer at various times. The top encapsulant layer shows an uneven moisture distribution while the bottom encapsulant is fully saturated after 1000 hours of Damp Heat 85/85.

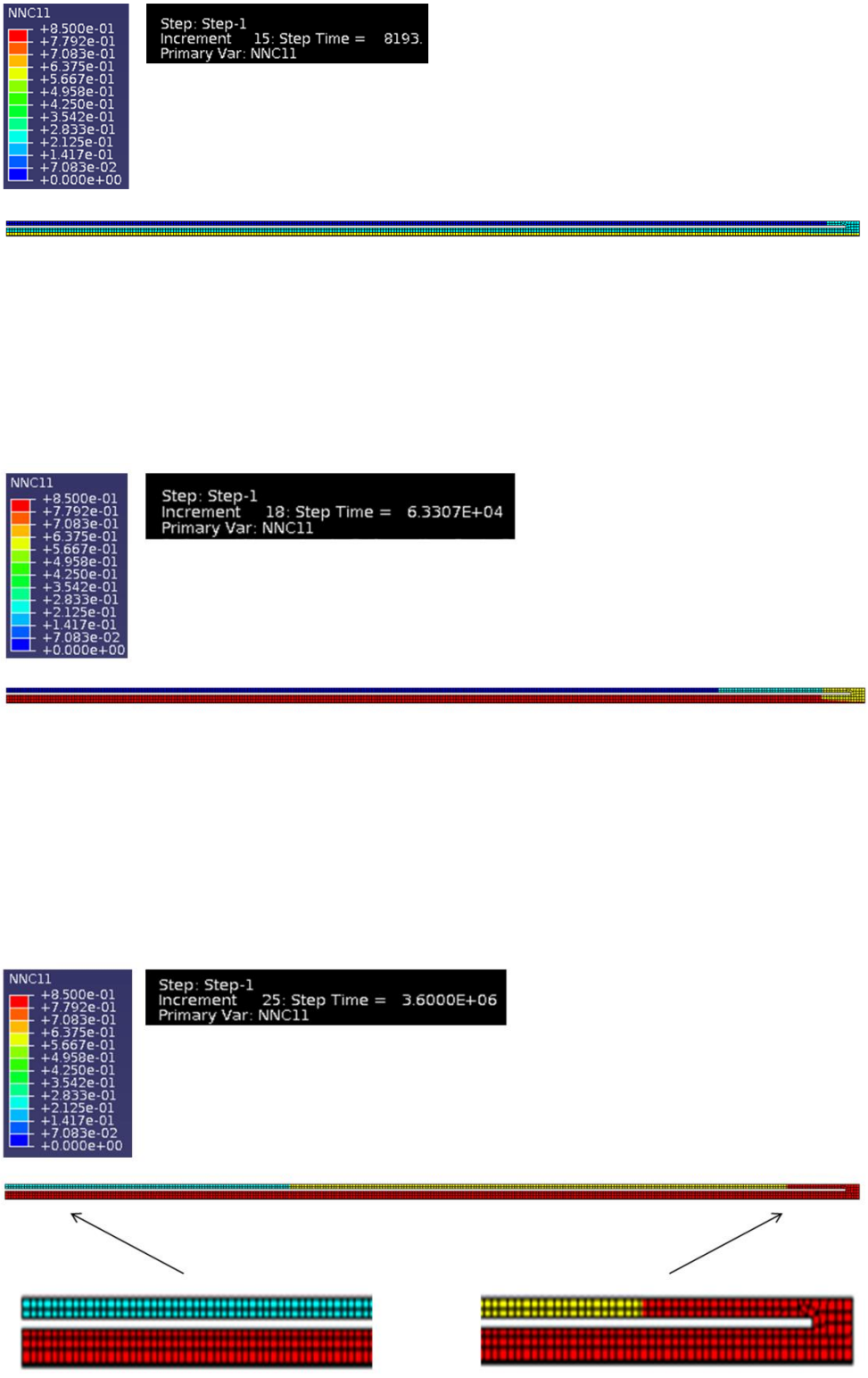

Fig. 9. Normalized moisture concentration in backsheet and encapsulant layers of a Si wafer PV module at 2 hours, 18 hours and 1000 hours in 85°C/85%R.H.

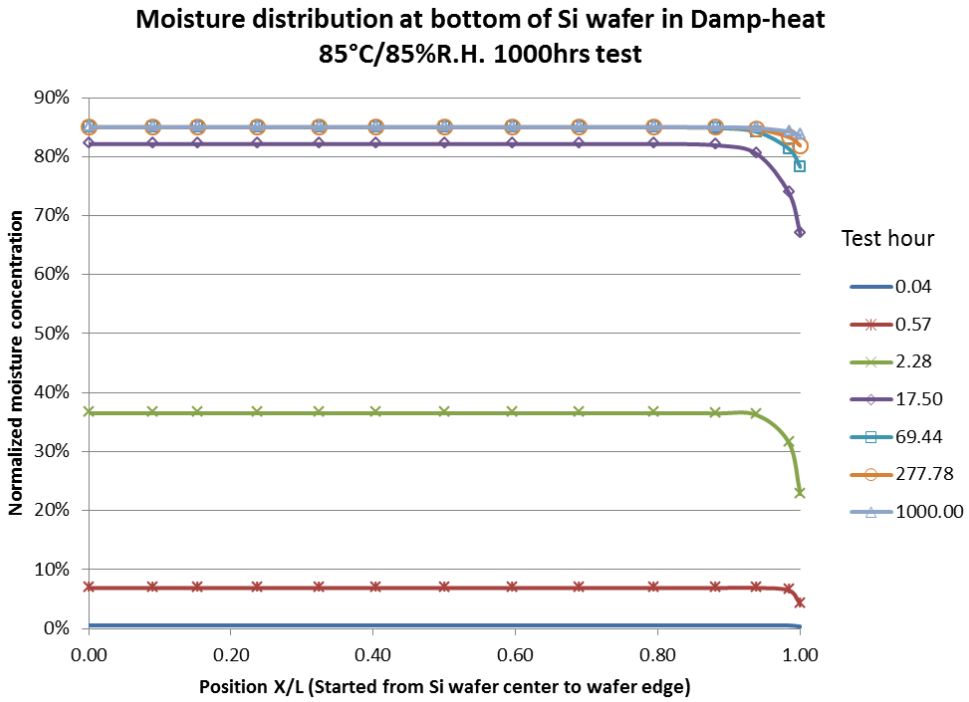

Fig. 10. Normalized moisture concentration C/Csat along the bottom of the Si wafer at various times during the Damp Heat 85°C/85%R.H. test

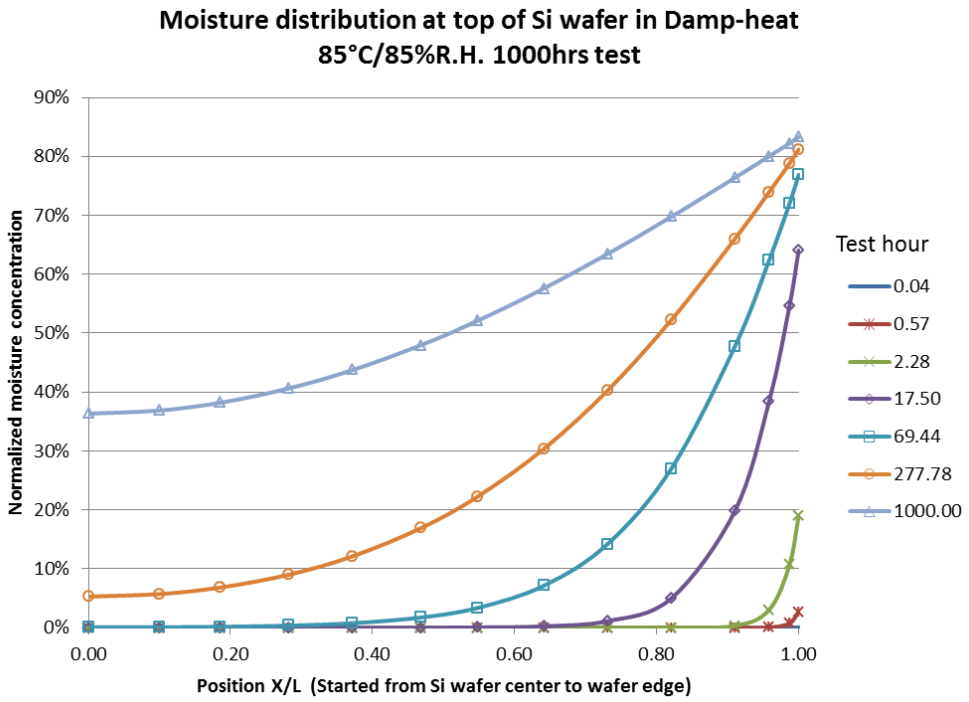

Fig. 11. Normalized moisture concentration C/Csat along the top of the Si wafer at various times during the Damp Heat 85°C/85%R.H. test

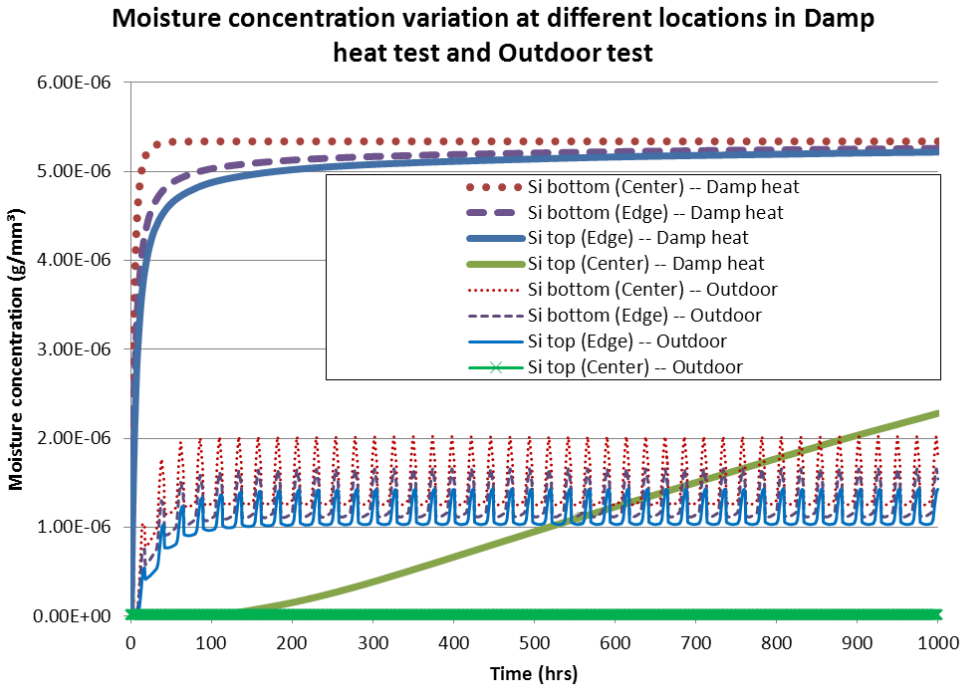

Fig. 12. Moisture concentration at various locations on the Si wafer interfaces in Damp Heat and Outdoor tests in Singapore

Figure 12 shows the variations of moisture concentrations with time at the top and bottom surfaces of the silicon wafer in Damp Heat and Outdoor test simulations. Under Damp Heat 85/85 soaking conditions, the centre of the bottom surface is found saturated within one day and the concentration at the centre of the top surface is just ~40% of that at the bottom surface after 1000 hours. The edge of the bottom surface shows lower moisture concentration than the centre of the bottom surface because moisture moves away from this region into the top encapsulant layer. The edge of the top surface shows even lower concentration than the edge of the bottom surface due to the same reason. Under the outdoor test conditions, assuming that the same sunny-day outdoor conditions would be repeated day after day without change, the centre of bottom surface of Si wafer reaches the highest concentration similar as that under Damp heat 85/85 test, followed by the edge of the bottom surface and the edge of top surface. The centre of the top surface shows very low moisture concentration as it keeps dry. With the cyclic variation of ambient relative humidity, a "cyclic"

phenomenon is exhibited as moisture concentration becomes the lowest at around 2pm in the afternoons and the highest during the nights. This is because the variations in the boundary conditions create different consequences in moisture diffusion. Under a condition that ambient relative humidity is higher than normalized moisture concentration (C/C_{sat}) inside the PV module during the day, moisture diffuses from the ambient into the module. When the difference in moisture concentration between ambient and module is reversed during the night, the direction of moisture diffusion becomes reversed too and the module will be in a "moisture desorption" process, instead of "moisture absorption" process. The varied module temperature results in differences in moisture diffusivity and solubility as both properties are functions of temperature.

It is interesting to note that after 5 days, the moisture concentration levels at the bottom surface of the Si solar cell and that at the edge of the top surface of the cell appear to have reached an "equilibrium" periodic daily variation, while the moisture concentration continues to increase even after 1000 hours.

The FEA work of Hülsmann *et al*. [75] showed a similar variation phenomenon for moisture concentration in the EVA layer for a Glass-Backsheet PV module under different climates. It showed that moisture intake was faster in warmer climates than in colder regions. It was also found that the equilibrium periodic moisture concentration in the tropical site was lower than those in the Alpine and the moderate climate sites due to the simlar absorption/desoprtion cycling described above.

As discussed in a subsequent chapter, water or its derivatives (hydroxide or hydrogen ion) is one of the reactants in the reactions of corrosion [45]. The kinetics of the chemical reactions is influenced by multiple factors while the supply of reactants is one of them. Higher moisture amount results in more metal atoms getting corroded. Hence total moisture amount experienced at corrosion sites is an important factor of

corrosion severity. By integrating the moisture concentrations shown in Fig. 12 with time, the total amount of moisture absorption (called moisture dose) after the damp heat and outdoor tests can be obtained. As shown in Fig. 13, moisture dose post Damp Heat 85/85 test is found to be 3-5 times of that post Outdoor test for the three regions of Si wafer (the centre of bottom surface, the edge of bottom surface, and the edge of top surface), while the ratio of Damp Heat test vs. Outdoor test is about 5 orders (100,000 times) higher at the centre of the top surface mainly due to the moisture blocking effect of Si wafer solar cells.

The above observation suggests different acceleration factors (AF) at different locations in the in the Damp Heat test. In other words, the extent of acceleration at the top and bottom EVA layers are significantly different when using the Damp Heat test to estimate the degradation by moisture ingress in the outdoor test. Thus the critical area (or the area of interest) needs to be identified first to correctly calculate the AF for a Damp Heat test. For example, based on the study of this simulation when temperature effect is excluded, the AF is 3-5 times if the critical area is the bottom surface of the Si wafer solar cell and it is 5 orders if it is the centre of top surface of Si wafer solar cell. This topic deserves further study with long-term weather data input into such simulations to verify the acceleration factor of the Damp Heat test with reference to the actual service conditions of the PV module.

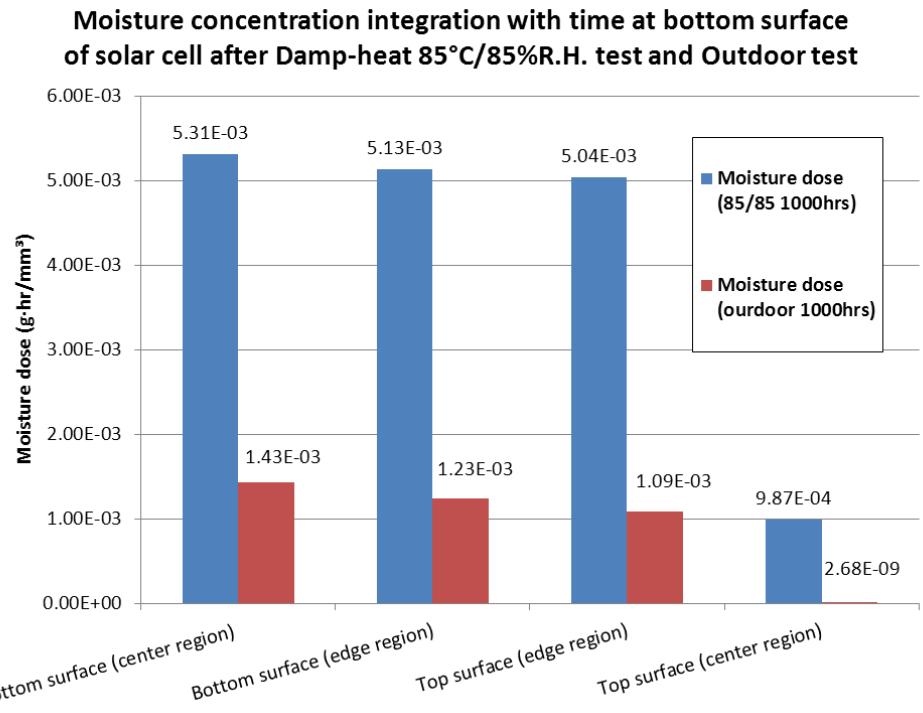

Fig. 13. Cumulative moisture amount (moisture dose) at Si wafer surfaces after 85°C/85%R.H. and Outdoor test of Singapore for 1000 hours.

3.5 Moisture diffusion simulation: Effect of backsheet thickness

This simulation aims at simulating the effect of backsheet thickness on moisture ingress by changing the thickness of PET layer while maintaining the thickness of Tedlar layers. Two thicknesses of the PET layer (254 µm and 76 µm) were used in the simulation. As shown in Fig. 5, PET possesses 2 orders (100 times) lower diffusivity than EVA, hence increasing PET thickness will increase moisture barrier capability for backsheet. In actual operation, the PV module experiences "moisture absorption" and "moisture desorption" processes depending on weather conditions as discussed in the previous section. The effect of the backsheet on moisture diffusion in outdoor conditions is the focus of this simulation. In this simulation, the same boundary condition (changed ambient humidity), initial condition (100% dry inside the PV module), and temperature loading (changed module temperature) are applied for the two geometries with different PET thicknesses.

Moisture concentration at the centre of the bottom surface of silicon wafer is plotted in Fig. 14 to compare the effect of backsheet thickness. It becomes stabilized after the 5 days when the previous mentioned reference-day outdoor conditions are repeatedly applied to the module, which indicates the balance of moisture absorption and moisture desorption from the 6^{th} day. Normalized moisture concentration C/C_{sat} ("wetness") decreases with increased module temperature and decreased air humidity in the mornings, and it increases in the afternoons. Thin TPT backsheet allows moisture diffusion out of the PV module more easily than thick TPT backsheet during the moisture desorption process, however, it absorbs moisture faster than thick TPT during the moisture absorption process. As the solubility of EVA increases with temperature, the moisture concentration curve shows a different trend from that of the normalized moisture concentration. But the same conclusion is obtained in that a thin TPT backsheet allows moisture effusion and moisture ingress more easily than thick TPT backsheet.

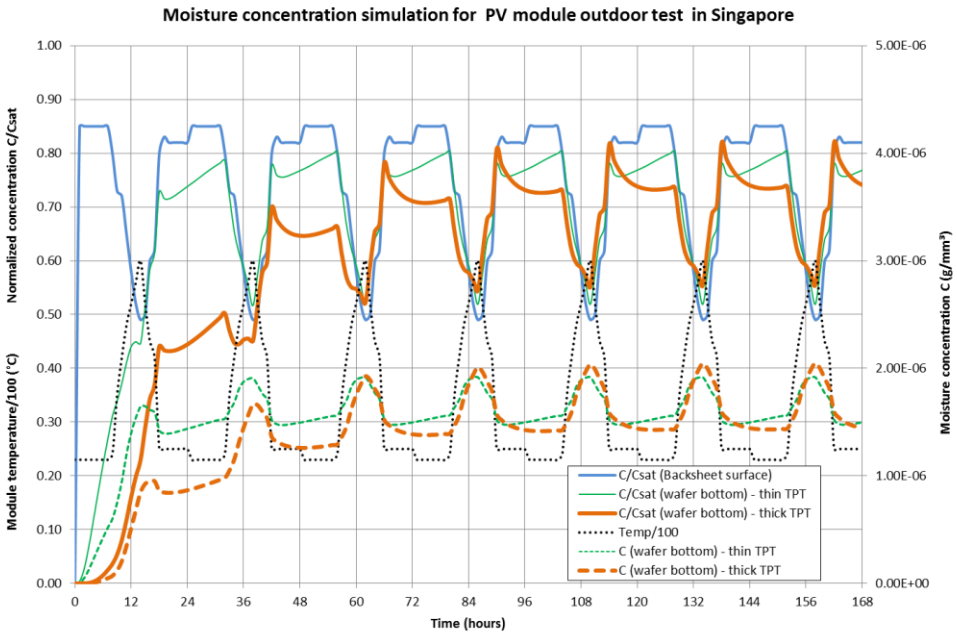

Fig. 14. Moisture concentration and normalized moisture concentration at the centre of bottom surface of Si wafer in outdoor test simulation.

3.6 Moisture diffusion simulation: Effect of encapsulant material

This simulation is on studying the effect of encapsulant on the silicon wafer PV module that was studied in the previous section. A 3-dimensional FEA model is established and symmetric planes are placed in the centres of cell-to-cell gaps to simplify the model. The same boundary conditions, initial condition and temperature loading are applied. Encapsulant layer is modelled with EVA and ionomer, respectively. Compared with EVA, ionomer possesses lower moisture permeability and higher mechanical adhesion strength than EVA. For DuPont® ionomer PV5300 encapsulant, its water vapour transmission rate (WVTR) is only 0.3 gram/m^2day, significantly lower than the common EVA encapsulant with WVTR about 30 gram/m^2day [49]. The model is loaded with 85% R.H. at the bottom of the backsheet as boundary condition and 85°C for the whole model as temperature loading.

Figure 15 shows the simulation results of moisture concentration in encapsulant and backsheet after 1000 hours 85°C/85%R.H. test. The tilted-angle view reveals mostly the distribution of moisture in the top encapsulant layer. Moisture absorption in the top encapsulant is low when ionomer is used, as compared to EVA. For example, at the centre region of top surface of the Si wafer, the normalized moisture concentration is about 0-8.5% when ionomer is used as encapsulant, while it is 51.0-59.5% for EVA. Moisture absorption in the bottom encapsulant has no difference as this layer becomes saturated for either case. The simulation shows moisture diffusion is much slower inside PV module when EVA encapsulant is replaced by ionomer encapsulant. The difference of moisture concentration on the top surface of the solar cell can result in different degrees of corrosion at the top metallization layer. The FEA work of Kim and Han [76] compared the effect of encapsulant materials in a Glass-Glass PV module in outdoor applications. The moisture concentration of a PV module built with ionomer encapsulant was found much lower than that built with

EVA or PVB encapsulant because of the low diffusivity and low solubility for ionomer material. The superior properties of ionomer on moisture absorption make it an attractive encapsulant material and further studies will be needed to test it against other degradation factors of field application.

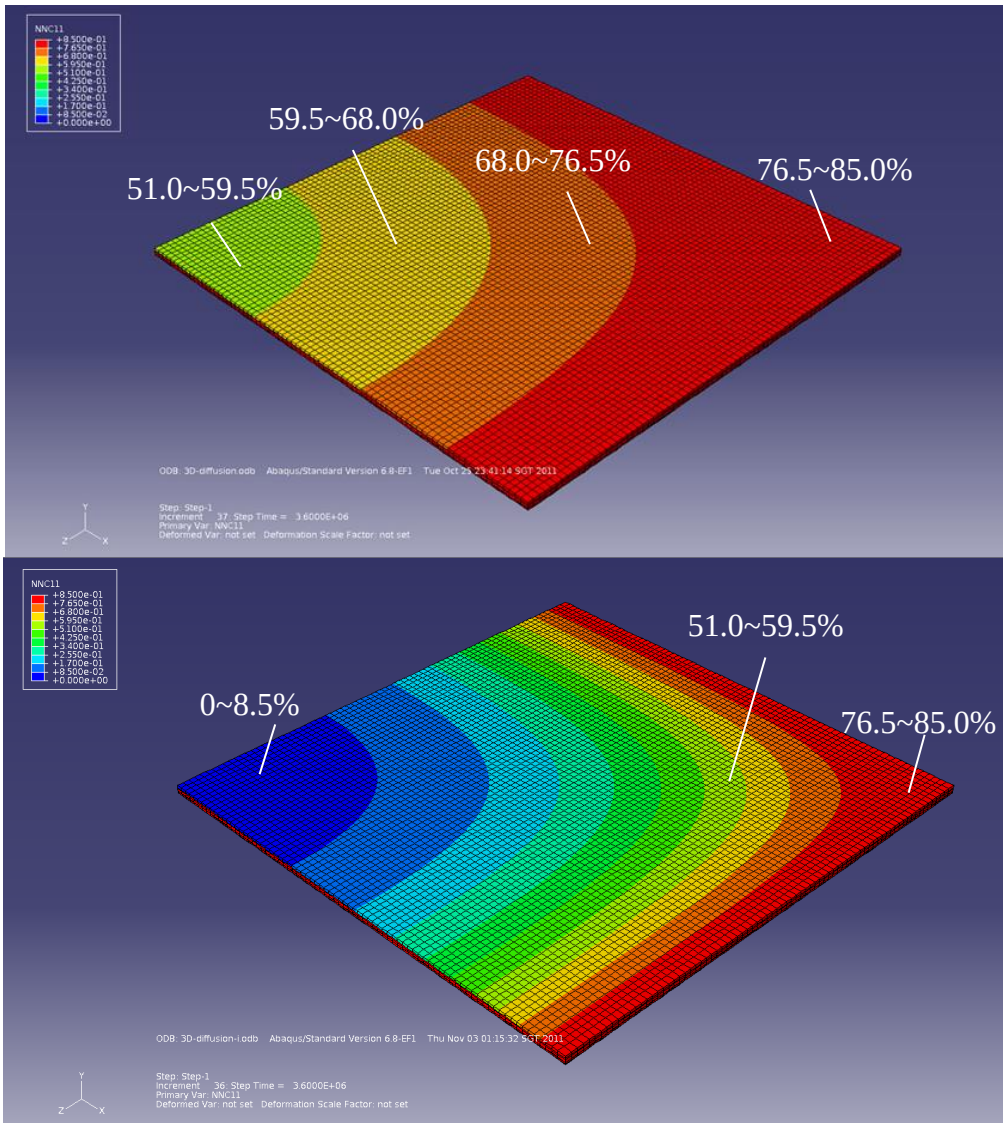

Fig. 15. FEA simulation of normalized moisture distribution in encapsulant layer after Damp Heat 85°C/85%R.H. 1000 hrs. Encapsulant: EVA (Upper) and ionomer (Lower).

3.7 Moisture diffusion simulation: Effect of module structure

Compared with Glass-Backsheet module, Glass-Glass module offers better protection against moisture ingress because glass is moisture impermeable thus it almost eliminates moisture ingress from the back of PV module, although a little moisture may penetrate from junction box on the back glass into PV module. Such module structure is widely used in Si-wafer based Building-Integrated PV modules and many thin-film PV modules. Moisture ingress occurs mainly from the edge region of such type of PV module between the two glasses. Edge sealant design is often adopted in order to minimize moisture ingress from the gap between front glass and back glass as edge sealant can be formulated with much lower moisture permeability than encapsulant material.

In the simulation, another structural feature (metal string) is studied to understand its effect on moisture diffusion. Metal string is usually a thin copper strip coated with solder. It is soldered with silicon-wafer solar cells to connect them together. In the model, 3 thicknesses of metal string are input into the model (Thickness: 0 mm, 0.10 mm, and 0.15 mm) and boundary condition 85°C/85%R.H. is applied at the edge of the EVA encapsulant (Total thickness: 0.60 mm; Single layer thickness: 0.30 mm). In a typical PV module, a silicon wafer of dimensions 156 x 156 x 0.2 mm is sandwiched between two layers of the encapsulant. The Si wafer in this study is located at the horizontal centre line of the Glass-Glass PV module. So, moisture diffusion occurs mainly from the module edge towards the centre of the Si wafer along the horizontal centre line and the moisture diffusion from the vertical direction becomes negligible.

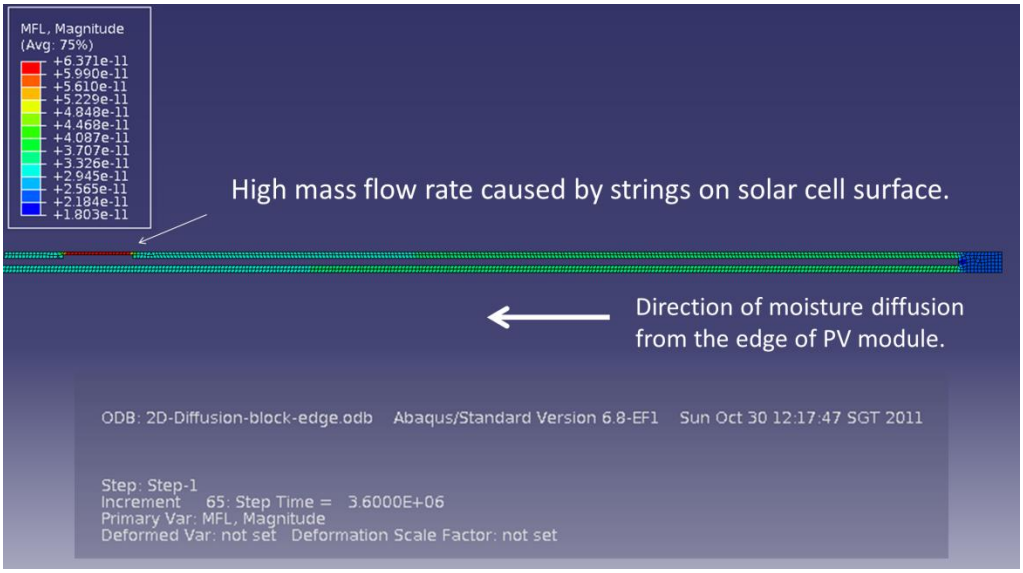

Fig. 16. Contour plot of mass flow rate in encapsulant layers of a Glass-Glass Si wafer PV module at a 30mm region from the edge of the module after Damp Heat 85°C/85%R.H. for 1000 hours. The string on Si wafer exhibits a blocking effect in retarding moisture diffusion towards wafer centre region.

Figure 16 plots mass flow rate in the encapsulant layer after 1000 hours of test. The region of encapsulant above metal string on silicon wafer reveals high mass flow rate as the string narrows the thickness of the encapsulant layer and plays a blocking effect in moisture diffusion. Normalized moisture concentration decreases with the string thickness increasing (Fig. 17). When the thickness ratio of string/encapsulant (single layer) is changed from 0.1/0.3 to 0.15/0.3, which means a 17% change on structure, the normalized moisture concentration at the centre of Si wafer after 85°C/85%R.H. 1000 hours test is reduced from 38% to 36% which means 5% improvement on moisture ingress. Further increasing the ratio by using a thicker string or using a thinner encapsulant is expected to gain more improvement in blocking moisture penetration from the edges of PV module. Adjusting the thicknesses of strings, silver finger, and/or encapsulants could be a convenient way against moisture ingress for Glass-Glass modules as well as Glass-Backsheet modules because the concept of blocking moisture is applicable for both types.

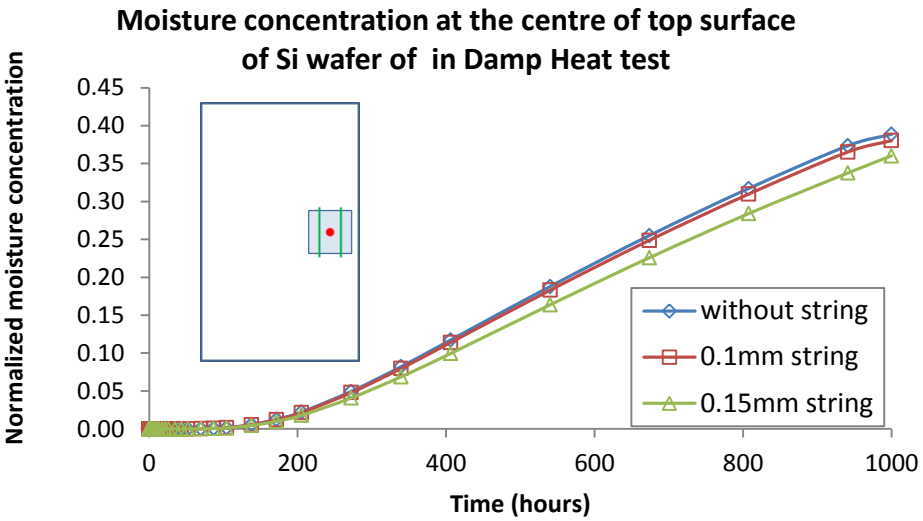

Fig. 17. Normalized moisture concentration C/Csat at the centre of top surface of the Si wafer near the edge of a Glass-Glass Si wafer PV module in Damp Heat test. The Si wafer is located along the horizontal centre line of the module.

3.8 Conclusions

The study [79] showed FEA simulations on moisture diffusion in a crystalline silicon PV module with certain assumptions for understanding moisture ingress process under different conditions. The following summary lists the findings in this study:

Because of the impermeable nature of front glass and Si wafer, moisture ingress in top EVA layer of Si wafer of a Glass-Backsheet PV module was found much slower than that in bottom EVA layer in both Damp Heat and outdoor tests. In Damp Heat test simulation, most of Si wafer bottom surface reached saturation fast while the normalized moisture concentration C/C_{sat} at the Top/Centre region of Si wafer was only about half of that at the Bottom/Centre region after the test. As moisture concentration is an important factor in corrosion, the result indicates different corrosion rates exist at different locations of Si wafer solar cell. The “blocking effect” of Si wafer significantly retarded moisture ingress to the top surface of the wafer. Other structural factor such as the thickness of metal string in a Si wafer Glass-Glass PV module also showed the similar “blocking” effect. The blocking effect deserves

further study for PV module design. For thin-film type PV module, the lack of such "blocking" effect would cause relatively rapid moisture diffusion from backsheet/ encapsulant to thin-film solar cell, which would eventually influence degradation rate of such type PV module.

The study also demonstrated another effect in Outdoor applications of PV module – "Breathable". The direction of moisture diffusion follows the gradient of moisture concentrations inside PV module and the process can be modelled by Fick's diffusion law. In the study, when boundary condition changed in that the ambient relative humidity is high during the night and becomes lower during the day, moisture absorption and desorption were found occurring alternatively during the night and day. Because of the effect, the centre region of top surface of Si wafer remains dry as shown in the outdoor test simulation result because moisture absorbed during the night gets desorbed during the day. For the other three selected locations of Si wafer, moisture concentrations become "stable" after 5 days of outdoor application while their concentrations are much higher than that at the centre region of top surface of Si wafer.

Other structural effects were revealed in the study by studying moisture concentrations at the bottom of Si wafer in outdoor application. Compared with thick TPT backsheet, thin TPT backsheet exhibited stronger "breathable" effect in that moisture absorption and desorption occurred faster. The implication is that thin TPT backsheet eases moisture escaping during the day but it allows more moisture absorption during the night. Thus backsheet selection needs to take this effect into consideration.

The comparison simulation of EVA encapsulant and ionomer encapsulant in Damp Heat test showed ionomer is a good material in mitigating moisture ingress into PV modules.

Also, the study disclosed the ratios of total moisture amount absorbed in accelerated stressing test (Damp Heat 85°C/85%R.H.) and in outdoor application under Singapore weather conditions, respectively. Compared with outdoor test, it shows the accelerated test gives 3~5 times moisture dose at Bottom/Centre, Bottom/Edge and Top/Edge regions of Si wafer Glass-Backsheet PV module and gives about 370,000 more dose at Top/Centre region of silicon wafer. The difference in moisture dose needs to be taken into consideration for developing accelerated stressing test for accelerated test.

CHAPTER 4

PV MODULE STRESSING TESTS

4.1 Ten types of commercial PV modules in the study

Ten types of commercially available PV modules from mass-production lines were selected (Table 4) from world-leading PV module companies in Germany, USA, Japan, and China for durability and performance tests to compare their performance and understand their weakness. For each module type, ten modules were obtained and each test sequence was allocated with one module. All the modules are from mass production line and bear manufacturers' quality certificate. All of them have front glass as superstrate for sunlight passing through to reach thin-film type or silicon wafer solar cells. They also have backsheet or back glass at the bottom of PV modules, and encapsulant to encapsulate solar cells with front glass/backsheet or back glass. Eight types of them have aluminium edge frame with edge-sealing tape/rubber/ adhesive at module edge region to enhance module mechanical strength as well as prevent module ingress from module edge, while 2 types of them adopt frameless design in that mechanical strength is ensured by front glass and back glass (Glass-Glass) structure. The No. 9 module is a Building Integrated Photovoltaic (BIPV) module with thick front glass and back glass to be applied as wall/roof/etc in a building. Mono-Si and mono-Si BIPV are with the same silicon wafer (mono-crystalline) while the wafers of the BIPV module are sparsely located. Back-contact mono-Si module has no metallization on top of Si wafer as all interconnects are at the back of wafers. The last module belongs to silicon wafer module type but its wafers have heterojunction with intrinsic thin amorphous silicon layer for cell efficiency improvement.

The three a-Si based thin-film modules are a-Si, micromorph tandem and a-Si/a-Si tandem. The thin-film structure of the latter two modules are in a stacking structure (known as "tandem") with microcrystalline Si on amorphous Si, and amorphous Si on amorphous Si, respectively. The remaining two thin-film modules (CdTe and CIGS) have their own stacking structure at thin-film layer. Table 4 lists main features of the modules and the details could be found with their manufacturers/internets. The photos of these modules are shown in Figs. 18 to 27.

Table 4. Ten types of commercially available PV modules under tests.

Types of PV Modules (Note: *"§" – Back glass; "f" – Frameless)*	**Power (W) Efficiency (%)**	**Length/ Width/ Thickness (mm)**
Cadmium telluride, (CdTe) [§ f]	75 W 10.4%	1200/600/6.8
Amorphous silicon, (a-Si)	60 W 6.3%	990/ 960/40
Tandem micromorph silicon, (micromorph-Si)	90 W 8.5%	1129/934/46
Tandem amorphous silicon, (a-Si/a-Si tandem)	95 W 6.2%	1308/1108/50
Copper Indium Gallium Selenide, (CIGS) [§]	70 W 9.2%	1235/641/35
Back-contact monocrystalline silicon, (mono-Si back-contact)	95 W 20.7%	1037/527/46
Monocrystalline silicon, (mono-Si)	180 W 14.1%	1581/809/40
Monocrystalline silicon, (mono-Si BIPV) [§ f]	170 W 10.0%	1795/950/12
Multicrystalline silicon, (multi-Si)	230 W 14.1%	1650/992/46
Monocrystalline Si amorphous Si heterojunction, (mono-Si a-Si hetero.)	210 W 16.7%	1580/812/35

Fig. 18. Photos of a-Si PV module. Size: 990 x 960 x 40 mm. Glass-Backsheet structure with frame and thick edge sealing rubber.

Fig. 19. Photos of CdTe PV module. Size: 1200 x 600 x 6.8 mm. Glass-Glass structure without frame but with edge sealant.

Fig. 20. Photos of a-Si/a-Si tandem PV module. Size: 1308 x 1108 x 50 mm. Glass-Backsheet structure with frame and edge sealing tape.

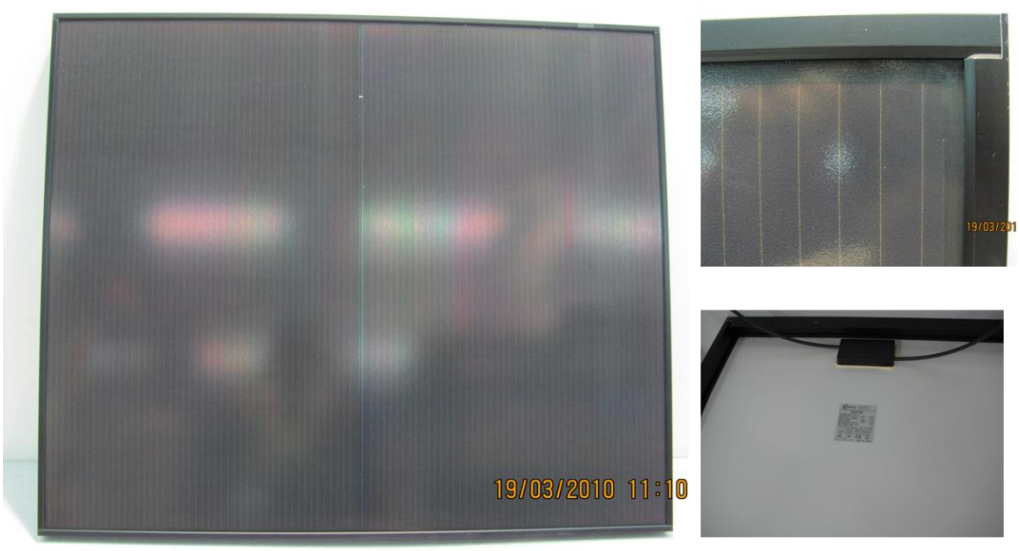

Fig. 21. Photos of micromorph PV module. Size: 1129 x 934 x 46 mm. Glass-Backsheet structure with frame and edge sealing tape.

Fig. 22. Photos of CIGS PV module. Size: 1235 x 641 x 35 mm. Glass-Glass structure with frame and edge sealant.

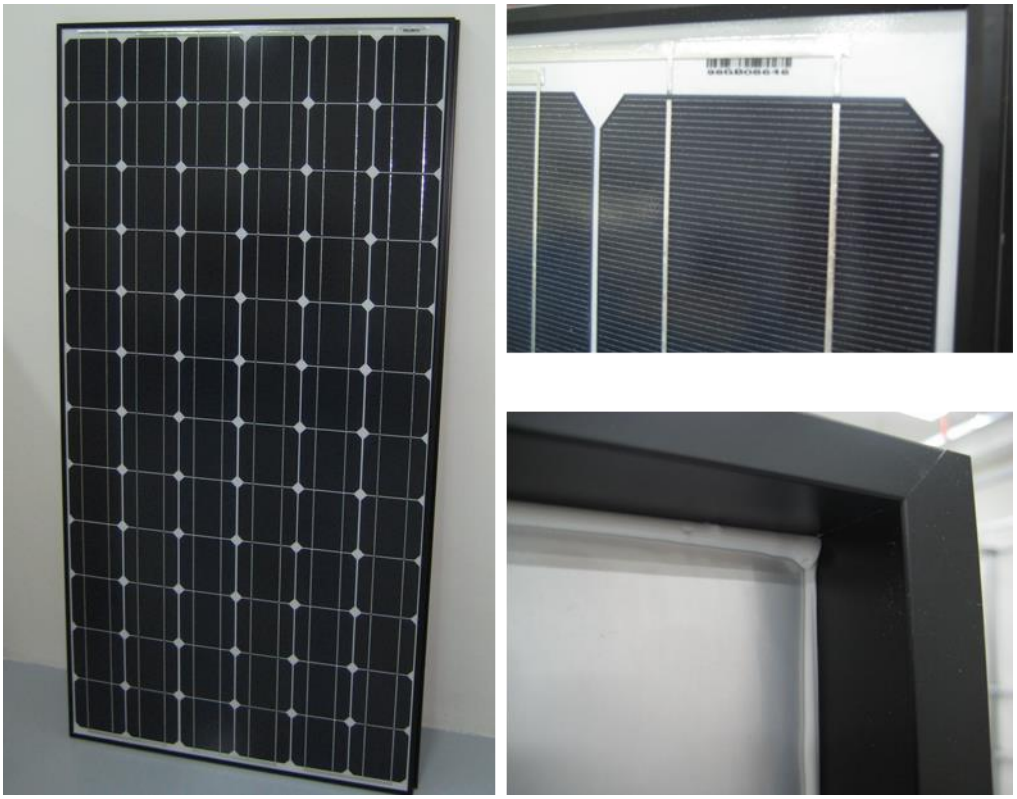

Fig. 23. Photos of mono-Si/a-Si heterojunction PV module. Size: 1580 x 812 x 35 mm. Glass-Backsheet structure with frame and edge sealing adhesive.

Fig. 24. Photos of multi-Si PV module. Size: 1650 x 992 x 46 mm. Glass-Backsheet structure with frame and edge sealing adhesive.

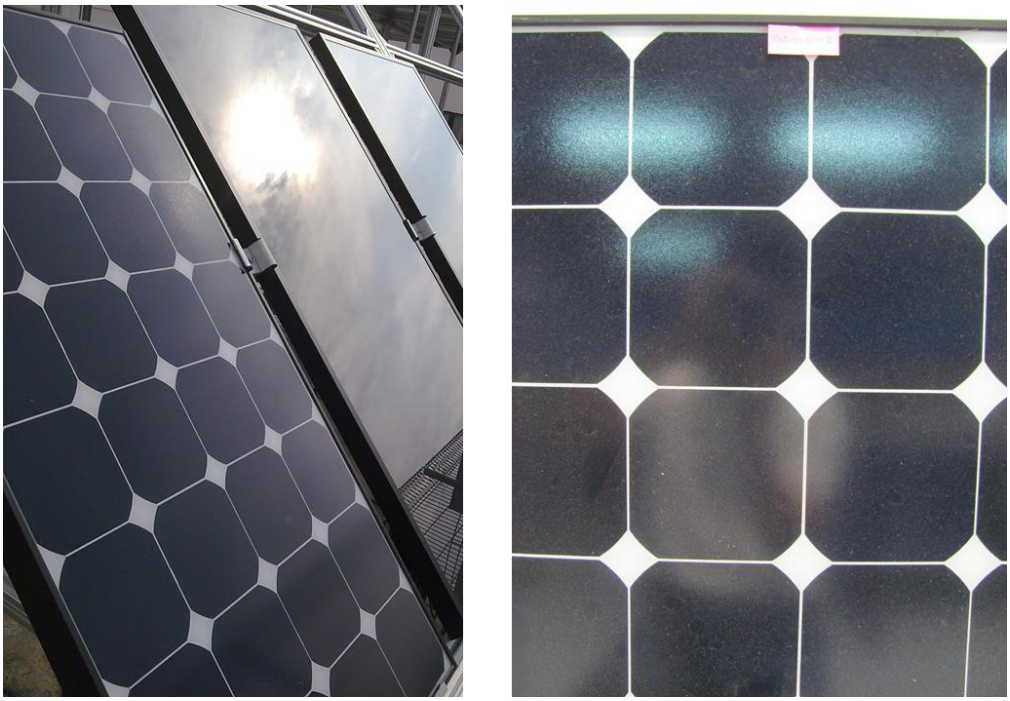

Fig. 25. Photos of back-contact mono-Si PV module. Size: 1037 x 527 x 46 mm. Glass-Backsheet structure with frame and edge sealing adhesive.

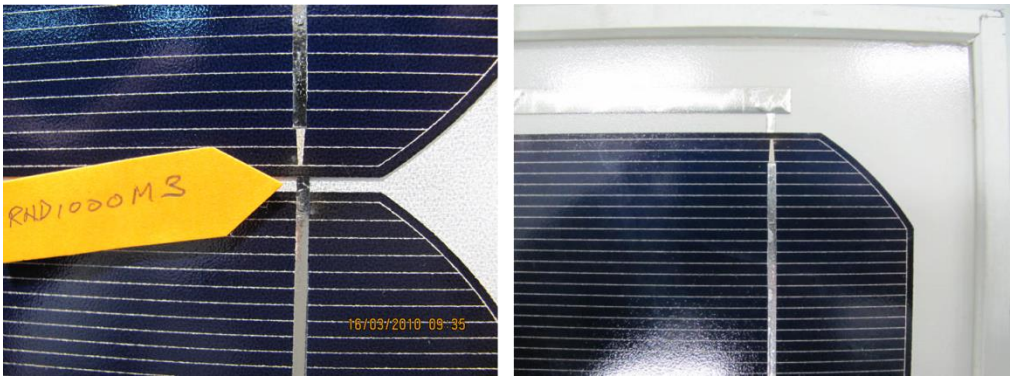

Fig. 26. Photos of mono-Si PV module. Size: 1581 x 809 x 40 mm. Glass-Backsheet structure with frame and edge sealing adhesive.

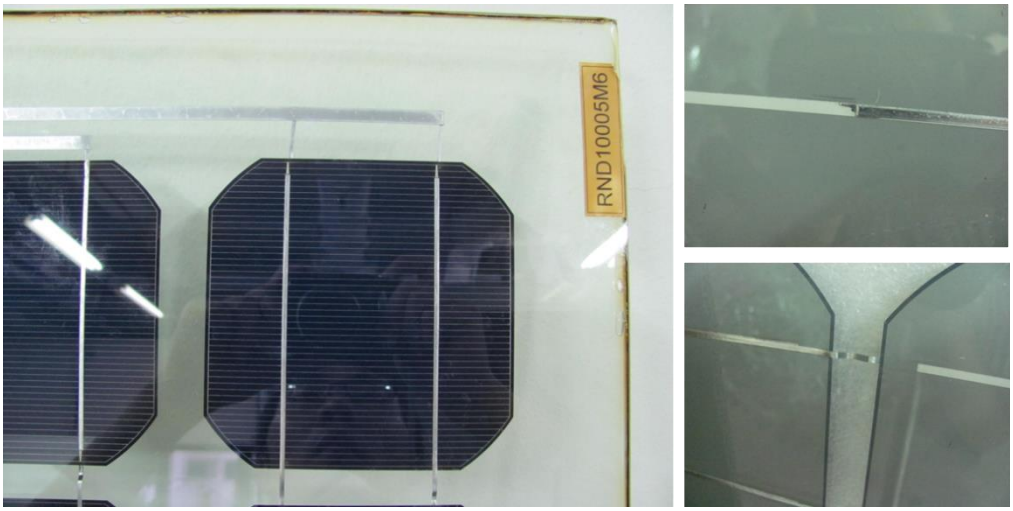

Fig. 27. Photos of mono-Si BIPV module. Size: 1795 x 950 x 12 mm. Glass-Glass structure without frame. Wafers are sparsely located to allow light to pass through the gaps between wafers.

4.2 Test plan and PV module performance assessment

The modules were exposed outdoors in open-circuit mode for 5 days as a pre-conditioning step to overcome initial light-induced degradation issues. Then, they were subjected to different characterization and accelerated stress tests specified in IEC standard 61215/61646 and also tightened stress tests with high stress acceleration factors and/or specific test conditions. For each test sequence, one panel of each PV module type was used. Module power after each test or each test sequence was tested with an IV curve flashing test system (better than Class ‘A” standard) at Standard

Test Condition (STC) – Irradiance 1000 W/m^2 and module temperature 25^{0}C (except for certain tests requiring different irradiance or temperature, e.g. performance at NOCT) in the PVPA unit of SERIS. A PT100 thermal sensor was attached at the back surface of the PV modules and the flasher was turned on when module temperature reached 25°C.

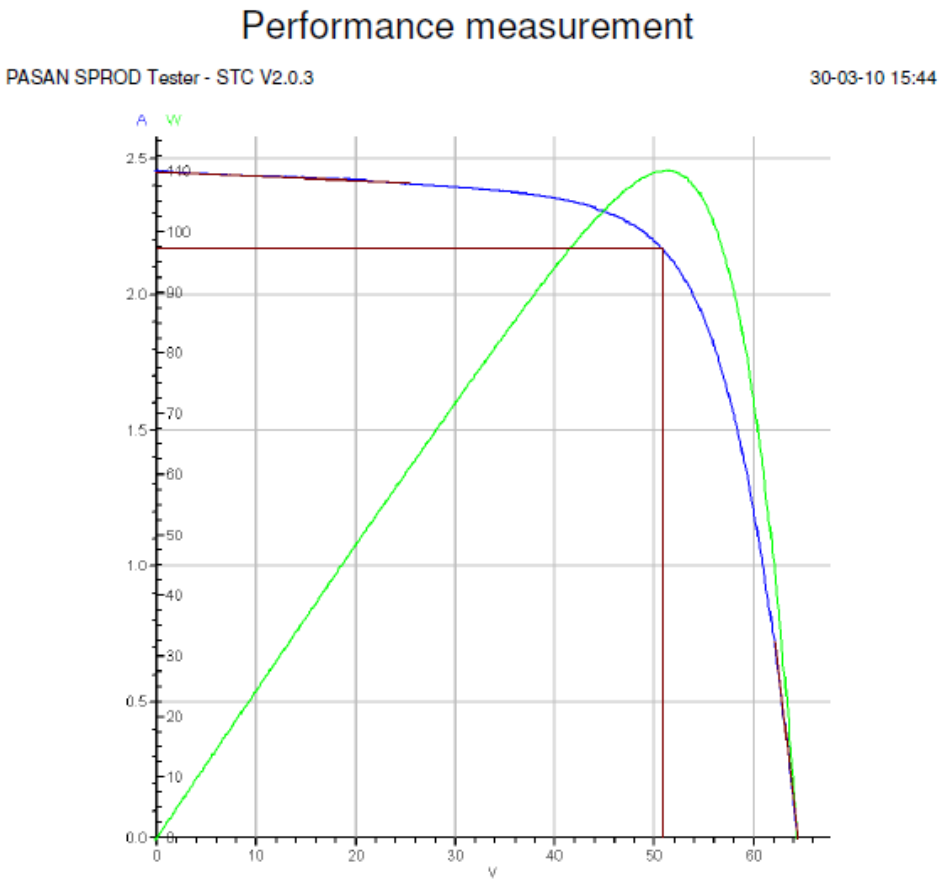

Measurement Data (Temp. compensated results)

PASAN Tester version	2.0.3		Operator	LOI	
Module ID Code	RND09004M5		Serial number		
Standard temperature	25.0	℃	Monitor Cell	OF 09-0663-1	
Mean Irradiance	0.999	kW/m²	Calibration Value	131.7	mV/(kW/m²)
Module Temp.	25.0	℃	Mon. Cell Temp.	24.1	℃
Mask	No Mask 1.000	-	Cell Area	109.5	cm²
Module Area	10509.0	cm²	Cells in Parallel	1	
Cells in Series	96		Isc	2.4523	A
Voc	64.40	V	Imp	2.1672	A
Vmp	50.83	V	Pmax	110.16	W
Reference vlt 1	0.00	V	Reference vlt 2	0.00	V
Power ar ref 1	-1.00	W	Power ar ref 2	-1.00	W
Current at ref 1	0.0000	A	Current at ref 2	0.0000	A
Fill Factor	69.7	%	Cell Efficiency	10.5	%
Module Efficiency	10.5	%	Shunt res.	600.92	Ohm
Serie res.	3.253	Ohm			

Fig. 28. An IV curve measured for a micromorph PV module by the flashing test system in PVPA of SERIS.

Figure 28 shows an IV curve measured by the flashing tester for a micromorph PV module. For thin-film modules, module powers post-test were obtained after further light-soaking to minimize the light-induced instability issue [7,15,80] and final power values were used for performance comparison in this study. All tests strictly meet IEC requirements from test conditions, module cleanliness, module handling, etc to minimize variations. To ensure the accuracy of the assessment, module surface cleaning was conducted to remove dust or contaminants from the cover glass surfaces before each IV measurement. Important parameters of the IV curve were obtained from the module flashing tests, e.g. maximum power point MPP (P_{max}), open-circuit voltage (V_{oc}), short-circuit current (I_{sc}), fill factor (FF), series resistance (R_s) and shunt resistance (R_{sh}).

4.3 Standard stress tests (Humidity Freeze, Thermal Cycling, Damp Heat)

Table 5 lists test sequences of the stress tests carried out in this study, which follows the IEC61215/61646 standard. For each test sequence, one module of each type was allocated. Performance assessments were done at STC at various test points.

Table 5. Test sequences of accelerated stress tests.

Humidity Freeze	**Thermal Cycling**	**Damp Heat**
Performance assessment	Performance assessment	Performance assessment
Preconditioning	Preconditioning	Preconditioning
Performance assessment	Performance assessment	Performance assessment
UV 15 kWh/m^2	Thermal cycling 200 cycles (85^{0}C to -40^{0}C)	Damp Heat 1000 hours (85^{0}C/85%R.H.)
Performance assessment		
Thermal cycling 50 cycles (85^{0}C to -40^{0}C)		
Performance assessment		
Humidity freeze 10 cycles (85^{0}C/85%R.H. to -40^{0}C)		
Light soaking (Thin-film modules only)	Light soaking (Thin-film modules only)	Light soaking (Thin-film modules only)
Performance assessment	Performance assessment	Performance assessment

A preconditioning exposure was done outdoors in open-circuit mode for 5 days to stabilize the PV modules. The modules were then subjected to specific accelerated stress tests. Final performance assessment at STC was done after the tests. Humidity freeze, thermal cycling and Damp Heat tests were done in multi-purpose climate chambers with the specified test parameters. UV 15 kWh/m^2 (UVB dose ~5%) was done in a special UV preconditioning chamber at 60^{0}C module temperature. Module powers were tested with the IV curve flashing tester at STC at different test points as shown in Table 5. For thin-film modules, module powers post-test were obtained after a further 5 days of outdoor light-soaking to mitigate the instability issue and the final power values were used for performance comparison in this study.

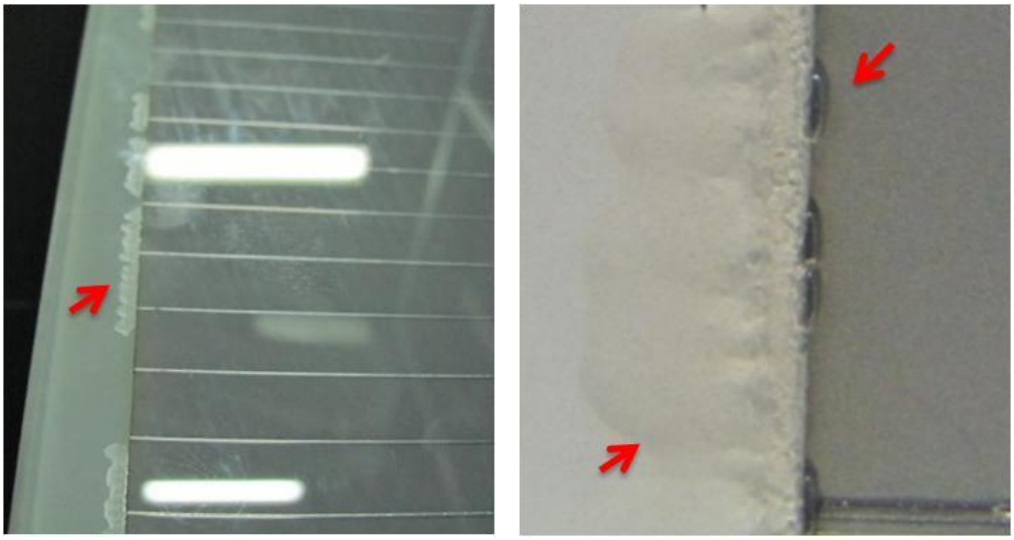

Fig. 29. Delamination and blisters at edge-sealant region of CdTe module after Damp Heat 85/85 test (Viewing from the back of the module). Right photo (amplified).

Various visual defects were found after the tests (e.g. adhesive yellowing, blistering, glass surface deterioration) which indicate weaknesses of the PV modules. Figure 29 shows the edge sealant region of the CdTe module after Damp Heat 85/85 test. The back glass shows partial delamination from edge sealant layer and there were a number of blisters emerging at various locations inside PV module. The deterioration of the front glass surface after moisture-involved tests (Humidity Freeze and Damp

Heat) was observed and it became more obvious after the tightened stress tests (e.g. Damp Heat 90/90).

Figure 30 plots the normalized power (normalized by module power at pre-conditioning) after the three main stress test series. All these modules show power variations within ±5% after all the tests. Degradation rates of the modules were summarized and compared at the end of this study. Also, the normalized powers after the three stress tests were averaged for ranking purposes to compare different PV technologies. From Fig.30, it can be seen that a-Si, mono-Si BIPV, mono-Si, and multi-Si performed relatively better than the other modules.

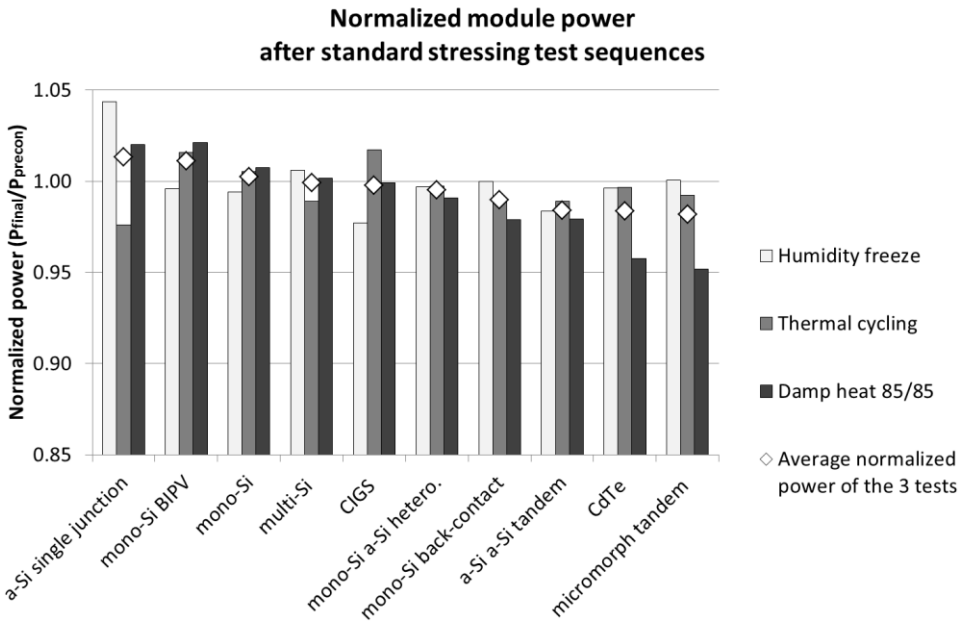

Fig. 30. Module efficiency after standard stress test series (Thermal Cycling 200 cycles, Humidity Freeze 10 cycles, and Damp Heat 85/85 1000 hours) normalized by their efficiency prior to the stressing.

4.4 Tightened stress test (Damp Heat 90/90)

In order to further differentiate the modules, a tightened test (Damp Heat 90/90) was conducted with the following test conditions: Damp Heat 1000 hours (90^0C/ 90%R.H.). For thin-film modules, module powers post-test were obtained after a

further 5 days of outdoor light-soaking to mitigate the instability issue and the final power values were used for performance comparison in this study.

The increased temperature and humidity level were meant to bring a more stringent stressing environment to the PV modules. The Damp Heat 90/90 test was conducted in the same way as Damp Heat 85/85 mentioned in previous section except that the humidity and temperature were increased in the chamber.

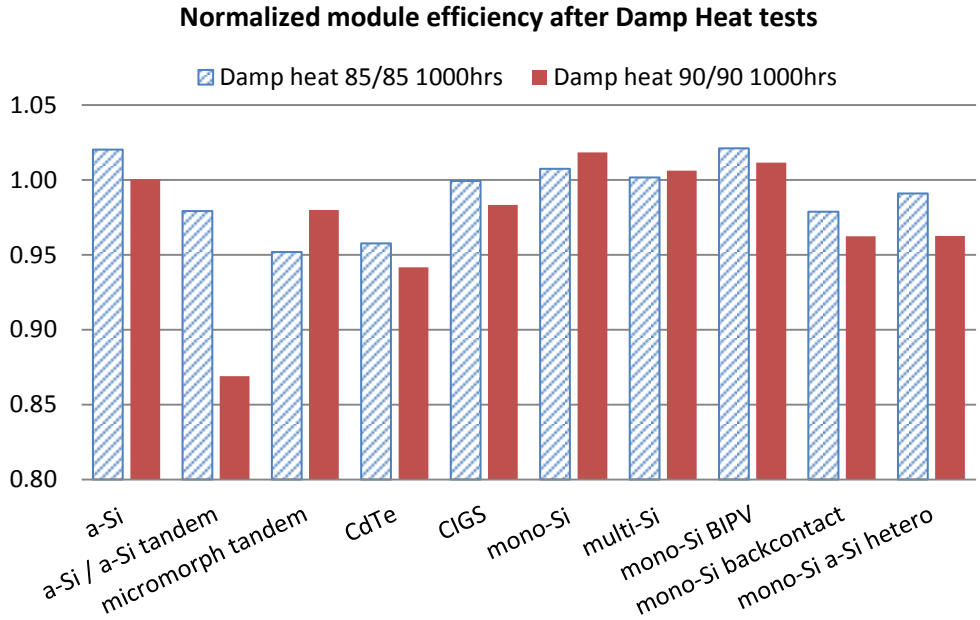

Fig. 31. Module efficiency after Damp Heat tests 85/85 and 90/90, normalized by their efficiency prior to the stressing.

Figure 31 compares the two Damp Heat tests for the PV modules. The more stringent condition results in more severe degradation in most modules. Moisture diffusion in polymeric materials (encapsulant, backsheet, edge sealant, etc) becomes faster as temperature increases diffusivity. The higher temperature should also increase reaction rate of corrosion. The moisture concentration inside the PV modules was also increased with higher moisture content in test environment which means more H_2O molecules for corrosion reactions. The degradation rates of these modules in the two test conditions are summarized and compared in this thesis. Interestingly, a-Si, mono-Si BIPV, mono-Si and multi-Si performed well again in the Damp Heat 90/90

test as in the standard stress tests. Such results could be attributed to material properties, module structure, and solar cell characteristics. For example, amorphous Si thin-film is susceptible to thermal annealing effect which will be discussed in Section 4.7. For mono-Si BIPV module, the sparsely located wafers are well protected between front glass and back glass and there is a large distance from Si wafer to module edge as shown in Fig. 27. So moisture ingress could only occur from the edge of the module and it will take longer time for moisture to reach the centre of the top of the Si wafers. Although CdTe and CIGS module are also in Glass-Glass structure, the distance of solar cell to module edge is much shorter. Surface deterioration of front glass (examples shown in Fig. 36) exhibited on mono-Si back-contact, mono-Si/a-Si hetero, and a-Si/a-Si tandem modules could have negative effects on module performance.

4.5 Tightened stress test (Damp Heat 85/85 with 1000 V DC bias)

The electrically-biased Damp Heat test introduces another stress factor into the accelerated test. The test was conducted on PV modules in Damp Heat test condition with additional electrical bias voltage between module frame and its active circuit. Such a bias condition can be faced in actual applications. As PV modules were connected in series and in parallel in PV arrays, the voltage potential of active circuit of the last module in serial-connected PV module chains can be very high as module frames (usually aluminium material) needs to be grounded for safety requirements. Such configuration results in a huge potential difference. It was reported that the biased Damp Heat test revealed some similar degradation phenomena encountered in field application such as Transparent Conductive Oxide (TCO) corrosion for thin-film PV modules. The failure mechanism was not well understood but it was reported to be caused by electro-chemical corrosion associated with sodium ion migration and moisture ingress. Some tests on thin-film modules exhibited the electro-chemical

corrosion phenomenon at the TCO layers under high voltage bias conditions (e.g. 600 V DC from module frame to active circuit) [19]. Back-contact silicon PV module was also reported with polarization issues which are associated with bias voltage from active circuit to module frame that resulted in module power output through a surface charging effect [81].

In this study [82], a higher DC bias voltage 1000 V was applied in the Damp Heat 85/85 tests with two different polarity settings for thin-film modules and Si wafer modules to observe the behaviours of PV modules under such high bias voltage conditions. For each type of module, one module each was used for a positive bias Damp Heat test and a negative bias Damp Heat test. For the frameless modules, an aluminium foil (about 30 mm wide) is wrapped along the module edges to "create" a pseudo frame connecting with one terminal of the high voltage power supply. The bias Damp Heat test was conducted in a dark multi-purpose climate chamber set at 85°C and 85% relative humidity. Inside the chamber, PV modules were loaded on a rack with non-conductive spacers and their frames/output cables were connected with a multi-channel high voltage power supply. The power supply applied ±1000 V DC bias voltage during the Damp Heat test for each module. In the positive bias test, the "+" terminal of the power supply was connected with the two output cables (shorted together) and the "-" terminal was connected with the module frame; In the negative bias test, the "+" terminal was connected to the module frame and the "-" terminal was connected to the cables of PV module. Test parameters such as voltage and current of each channel are recorded by a computer every minute. The maximum current for each channel was limited to 5mA. Prior to the test, all the modules had experienced outdoor preconditioning (> 5kWh/m^2) in open circuit mode as suggested in IEC61215, and module performance assessment was done after the pre-conditioning. Then the modules were loaded into the climate chamber for the 650 hours biased Damp Heat test. For thin-film modules, outdoor light-soaking was done

again after the Damp Heat test in order to stabilize the modules before the IV curve measurement. Finally module performance assessment was done again to obtain the result after the accelerated stress test.

As shown in Fig. 32, the 1000 V Damp Heat 85/85 tests show apparent differentiation on module performance and the bias polarity was found to be a critical factor. Different defect modes were exhibited after the tests as summarized below.

After the negative bias test, CIGS and CdTe modules totally lost their power output due to internal short circuits developed during the test. The V_{oc} was found also zero for the two modules and the resistance of active circuit between output cables (measured in a dark condition) was found to have dropped by 4-5 orders as compared to their reference modules which were not put through this test. All the above indicates the formation of a serious shunt (Ohmic short) inside the solar cells of the modules. CdTe, a-Si/a-Si tandem, and micromorph modules showed significant delamination at the thin-film layer under their front glass. Such "hair-like" delamination occurred near the frame/peripherals of these thin film modules as shown in Figs. 33 and 34. An interesting finding is that the a-Si module was exempt from this defect mode.

After the positive bias test, most PV modules show white stains on the external surface of front glass as surface deterioration. Also white powdery lumps were shown bridging module frame/peripheral and the surface of the glass, as shown in Figs. 35 and 36, which is believed to be the result of sodium, H^+, OH^- ion migration in the direction of the electric field. Such surface deterioration on the front glass was shown for almost all the modules in the positive bias test but not on any module in the negative bias test. Back-contact mono-Si module showed a large power reduction (~42%) which is consistent with what other studies reported due to a charging effect for this type of PV module.

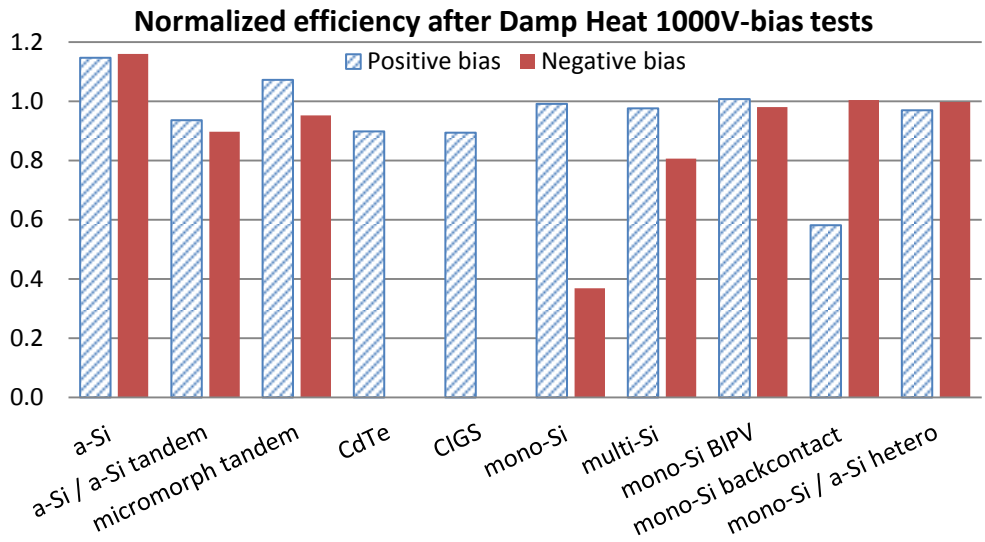

Fig. 32. Module efficiency after bias Damp Heat tests normalized by their efficiency prior to the stressing.

Fig. 33. “Hair-like” delamination at thin-film layer under the front glass of CdTe module after the negative bias Damp Heat 85/85 test.

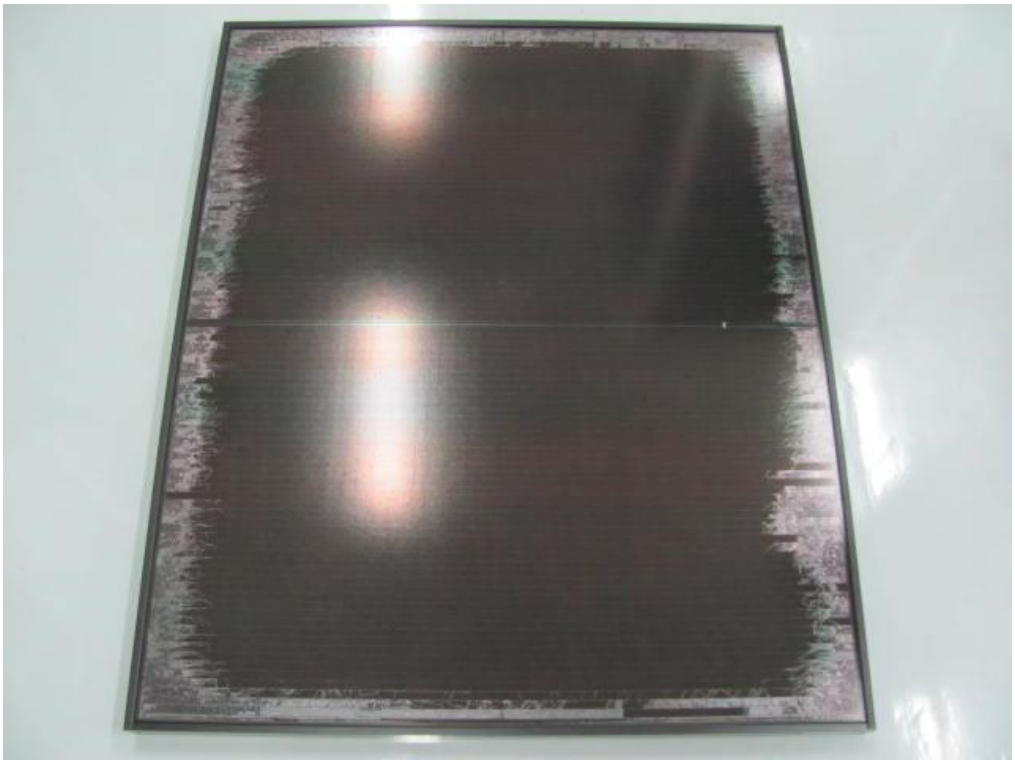

Fig. 34. “Hair-like” delamination along the edge frame of micromorph PV module after the negative bias Damp Heat 85/85 test. The delamination is located at the thin-film layer under the front glass.

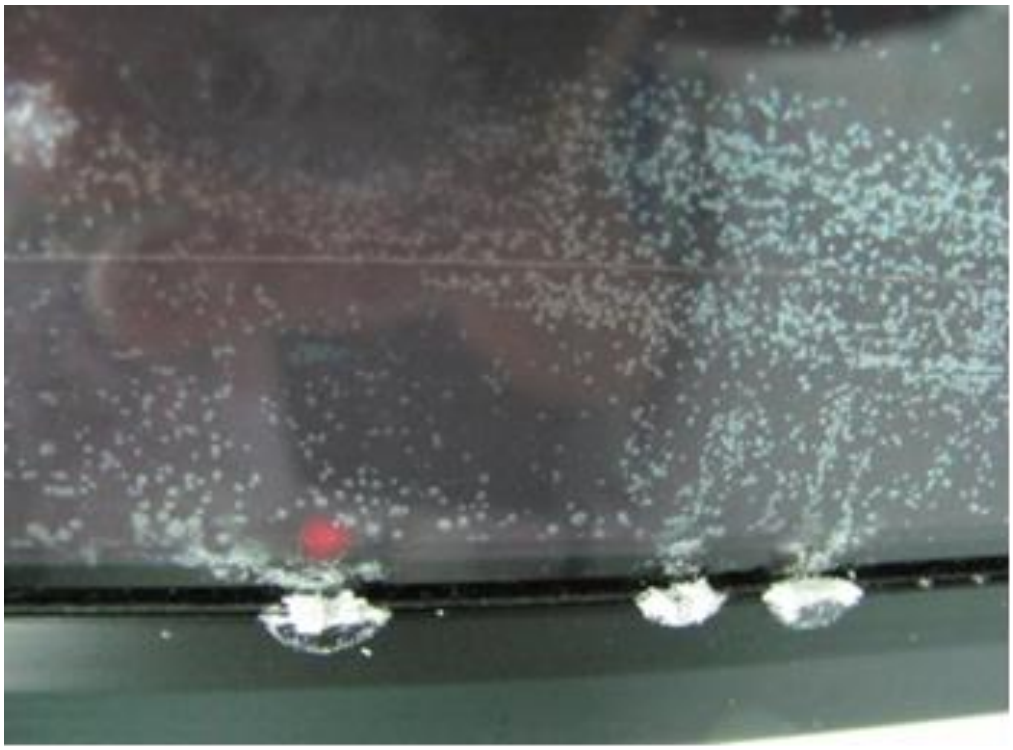

Fig. 35.“Dot-like” delamination at thin-film layer under the front glass of a-Si/a-Si tandem module after the positive-bias Damp Heat 85/85 test; Frame corrosion is also shown.

Fig. 36. Glass surface deterioration of mono-Si backcontact module after the positive bias Damp Heat 85/85 test. White “mist” on front glass and frame corrosion are also shown.

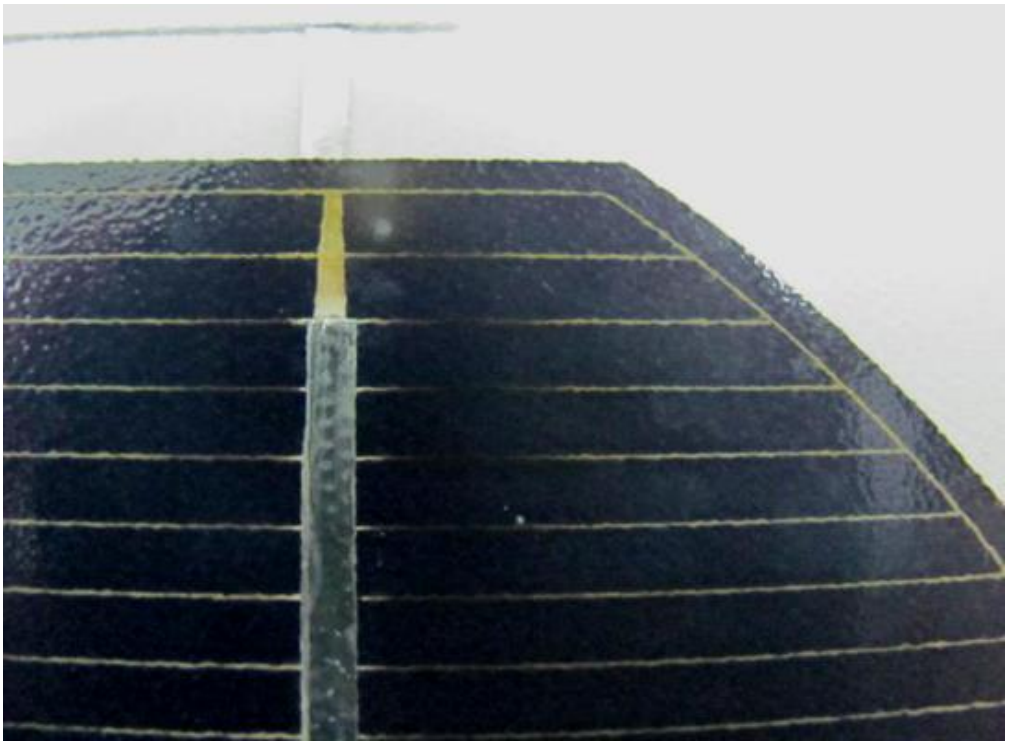

Fig. 37. Discoloration of silver metallization on the solar cell of mono-Si module after the positive bias Damp Heat 85/85 test

Discoloration phenomenon at metal string was shown on two mono-Si modules only at positive bias test. As shown in Fig. 37, the silver metallization turns yellow for the solar cells close to the module frame and the grids beside the tab-string turn darker, which could be the result of silver oxidation caused by electrical chemical corrosion. This effect is similar to the "Snail effect" [83] found for Si-wafer PV modules in field applications where silver metallization got oxidized under the effect of water and Chloride. The phenomenon usually occurs more obviously near the tab-string which could be because of Chlorine migration from flux residue near the tab-strings. One future work could be a further study of different flux or special cleaning process to get rid of the corrosive effect from flux residues.

Table 6. Visual defects after 1000 V 85°C/85%R.H. Damp Heat for 650 hours in positive bias (PB) and negative bias (NB) modes.

Module type *"§" – Back glass; "f" – Frameless*	**Delam. under glass**		**"White Mist" on glass**		**Frame corrosion/ powders**		**Discolour at cell/ metal grid**	
Bias polarity	*PB*	*NB*	*PB*	*NB*	*PB*	*NB*	*PB*	*NB*
a-Si	☐	☐	☐	☐	☒	☐	☐	☐
a-Si/a-Si tandem	☒	☒	☒	☐	☒	☐	☐	☐
micromorph tandem	☐	☒	☒	☐	☒	☐	☐	☐
CdTe *§ f*	☐	☒	☒	☐	☒	☐	☐	☒
CIGS *§*	☒	☐	☒	☐	☒	☐	☐	☐
mono-Si	☐	☐	☒	☐	☒	☐	☒	☐
multi-Si	☐	☐	☒	☐	☒	☐	☐	☐
mono-Si BIPV *§ f*	☐	☐	☒	☐	☒	☐	☒	☐
mono-Si back-contact	☐	☐	☒	☐	☒	☐	☐	☐
mono-Si/a-Si hetero.	☐	☐	☐	☐	☒	☐	☐	☐

The visual defects are summarized in Table 6. After the positive bias test, common defect modes for almost all modules were glass surface deterioration and module frame corrosion. A "milky-white" stain layer emerges on the module glass surface which was found hard to be removed by scrubbing. Energy-dispersive X-ray spectroscopy confirms its content to be the same as normal glass. The layer looks more obvious at the glass surface closer to module frame. Also, all module frames were

found corroded with white powder on the aluminium frame surface. In contrast, the above-mentioned surface deterioration or frame corrosion was never shown for any modules after the negative bias Damp Heat test.

Thin-film module types with TCO layers were known to be degraded under negative bias tests [19], and the mono-Si back-contact module type is known to suffer surface charging issue under positive bias due to its unique back-contact module structure [81]. However it is really surprising to see the standard mono-Si and multi-Si modules suffer efficiency drops of 63% and 19%, respectively, and CdTe and CIGS modules totally lost their power output after negative bias test. The Fraunhofer Centre for Silicon Photovoltaics [84] reported a similar large power reduction for crystalline silicon PV modules and attributed this to sodium ion migration that caused shunts. Seven of nine module types (excluding the mono-Si back-contact module) show the negative bias test causes more efficiency drop as compared to the positive bias test, although the latter test results in glass surface deterioration issue that could affect light transmission. Discoloration of silver metallization, thin-film delamination, and glass surface deterioration are believed to be the result of electro-chemical corrosions.

The mechanisms of efficiency drop could be different among the modules because of the differences in module structure and PV materials. Ion migration is an important factor. Sodium ion (Na^+) was known as a mobile ion from glass [55]. Under high voltage bias and wet/hot test condition, Na^+ migration occurs from the front glass to module frame in positive bias test and the glass surface deterioration is a result of pH value change at glass surface that results in glass corrosion and also aluminium frame corrosion. Under negative bias mode, Na^+ moves from the front glass towards the solar cells. Such bias suppresses the occurrence of surface corrosion for the front glass, however, solar cells receive the mobile Na^+ ions in this case. Thin-film layers could be susceptible to the "attack" of Na^+ ions as the migration could change

material properties. For Si wafer modules, the migration could happen through EVA encapsulation. Besides sodium ion migration, there could be other mobile ions inside the modules that contributed to the efficiency drop problem. A detailed study is necessary to further understand the mechanisms. As most PV modules severely suffer an efficiency drop under biased Damp Heat test conditions and more modules were affected by the negative bias mode as compared to the positive bias mode under the same Damp Heat test conditions, design solutions at the module level and the system level might be worthy of consideration in order to mitigate the impact of this failure mechanism. In this study, it was found that the a-Si thin-film module shows no delamination at the thin-film layer or no degradation in either bias polarity tests, thanks to its thick rubber sealing between edge frame and front glass. The rubber results in a high insulation resistance between the module and its edge frame that minimizes the amplitude of the bias current during the tests as shown in the current monitoring of the tests, which limits the occurrence of thin-film corrosion eventually.

4.6 Tightened stress test (UV exposure 50 kWh/m^2)

Polymeric materials are known to be subjected to UV light degradation. The qualification test standard (IEC61215) specifies the minimum UV dose to assess differences between PV modules. Modules were placed into a UV exposure chamber with 60°C chamber temperature and under UV source between 280 and 385 nm with minimum 5 kWh/m^2 between 280 and 320 nm. In order to further study the performance of PV modules, UV 50 kWh/m^2 is used in this study as a tightened UV test as compared to the UV 15 kWh/m^2 test of the standard IEC test. The test hour of the new test is 3.3 times of that in the original UV test.

Most modules do not show obvious signs of degradation in appearance except a certain degree of “yellowing” in their encapsulant. Figure 38 shows the yellowing issue of the CdTe module at 3 stages (prior to UV test, post 5 kWh/m^2 exposure and

post 50 kWh/m^2 exposure). The module power assessment at STC as shown in Fig. 39 does not reveal the increased UV exposure time would cause more module power degradation. However, Si wafer based modules all show relatively more stable performance as compared to thin-film modules. One reason of instability for amorphous silicon-based modules is discussed in the following section.

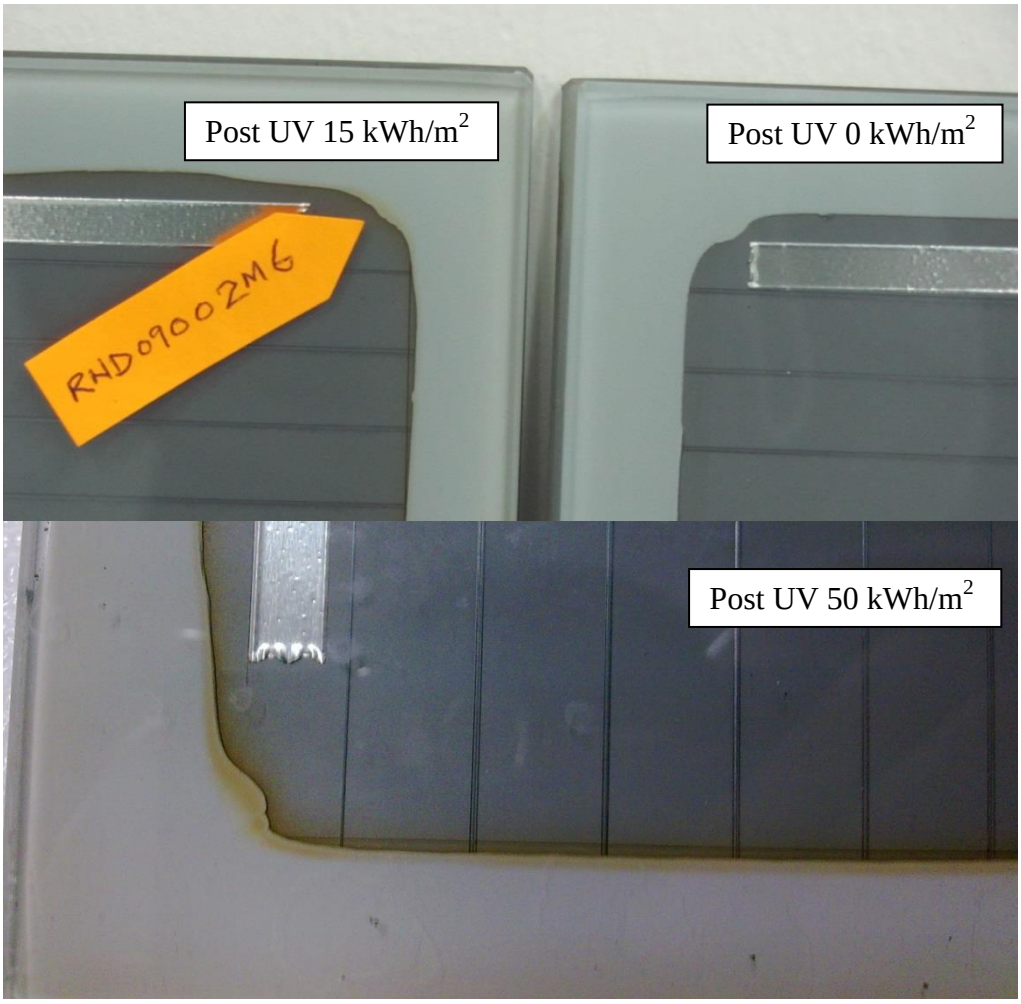

Fig. 38. CdTe PV module shows yellowish colour at the edge sealant region (viewed from the back of the modules) post the UV test. The yellowish colour becomes more obvious with extended UV test duration.

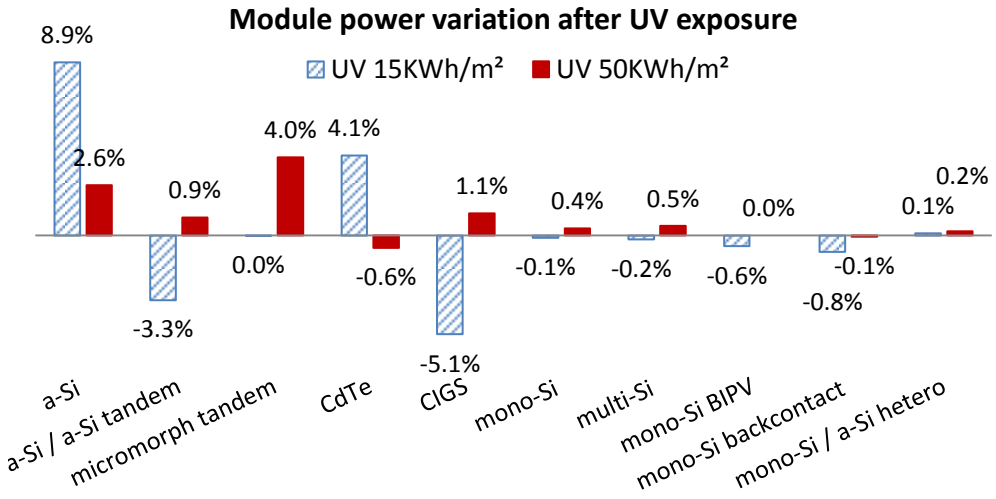

Fig. 39. Module power variation after UV 15 kWh/m^2 and UV 50 kWh/m^2 tests.

4.7 Study of instability of thin-film modules

A light-soaking test was conducted for thin-film modules to assess their stability in a light soaking chamber with simulated sunlight source in the PVPA Unit of SERIS. After certain hours of light soaking, PV modules were measured at STC with an IV curve flashing tester. The total degradation percentages for the three a-Si based modules were about 19%, 14%, and 12% (Fig. 40). The amorphous-Si single-junction module suffered the most serious degradation induced by sunlight, which could be because its amorphous-Si layer is thick, which is usually done by PV module manufacturers in order to harvest solar energy better and achieve higher efficiency as a compensation for the poorer light absorption coefficient of amorphous Si material. Thin-film silicon modules are known to have an instability issue caused by light-induced degradation and the degradation can be reversed by annealing above 150°C for a few hours (Staebler & Wronski effect, SWE) [80]. The CIGS module also displayed a similar degradation induced by light with 10% maximum power degradation, however, the CdTe module exhibited a power gain phenomenon (+6%) after light soaking. The different responses to the light soaking test may be attributed

to the different characteristics of the CdTe and CIGS thin-film materials as compared to the three amorphous-silicon-based thin-film materials.

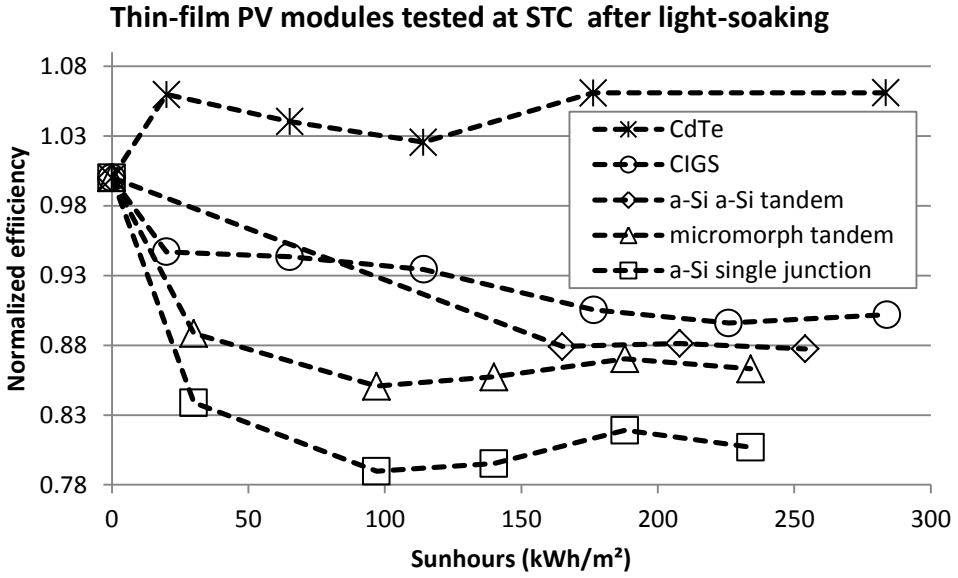

Fig. 40. Module efficiency at different test points of light-soaking test, normalized by their initial efficiency.

To further study SWE effect of thin-film Si modules, a thermal annealing test was conducted for the three amorphous Si-based thin-film modules as well as two other reference modules (CdTe thin-film module and mono-Si/a-Si hetero module). After the performance assessment post the last test points of the stress tests, the modules were baked for 96 hours in 65°C and 85°C, respectively. As shown in Fig. 41, the Si wafer module (mono-Si/a-Si hetero) shows almost no change with thermal annealing, while the thin-film modules exhibit obvious variations as a result of the annealing. The thermal annealing results in the power gain phenomenon for all the 3 amorphous Si-based PV modules. A higher annealing temperature (85°C) gave a stronger annealing effect as compared to 65°C. For the CdTe module, thermal annealing had an inverse effect in that the module power dropped after the heating. A higher annealing temperature appeared to cause less power degradation for CdTe.

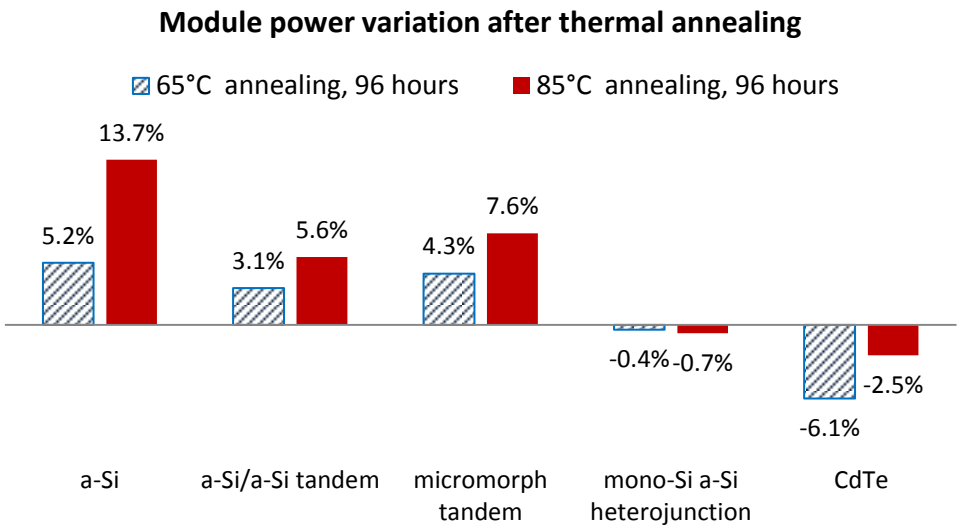

Fig. 41. Module power variation after thermal annealing. A higher annealing temperature generally leads to an increase in power for a-Si based modules.

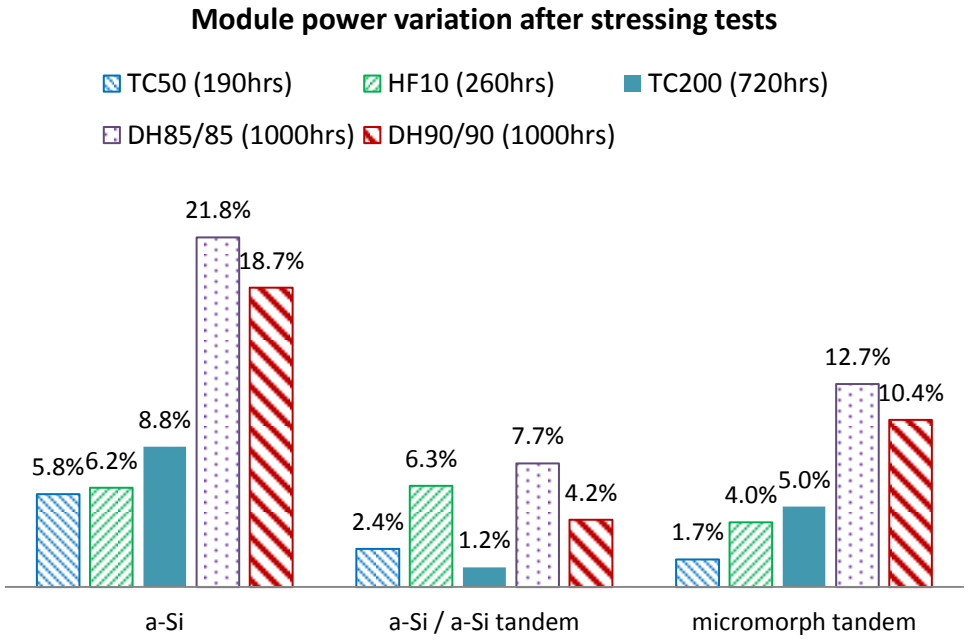

Fig. 42. Module power variation after stress tests to show the effect of thermal annealing on a-Si based modules. The duration above 50°C are shown for these tests. Longer heating times generally lead to more power gain due to thermal annealing effect.

Figure 42 summarizes module power variation percentages for the three amorphous Si-based PV modules after different stress tests without additional outdoor light soaking stabilization post the relevant stress tests. The time above 50°C was

calculated for each test. The module power increasing shows thermal annealing plays a stronger effect than the stressing in these tests. The power increasing due to thermal annealing effect in these tests generally becomes larger with the increasing heat time (above 50°C) in these tests. The result proves the effect of thermal annealing for thin-film Si modules. In order to overcome the effect from thermal annealing and assess module performance change due to accelerated stressing (e.g. moisture ingress), that is why additional light soaking in outdoor open-circuit mode was conducted after these stress tests in this study to stabilize the modules first before their performance assessment at relevant test points defined in their stress test sequences.

4.8 Analysis of IV curve parameters on power degradation

In the section, the IV curve parameters were analyzed to underdstand the relationship between IV curve parameters and module power output. It is known that V_{oc} reduction could be due to bandgap decreasing or shunt problem at the semiconductor materials of solar cells. EVA yellowing or the reduction of light transmission usually result in the reduction of the current so the effects can be shown on the variation of I_{sc}. Series resistance R_s relates to the continuity of solar cell circuit and the resistance of conductors. R_s increasing could be due to interconnect degradation that increases contact resistance. Corrosion and solder joint problem (e.g. fatigue, crack, hot spot) can cause R_s increasing too. When shunt happens, parrallel resistance R_{sh} decreases. Fill Factor (FF) variation can be associated to the influences of the parameters $V_{oc,}$ I_{sc}, R_s and $R_{sh.}$.

The effects of the IV curve parameters on module power were plotted in the scatter plots of Figs. 43 to 47. All the relevant parameters and module powers were taken from the result of test sequences of Damp Heat 85/85, Damp Heat 90/90, Thermal Cycling 200, and Humidity Freeze 10 test series. The gradients of the curves of linear regression show that V_{oc}, followed by I_{sc}, FF, R_s and R_{sh}, plays as the number one

significant factor that influences module power at maximum power point (MPP). Hence design improvement on avoiding V_{oc} degradation should be taken into consideration as top priority for PV module durability.

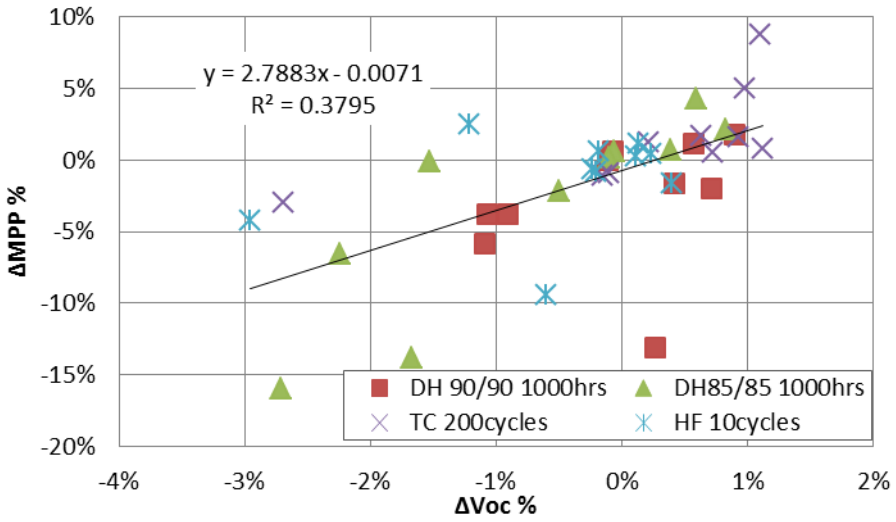

Fig. 43. Interaction graph of V_{oc} and MPP variations after stress tests.

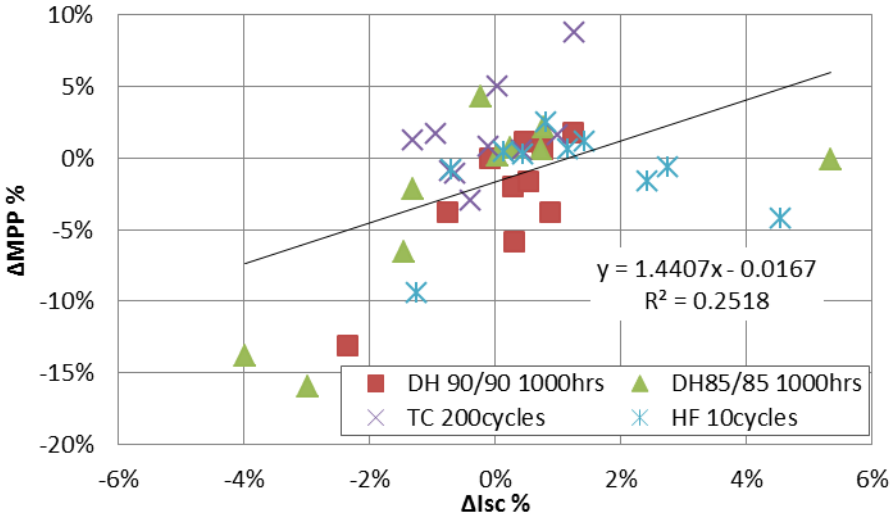

Fig. 44. Interaction graph of I_{sc} and MPP variations after stress tests.

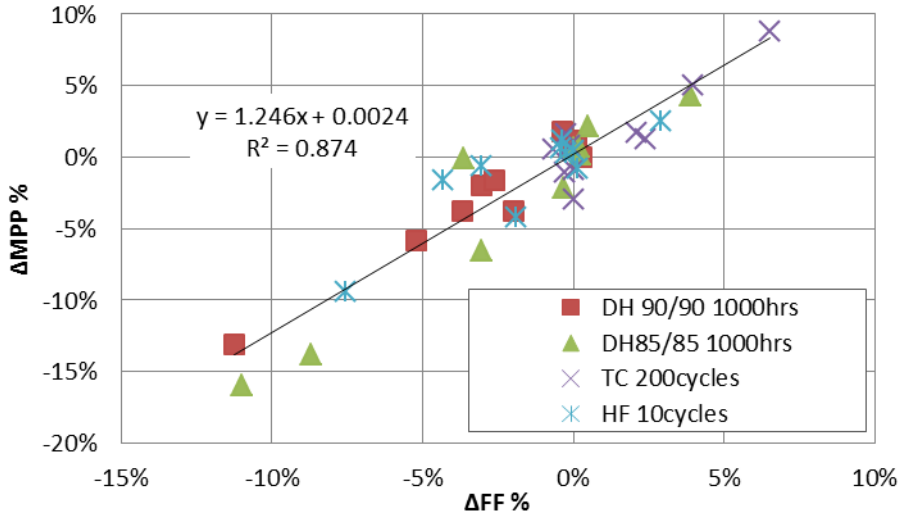

Fig. 45. Interaction graph of FF and MPP variations after stress tests.

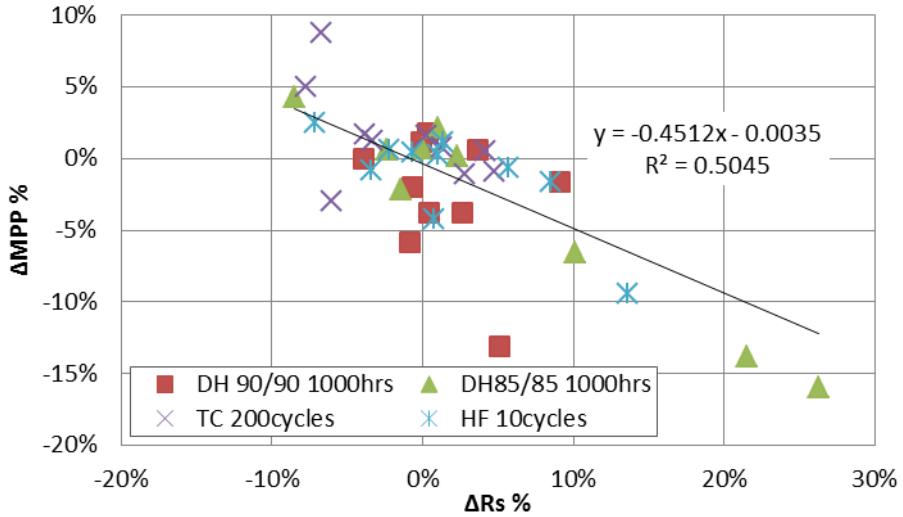

Fig. 46. Interaction graph of R_s and MPP variations after stress tests.

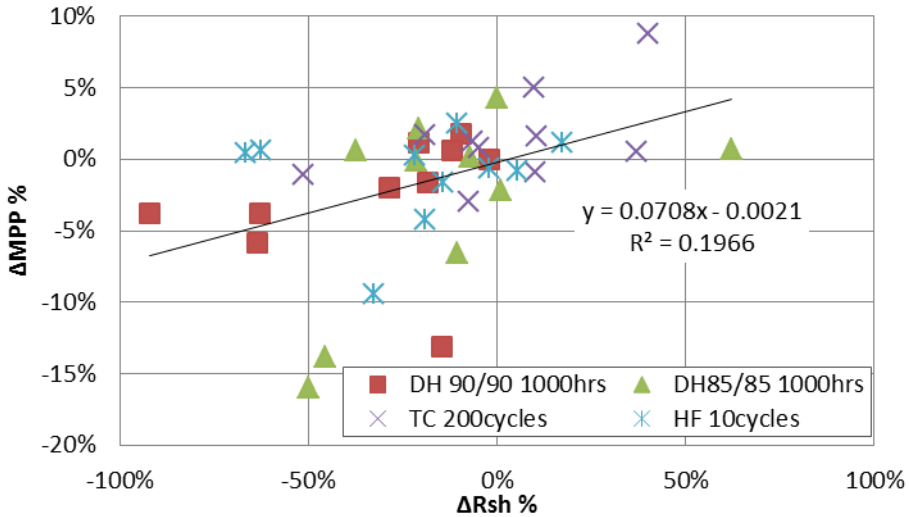

Fig. 47. Interaction graph of R_{sh} and MPP variations after stress tests.

4.9 Conclusions

In the chapter, ten types of PV modules were tested with IEC 61215/61646 standard stress tests, e.g. Damp Heat 85/85, Temperature Cycling, Humidity Freeze, UV exposure, Light Soaking, and tightened stress tests (e.g. bias Damp Heat). After standard stress tests, the normalized powers after the three stress tests (DH, TC, HF) were averaged for ranking and a-Si, mono-Si BIPV, mono-Si and multi-Si performed relatively better than the other module types. For the tightened stress test Damp Heat 90/90, the more stringent condition resulted in more severe degradation for most modules and a-Si, mono-Si BIPV, mono-Si and multi-Si were shown again as the 4 best modules after the test. After the tightened stress test Damp Heat 85/85 1000 V DC bias test, the modules exhibited different behaviours under positive bias and negative bias modes that could be mainly attributed to ion migration. CdTe and CIGS module totally lost their power output after the negative bias test, probably due to internal shunt caused by the negative bias. Such effects also took place on mono-Si and multi-Si modules. Mono-Si back-contact module was seriously affected by the positive bias that caused a surface charging effect to this unique type of PV module. Interestingly, the a-Si module performed very stably in both bias tests, thanks to its module structure with additional edge sealing rubber that increased insulation resistance between module frame and its active circuit. Another tightened stress test UV 50 kWh/m^2 did not significantly impact module power although encapsulant yellowing became more obvious. After the light soaking test, three amorphous silicon-based PV modules (due to SWE effect) and CIGS module revealed significant degradation (10-20%) while CdTe module showed power increasing after light soaking.

Thermal annealing effect was demonstrated on amorphous silicon-based PV modules in the study. In the 65/85°C 96 hours annealing experiement, while the Si wafer

module showed almost no change in module power, all the 3 amorphous silicon-based PV modules exhibited 3-14% power gain phenomenon and CdTe module showed an inverse effect by the annealing in that the module power dropped by 3-6%. A higher annealing temperature appeared to cause less power degradation for CdTe and strengthened the annealing effect for amorphous silicon-based PV modules. Correlating annealing time with module power in the five stress tests for the three amorphous silicon-based modules showed annealing time was another significant factor for the power gain phenonmenon.

Lastly, an analysis of IV curves from Damp Heat 85/85 and 90/90, Humidity Freeze, and Thermal Cycling tests was performed to understand the relationship between IV curve parameters and module power output. V_{oc}, followed by I_{sc}, FF, R_s and R_{sh}, were found to have a significant effect on module power in order of importance.

CHAPTER 5

PV MODULE CHARACTERIZATION TESTS

5.1 Nominal Operating Cell Temperature @ Singapore ($NOCT_{sg}$)

NOCT is a characteristic of PV module to tell how hot solar cell could become under sunlight which associates with heat dissipation capability of PV modules. As temperature affects power output, lower NOCT is preferred. In this test, module temperature T_m was monitored with PT100 temperature sensors attached on the back surface of PV modules. Total irradiance (G) was obtained with a pyranometer exactly aligned with module surface. An integrated ultrasonic weather transmitter was installed at approximately 0.7 meter above PV module to monitor wind speed, wind direction, ambient temperature T_{amb}, relative humidity, precipitation, and air pressure. A data-logger system recorded all the above-mentioned data in every 5 sec. Finally a data-processing (filtering) was done to obtain NOCT at 20^0C ambient temperature, wind speed 1 m/s and total irradiance 800 W/m^2 with the primary method defined in IEC standard 61215 and 61646 as shown in equation (6):

$$NOCT = (T_m - T_{amb})_{800w/m^2} + 20℃ + Correction\ factor \quad (6)$$

IEC standard requires 45° installation angle for this test but PV modules in Singapore were usually installed with 5-10° inclination angle to better harvest solar energy. In this study, NOCT tests were done in both inclination angle conditions and $NOCT_{sg}$ (10° installation angle as shown in Fig. 48) was found about 1.5°C (maximum) lower than NOCT (45°installation angle) for different modules. $NOCT_{sg}$ was selected to be the appropriate parameter for PV module installed in tropical countries.

Fig. 48. $NOCT_{sg}$ test for an amorphous Si tandem PV module and a heterojunction mono-Si/a-Si module in Singapore.

Figure 49 shows a daily measurement of two PV modules in open-circuit condition, showing module temperature at the back of modules and ambient temperature T_{amb} measured at average wind speed 1.0 ± 0.2 m/s with the change of solar irradiance in a sunny day. The two modules were tested simultaneously. The ~5^0C temperature difference could have resulted from module structure, materials used, etc.

Figures 50 and 51 further reveal the temperature difference at top and bottom surface of PV module under the $NOCT_{sg}$ test. Front glass was found always cooler than backsheet or back glass, as front glass absorbs less sunlight than the backsheet and it has a better heat dissipation condition by air convection than that of the back surface of PV module. For Glass-Glass module, the difference was found much larger than Glass-Backsheet module.

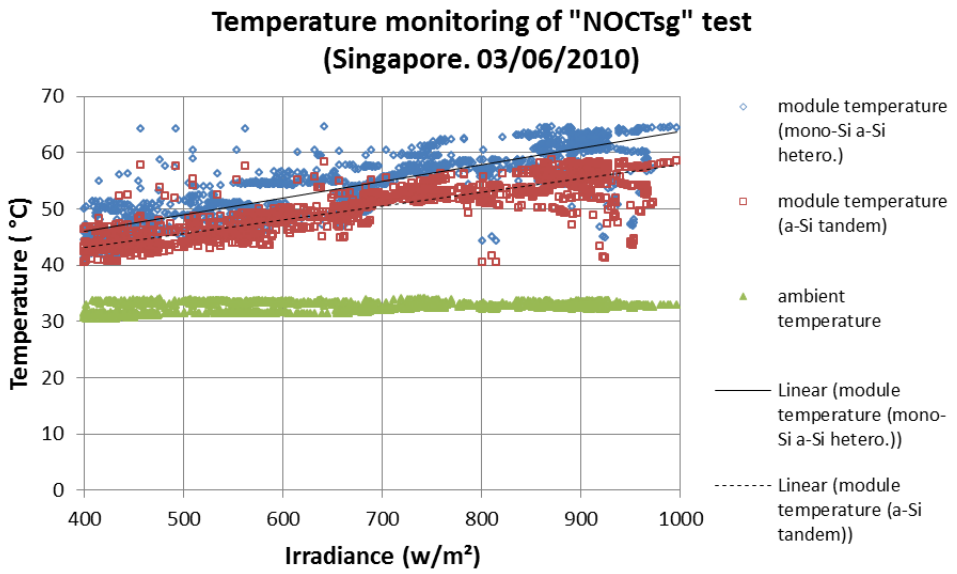

Fig. 49. A daily measurement of $NOCT_{sg}$ for two PV modules in the study. Apparent differences of module temperature attribute to module structure, materials, etc.

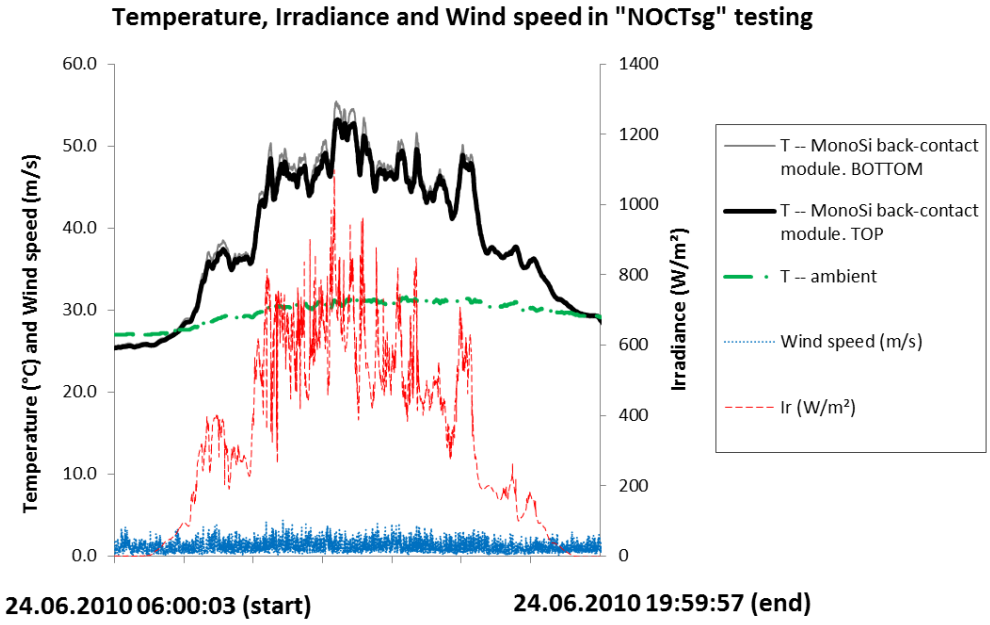

Fig. 50. Temperature monitoring in $NOCT_{sg}$ test of a mono-Si back-contact PV module in Glass-Backsheet structure. Top surface was found ~3°C (max.) cooler than bottom surface of the module.

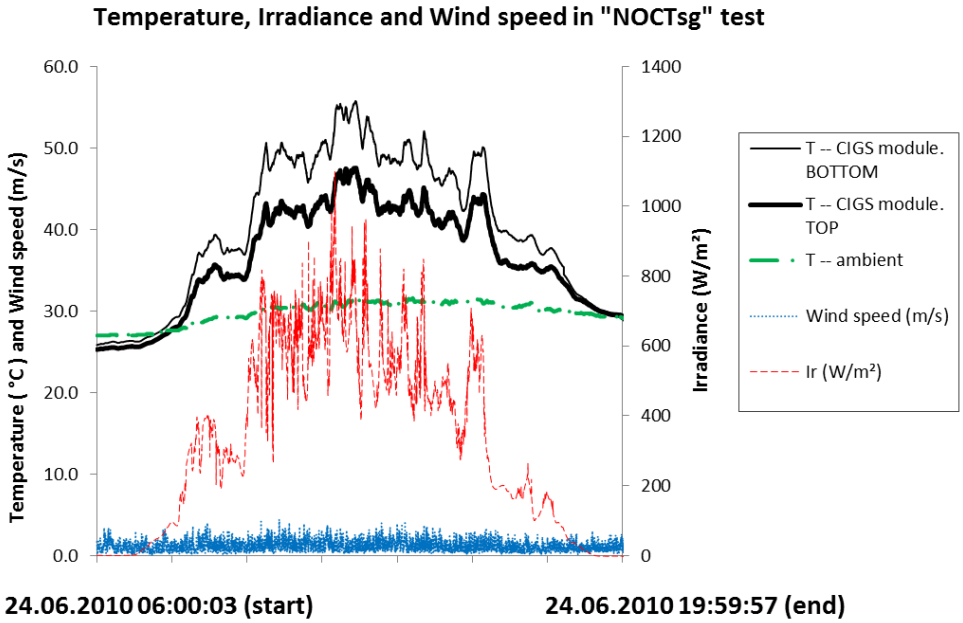

Fig. 51. Temperature monitoring in $NOCT_{sg}$ test of a CIGS PV module in Glass-Glass structure. Top surface was found ~10°C (max.) cooler than bottom surface.

In Fig. 52, $NOCT_{sg}$ result for the ten type of PV modules are plotted. The result can be attributed to multiple factors, including backsheet thickness, backsheet colour, module frame size, etc that influenced sunlight absorption and/or heat dissipation.

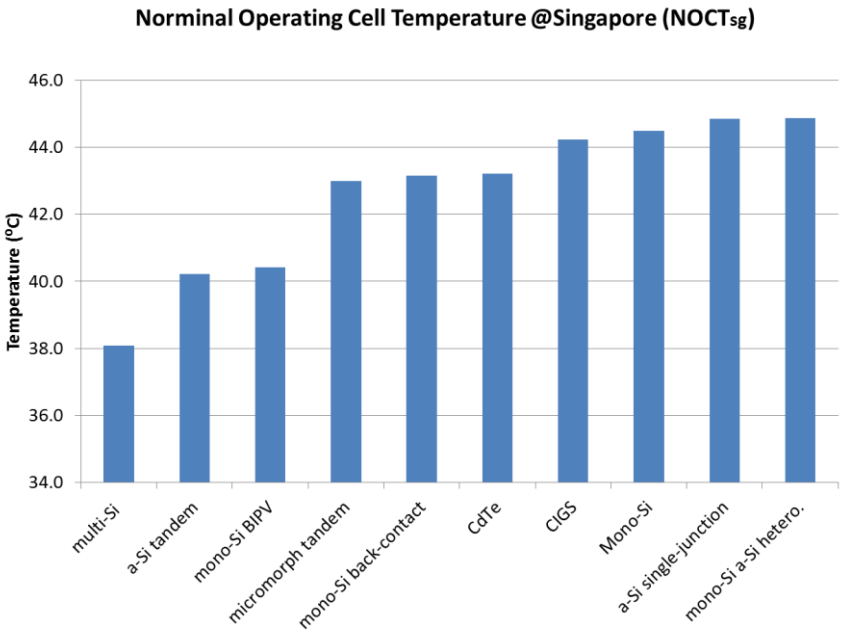

Fig. 52. $NOCT_{sg}$ temperature measured in Singapore for ten types of PV modules.

5.2 Temperature Coefficient

Temperature coefficient measurement was done in the PVPA Unit of SERIS with the IV curve flashing test system and a temperature controlled chamber sealed by a glass screen to allow flashing light to pass through when the module was heated or cooled in the chamber. A PT100 thermal couple was attached at the back of PV module inside the chamber to monitor module temperature. The flasher turns on automatically at different module temperatures (35-65^{0}C) to obtain a series of IV curves @ 1000 W/m^2 as shown in Fig. 53. Different responses are shown from IV curves for different module types. The maximum power points of a-Si thin-film module and mono-Si wafer module show obvious shifts in different ways which represents different characteristics of these two types of PV modules.

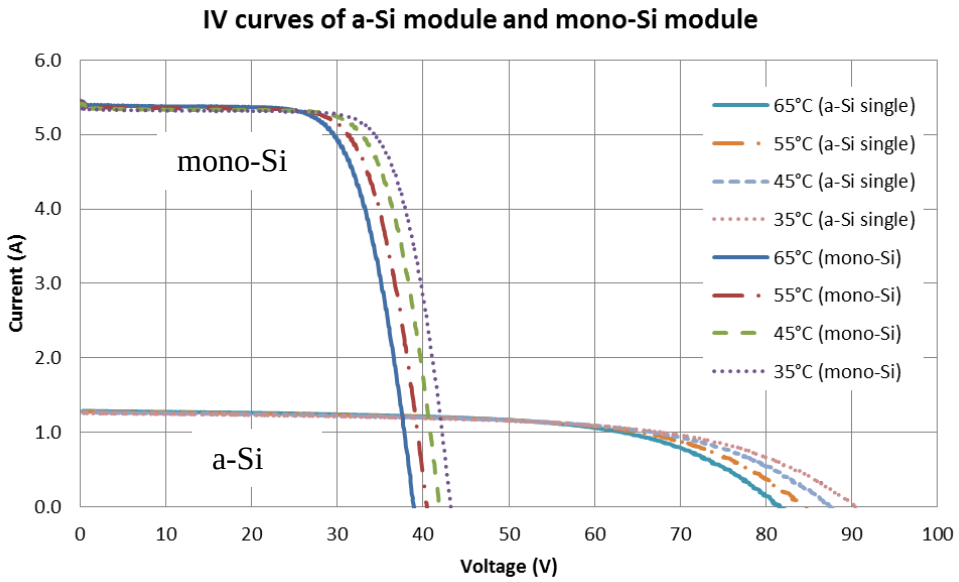

Fig. 53. IV curves measured at different temperatures of a-Si and mono-Si PV modules.

Temperature coefficients were extracted by plotting the percentages of variations for module power, I_{sc}, and V_{oc} with regard to temperature as shown in Table 7. Amorphous silicon-based thin-film modules and CdTe module exhibit less reduction in module power at maximum power point while mono-Si, multi-Si and mono-Si

BIPV modules show more obvious influence of module temperature. The difference in temperature coefficient could attribute to bandgap characteristics of different semiconductor materials and those with larger bandgap would be less susceptible to power reduction in high operating temperature conditions [16].

Table 7. Temperature coefficient of ten PV modules measured in the PVPA Unit of SERIS.

Module type		Temperature coefficient		
		Isc	Voc	Max. power
		%/°C	%/°C	%/°C
a-Si single junction	thin-film	0.09%	-0.35%	-0.22%
CdTe single junction	thin-film	0.03%	-0.26%	-0.25%
a-Si tandem	thin-film	0.08%	-0.35%	-0.32%
micromorph tandem	thin-film	0.09%	-0.43%	-0.39%
mono-Si a-Si heterojunction	wafer	0.04%	-0.27%	-0.40%
Mono-Si backcontact	wafer	0.04%	-0.30%	-0.41%
CIGS	thin-film	-0.01%	-0.34%	-0.42%
Multi-Si	wafer	0.04%	-0.35%	-0.48%
Mono-Si	wafer	0.04%	-0.35%	-0.49%
Mono-Si BIPV	wafer	0.04%	-0.36%	-0.49%

5.3 Performance at $NOCT_{sg}$

Temperature coefficient and NOCT are two important characteristics as the former determines how much loss a PV module will be when it becomes hot and the latter determines how hot a PV module will be. Temperature coefficient depends on the features of solar cell itself (e.g. bandgap of semiconductors) and NOCT can be attributed to the factors from module structure, module materials, heat transfer condition, etc.

Figure 54 plots $NOCT_{sg}$, temperature coefficient as well as the measured performance at $NOCT_{sg}$ temperature for each module. Among the modules, the best performers at $NOCT_{sg}$ are a-Si, multi-Si, and CdTe, which shows lower value of temperature and the worst performers are mono-Si back-contact, mono-Si, and micromorph tandem.

The result of "performance at $NOCT_{sg}$" shows the combined effects from temperature coefficient and $NOCT_{sg}$ on these modules.

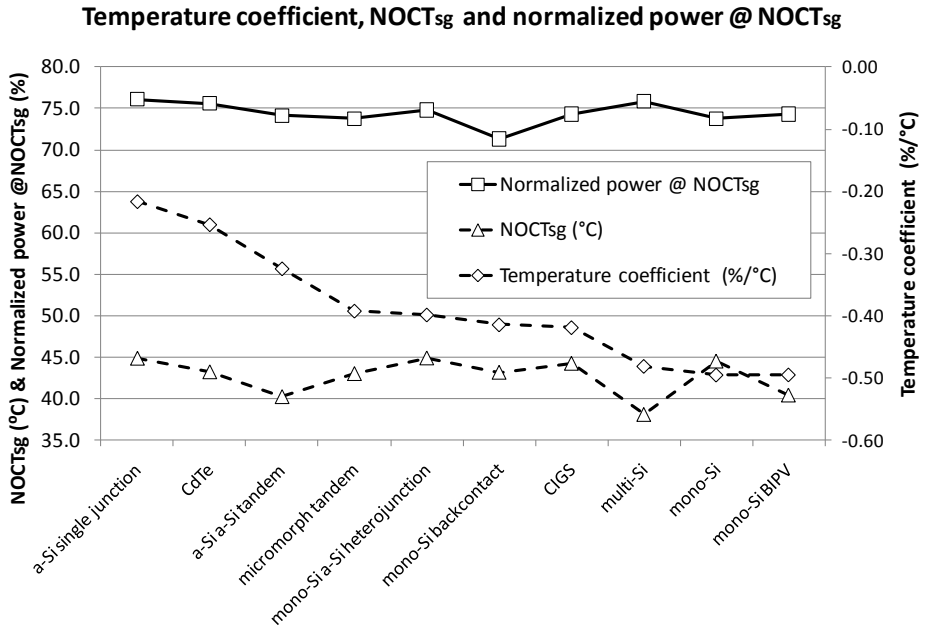

Fig. 54. Temperature coefficient, $NOCT_{sg}$ and normalized module power at $NOCT_{sg}$.

5.4 Outdoor exposure test

The test is to study stability for thin-film modules and Si wafer modules when exposed to sunlight. Amorphous silicon (a-Si) is known to suffer light-induced degradation due to Staebler-Wronski Effect. For micromorph module (amorphous Si and microcrystalline Si tandem, known as micromorph), the different degradation rates of a-Si cell and microcrystalline Si cell can cause mismatch problem that further affects module power due to current mismatch problem between the top and the bottom cell. The initial degradation on boron-doped Czochralski (Cz) crystal silicon cell was found related to activation of a boron-oxygen complex [26]. In IEC standard, outdoor exposure (60 kWh/m^2) test aims "to make a preliminary assessment of the ability of the module to withstand exposure to outdoor conditions and to reveal any synergistic degradation effects which may not be detected by laboratory tests". In this

study the test was conducted on the rooftop of the PVPA unit of SERIS to first precondition PV modules in open-circuit mode for ~5 kWh/m^2 first and then the PV modules were set in loading mode with dedicated resistor loads to work at their maximum power point conditions during the test.

Figure 55 plots module power variation after preconditioning and outdoor exposure 60 kWh/m^2 tests. The module powers were measured at STC with the IV curve flashing tester. Most modules show power reduction after the two test steps. The three amorphous silicon-based modules show large initial degradation after preconditioning and their powers were further reduced after outdoor 60 kWh/m^2 but in a slower degradation rate. A-Si based modules (solid lines) exhibit considerable power reduction than Si wafer based modules (dash lines). For the other two thin-film modules, CIGS module shows < 5% degradation, and CdTe module shows different behaviour with power slightly increasing after preconditioning but the final variation of power is within ±5%. All wafer based modules give relatively stable performance (less than 4% degradation) as compared to thin film modules.

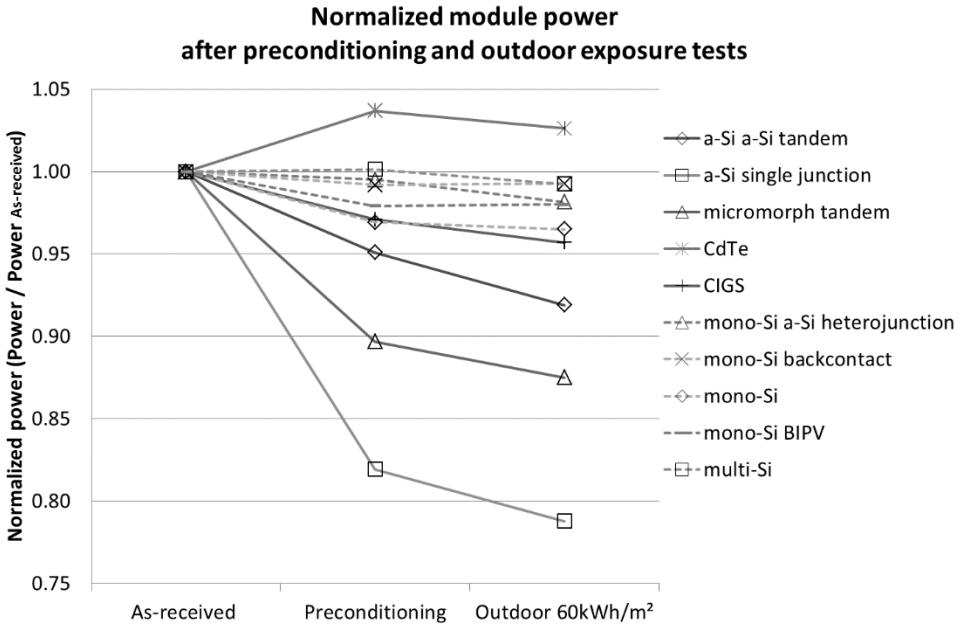

Fig. 55. Module power variation after preconditioning and outdoor exposure tests.

5.5 Low-irradiance performance

This test was done with an IV curve flashing tester at module temperature 25^{0}C and 200 W/m^2 low irradiance conditions to assess module performance at weak light condition, as different PV technologies showed different performance characteristics at low light conditions such as early mornings, late afternoons, or cloudy days, as well as at high-latitudes.

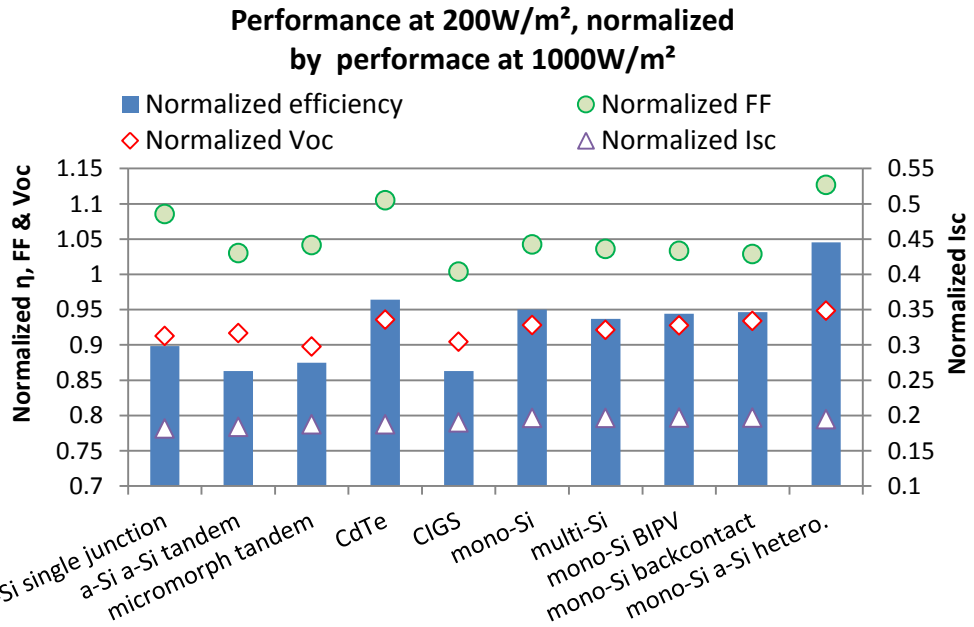

Fig. 56. Low-irradiance test at 200 W/m^2 irradiance and module temperature 25^{0}C.

Figure 56 plots the four normalized parameters (efficiency, I_{sc}, V_{oc}, and fill factor) normalized by their counterparts tested at STC, e.g. the normalized efficiency stands for the efficiency at 200 W/m^2 normalized by efficiency at 1000 W/m^2. For all modules, fill factors at 200 W/m^2 are higher than those at 1000 W/m^2. V_{oc} and I_{sc} are lower at 200 W/m^2 than those at 1000 W/m^2. The decreasing of V_{oc} mainly represents the effect of the internal shunt inside the solar cells at low irradiance. I_{sc} reduction could be attributed to the reduction of photon flux and/or the difference of spectral response. Compared with the other modules, mono-Si/a-Si heterojunction module showed the best performance as its weak-light efficiency was found even better than

that at STC. The thin-film modules (except for CdTe) show relatively poorer performance in this test as compared to Si wafer modules, which could be because of the nature of thin-film fabrication which inherently produces more shunt defects in the solar cells.

5.6 Hot-spot test

When a PV module is partially shadowed, the affected cell or group of cells are forced into reverse bias and the dissipating power can cause overheating that deteriorates the encapsulation of PV module. In this study, five PV modules were tested by following the IEC 61215/ 61646 standard in hot spot test chamber at PVPA of SERIS. Modules were shadowed partially to find out the worst bias condition under a sun simulator. An IR camera was used to measure the hot spot temperature under the test condition as shown in Fig. 57. Figure 58 plots the peak hot-spot temperatures for these modules and the module power variation measured at STC condition post the test. CdTe module, mono-Si/a-Si hetero module, and a-Si module show high hot-spot temperature. The module power of the first two modules drop by 11.2% and 6.6%, while a-Si module exhibits power gain phenomenon (due to thermal annealing effect as discussed previously) despite of the hot spot issue.

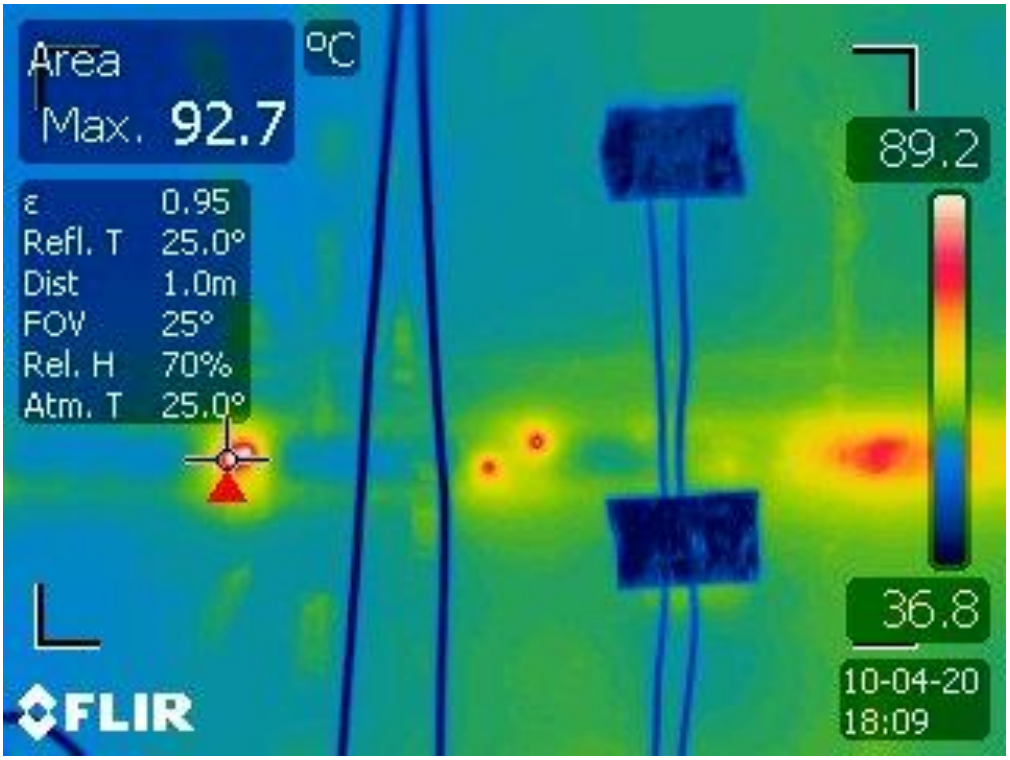

Fig. 57. Hot spots detected at the back of micromorph tandem PV module by an IR camera in hot-spot test.

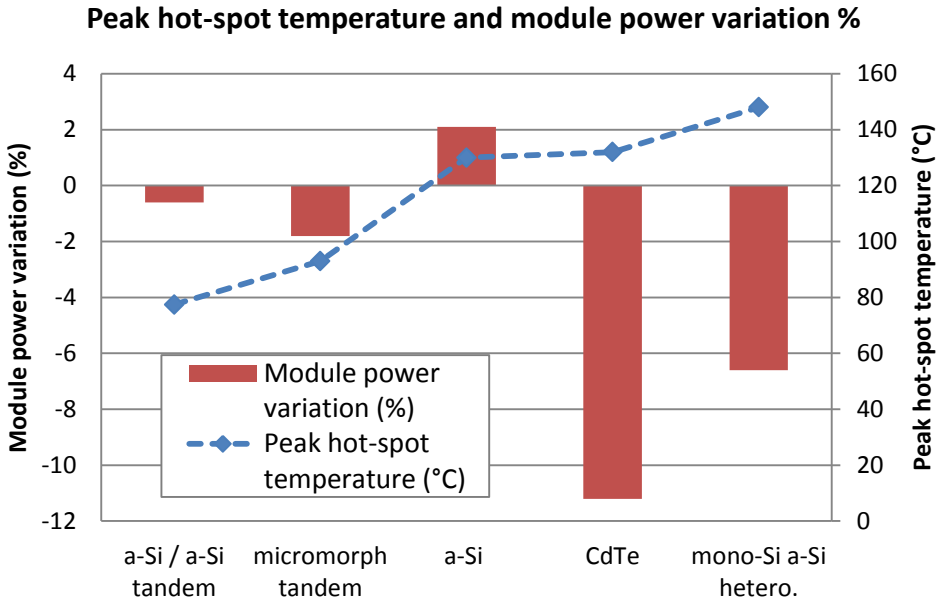

Fig. 58. Module power variation influenced by hot-spots for four thin-film PV modules and a Si-wafer PV module.

5.7 Conclusions

In this chapter, a series of PV module characterization tests were performed. $NOCT_{sg}$ (NOCT test at Singapore outdoor condition) ranged from 38°C to 45°C, influenced by backsheet thickness, backsheet colour, module frame size, etc. Temperature coefficient tests showed a-Si, CdTe, and a-Si tandem were the best while mono-Si, multi-Si and mono-Si BIPV modules suffered the highest loss when temperature was increased. Combining the two effects, the "Performance at $NOCT_{sg}$" test showed a-Si, multi-Si, and CdTe modules as the best performers while mono-Si back-contact, mono-Si, and micromorph tandem performed the worst.

Outdoor exposure tests at 60 kWh/m^2 showed the three amorphous silicon-based modules performed the worst with 8-21% degradation while Si wafer based modules performed very stably with less than 4% degradation. For the other two thin-film modules, CIGS module showed less than 5% degradation, and CdTe module instead showed 3% power enhancement.

Low-irradiance performance tests showed a superior performance for mono-Si/a-Si hetero module, followed by CdTe and mono-Si modules. The other 4 thin-film modules exhibited poorer performance under weak light condition as compared to their Si-wafer counterparts.

Lastly, hot spot tests on 5 PV modules showed the Si-wafer module (mono-Si/a-Si hetero) experiencing the highest hot-spot temperature, followed by CdTe thin-film module. The module power of the CdTe and mono-Si/a-Si hetero modules dropped by 11.2% and 6.6%, while the module power variation for the three amorphous silicon-based thin-film modules was within ±2%.

CHAPTER 6

PREDICTION OF PV MODULE PERFORMANCE

6.1 Summary of PV module performance

Table 8 summarizes the degradation rates of major stress tests and outdoor exposure test in Singapore for different PV module technologies conducted in this study, and Fig. 60 compares them with the target degradation rate (-0.0001%/hr), equivalent to 20% max degradation of module power in 25 years of field service.

Table 8. Degradation rate (%/hr) measured for different PV technologies by stress tests and outdoor exposure test

Tests	**HF10**	**DH85/85**	**DH90/90**	**DH85/85 bias (PB)**	**DH85/85 bias (NB)**
Stressing hours	**240**	**1000**	**1000**	**650**	**650**
a-Si	0.0182%	0.0020%	0.0000%	0.0226%	0.0246%
a-Si /a-Si tandem	-0.0068%	-0.0021%	-0.0131%	-0.0099%	-0.0158%
micromorph tandem	0.0003%	-0.0048%	-0.0020%	0.0112%	-0.0074%
CdTe	-0.0015%	-0.0042%	-0.0058%	-0.0157%	-0.1537%
CIGS	-0.0096%	-0.0001%	-0.0017%	-0.0162%	-0.1537%
mono-Si	-0.0025%	0.0007%	0.0018%	-0.0012%	-0.0971%
multi-Si	0.0026%	0.0002%	0.0006%	-0.0035%	-0.0298%
mono-Si BIPV	-0.0017%	0.0021%	0.0011%	0.0013%	-0.0030%
back-contact mono-Si	0.0000%	-0.0021%	-0.0038%	-0.0643%	0.0006%
mono-Si/a-Si hetero	-0.0012%	-0.0009%	-0.0037%	-0.0046%	-0.0003%
Tests	**TC200**	**UV15**	**UV50**	**Outdoor exposure**	
Stressing hours	**666**	**264**	**880**	**480**	
a-Si	-0.0036%	0.0338%	0.0029%	-0.0080%	
a-Si /a-Si tandem	-0.0016%	-0.0126%	0.0010%	-0.0070%	
micromorph tandem	-0.0011%	-0.0001%	0.0046%	-0.0051%	
CdTe	-0.0005%	0.0156%	-0.0007%	-0.0021%	
CIGS	0.0026%	-0.0193%	0.0013%	-0.0030%	
mono-Si	0.0008%	-0.0005%	0.0004%	-0.0009%	
multi-Si	-0.0016%	-0.0008%	0.0006%	0.0002%	
mono-Si BIPV	0.0024%	-0.0021%	0.0000%	-0.0019%	
back-contact mono-Si	-0.0014%	-0.0032%	-0.0001%	0.0002%	
mono-Si/a-Si hetero	-0.0004%	0.0004%	0.0002%	-0.0028%	

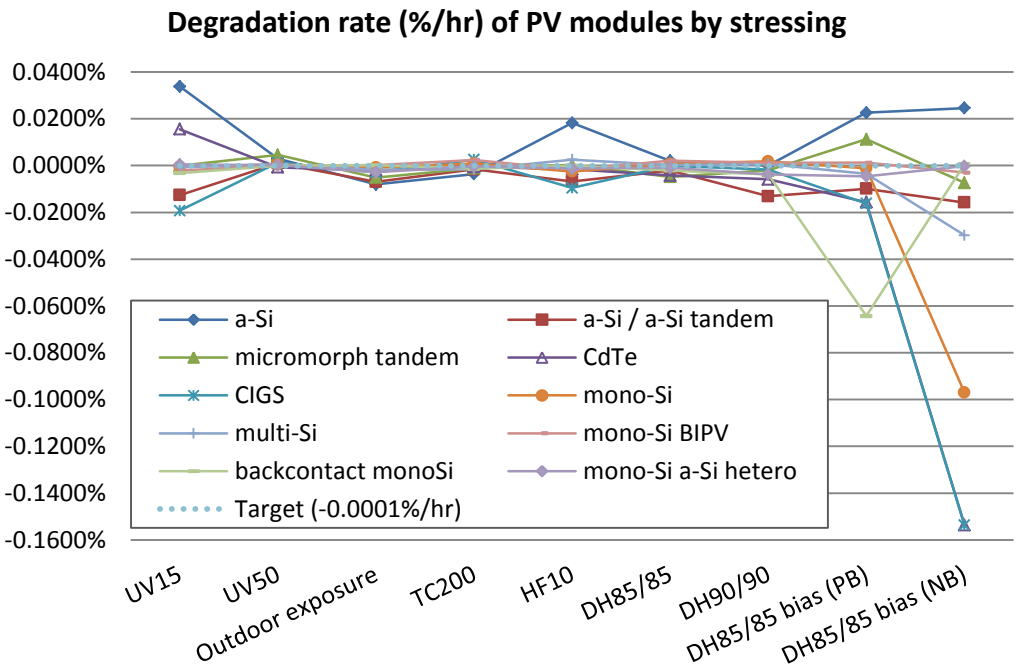

Fig. 60. Degradation rate of PV modules after stress tests and outdoor exposure test, compared with the target rate (-0.0001%/hr) for 25 years of service.

The above results show that degradation rates generally become worse in moisture related tests and worsens further when the moisture test condition becomes more severe (e.g. 85°C/85%R.H. to 90°C/90%R.H.) or when additional electrical bias is applied during Damp Heat test. Certain module types exhibit different behaviours due to their own unique features, e.g. back-contact mono-Si affected by surface charging effect under positive bias, a-Si based modules affected by thermal annealing effect by heating during the tests. Even for PV modules with the same type of solar cell technology, PV module design (e.g. structure) influences the test result too, e.g. the thick rubber sealing on a-Si module minimizes the bias current under biased Damp Heat test; the Glass-Glass structure of the BIPV mono-Si module enables it to have low moisture ingress (as compared to mono-Si module and multi-Si module) and eventually exhibit stable performance in tests. As compared to the target degradation rate of -0.0001% per hour (20% degradation max for 25 years), in general, all the tests give different degradation rates.

For the viewpoint of durability, those modules with degradation rates close to the 0% line in all the tests should be the best as they are most likely to generate stable and expected power output in field service. However, as field service conditions vary (e.g. weather, installation), certain stress conditions could be significant in one location but not in another location. Thus the assertion that one PV technology is the best in durability has to be verified through extensive field tests at different locations. The merit of accelerated tests is that one can design a series of tests to include the most significant factors for field service and estimate the long term performance from these tests. The differences in degradation rates found for different stress tests shows that different module technologies have different sensitivities to different stress types. Thus a dedicated test design needs to include appropriate stress tests in order to predict performance durability.

6.2 Prediction of PV module performance

Performance ratio is a parameter used to measure solar photovoltaic performance to assess the ratio of actual electricity generated in outdoor condition and calculated energy that would be expected from the panel nameplate rating. This metric quantifies the overall effect of losses [68] due to: inverter inefficiency, wiring, cell mismatch, elevated PV module temperature, reflection from the module front surface, soiling, system down-time, shading, and component failures. PR can be calculated using equation (7) as follows [85]:

$$Performance\ Ratio\ (PR) = \frac{Production\ energy\ (Wh)}{\sum_t \left[Irradiance\left(\frac{W}{m^2}\right) \times \frac{W_p}{1000\left(\frac{W}{m^2}\right)} \right] \times [\,1 + (Temp - 25℃) \times Temp\ Coeff.\left(\frac{\%}{℃}\right)]} \quad (7)$$

Temp stands for module temperature, which is measured temperature at module back surface. W_p is watt peak power which is the rated power provided by PV module manufacturers under STC conditions (irradiance 1000 W/m^2 and temperature 25°C). *Temp Coeff.* is the measured temperature coefficient of a particular PV module that reveals the effect of temperature on module performance. *Irradiance* is the intensity of solar irradiation at time *t*.

A predicted Performance Ratio ($PR_{predicted}$) is proposed in this work to take Comprehensive Stress Factors (CSF) into consideration to predict PV module performance in the long term, as shown in formula (8).

$$Predicted\ Performance\ Ratio\ \left(PR_{predicted}\right) = \frac{Production\ energy\ (Wh) \times CSF}{\sum_t \left[Irradiance\left(\frac{W}{m^2}\right) \times \frac{W_p}{1000\left(\frac{W}{m^2}\right)} \right] \times [\,1 + (Temp - 25℃) \times Temp\ Coeff.\left(\frac{\%}{℃}\right)]} \quad (8)$$

$$CSF = C \cdot f\left(\frac{P_{stress1}}{P_{initial}}, \frac{P_{stress2}}{P_{initial}}, \frac{P_{light-soaking}}{P_{initial}}, \dots\dots\right) \quad (9)$$

$$CSF' = 1 + \alpha \cdot t \quad (10)$$

As shown in formula (9), the CSF includes the influencing factors of moisture, thermo-mechanical stress, thermal annealing, etc through a function to reflect a synergistic effect on product performance. *C* is a constant in the formula. The terms of the function are from the result of accelerated stress tests (e.g. if stress 1 is treated as moisture induced corrosion, $P_{stress1}/P_{initial}$ will be the normalized power after Damp Heat test). The extremely long PV module lifetime of 20-25 years makes it beneficial to use the result of accelerated stress tests to predict module performance. For long-term performance, the CSF' links to the degradation rate α of PV module/system in a

time function as shown in formula (10). For example, a PV system with an annual degradation rate 0.8% for 10 years will result in a 0.92 CSF' as shown in formula (10). The prediction obtained by accelerated stress tests and the synergistic factor CSF through formula (9) aims to forecast the same extent of degradation shown through CSF' of formula (10) in shorter test time.

In the work, the function of CSF was selected to be the average of the normalized module powers from Humidity Freeze 10, Thermal Cycling 200, Damp Heat 85/85 1000hrs tests times the effect of light-induced degradation as these tests cover the stressing factors of UV, moisture, thermo-mechanical stress, and light. As module frames were not grounded in the outdoor test, the result of the Damp Heat biased test was not included in the calculation of CSF. By taking the assumption that the result of these accelerated stress tests corresponds to certain lifetime of PV module, the CSF approximates to the total degradation after field application of that lifetime.

Production energy Wh was calculated according to formula (7) and (8). The calculated energy yield and the predicted energy yield (Wh/W_p.day) are shown in Figure 59. Also, the result of an outdoor test in Singapore is included. Assumptions taken in the calculation: The sunshine hours of a sunny day are divided into two stages – "Nominal Operating" stage with 800 W/m^2 irradiance and "Low-Irradiance" stage with 200 W/m^2 irradiance while the total daily solar insolation after the staging meets the measured result (4.6 kWh/m^2 as measured in $NOCT_{sg}$ test) of a typical sunny day in Singapore. Performance ratios at 800 W/m^2 and 200 W/m^2 are input from the results of "Performance at $NOCT_{sg}$" (Fig. 54) and "Performance at Low-Irradiance" (Fig. 56). Module temperature at 800 W/m^2 irradiance is obtained from $NOCT_{sg}$ test (Fig. 52) and module temperature is set as 25°C when the low irradiance 200 W/m^2.

The energy yield $Wh/W_p.day$ is plotted in Figure 59 for ranking purpose. The two bars show the calculated energy yield without including the CSF effect and the predicted energy yield including the CSF effect. The outdoor test result represents the average daily energy yield (DC) of the ten commercial PV modules in Singapore for the period from September 2010 to April 2011 [86]. The commercial PV modules in this study were monitored for their performance under Singapore weather condition and they (one panel each type) were mounted on open racks at the rooftop of a building in National University of Singapore (NUS) with a Maximum Power Point Tracking (MPPT) system collecting IV curves for each module at 10 sec intervals.

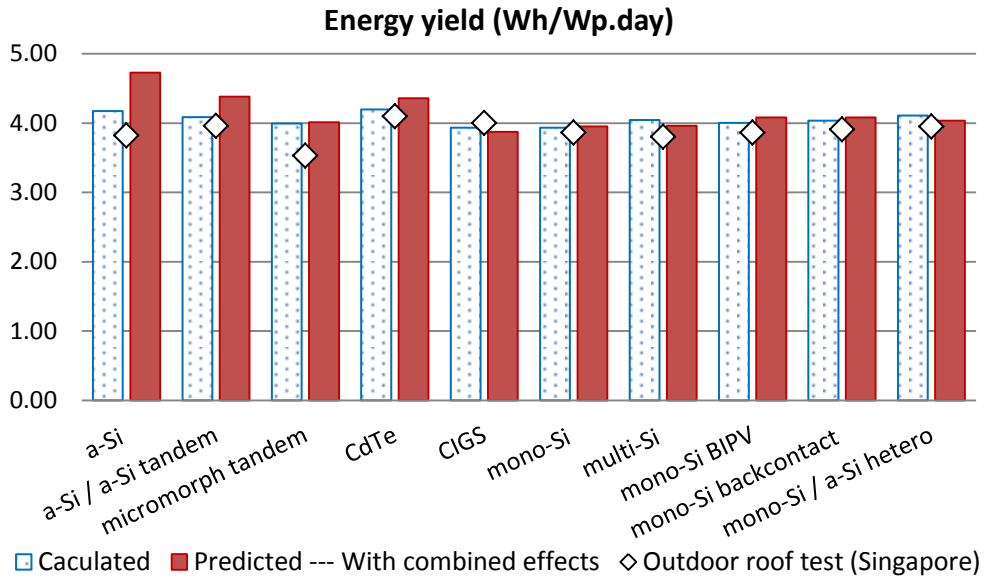

Fig. 59. Calculated, predicted and measured energy yield of ten types of commercial PV modules. Outdoor measurements were done between September 2010 and April 2011 on a rooftop at the National University of Singapore.

For the calculated energy yield without CSF effect, the 3 best performers of PV modules are found as CdTe, a-Si and mono-Si/a-Si hetero. The 3 least good performers are CIGS, mono-Si, and micromorph tandem. For the predicted energy yield in which stress effects (Thermo-mechanical, moisture ingress, thermal annealing, etc) and light-induced degradation are taken into consideration, the 3 best performers are found as a-Si, a-Si/a-Si tandem and CdTe. The 3 least good performers are CIGS,

multi-Si and mono-Si. For the outdoor test, the 3 best performers are CdTe, CIGS, and a-Si/a-Si tandem and the 3 least good performers are micromorph tandem, multi-Si, and a-Si.

When stress effects (e.g. degradation due to moisture induced corrosion) are not considered, the least good choice are the CIGS module and the mono-Si module selected in this study, mainly because of their higher $NOCT_{sg}$ and/or higher temperature coefficient, which means their performance could be badly affected by Singapore's hot weather. The other modules show about the same performance as estimated. When stress effects (Thermo-mechanical, moisture ingress, etc) and light-induced degradation are taken into consideration, amorphous silicon-based modules and CIGS module are affected by light-induced degradation problem. A-Si module shows larger increasing in predicted yield because thermal annealing effect strongly influences its performance (even greater influence than light-induced degradation). The CdTe module instead would perform even better because it exhibits a reverse behaviour as the rest 4 thin-film modules in light-induced degradation and it also has low temperature coefficient. CdTe repeatedly shows power increasing in outdoor tests that seems to indicate light and/or heat influences its performance in some way. From the actual outdoor test, CdTe module also is the one giving the highest energy yield. Compared with other PV modules, while the performances of these module types are fairly close to each other, CdTe module seems to be a good choice in terms of module energy yield Wh/W_p for Singapore weather. It should be taken into consideration that the comment is based on a limited number of test samples, limited test hours, and limited tests performed in this study. Further studies with larger sample size, increased test hours, and/or large-size outdoor test arrays should be performed to better distinguish their difference for tropical weather.

CHAPTER 7

CONCLUSIONS AND FUTURE WORK

7.1 Conclusions

PV module durability

From the IEC 61215/61646 standard stress tests, e.g. Damp Heat 85/85, Temperature Cycling, Humidity Freeze, UV exposure, Light Soaking, etc, the normalized powers averaged from three stress tests (DH, TC, HF) shows a-Si, mono-Si BIPV, mono-Si and multi-Si performed relatively better than the rest of the modules. For the tightened stress test Damp Heat 90/90, the more stringent condition resulted in more severe degradation for most modules and a-Si, mono-Si BIPV, mono-Si and multi-Si were shown again as the 4 best modules after the test. Another tightened stress test UV 50 kWh/m^2 doesn't cause big impact on module power. After light soaking test, three amorphous silicon-based PV modules (due to SW Effect) and CIGS module revealed significant degradation 10-20% for while CdTe module showed opposite behaviour with power increasing after light soaking.

IV curve parameter analysis

From IV curve parameters analysis on the result of Damp Heat 85/85, Damp Heat 90/90, 1000V bias Damp Heat 85/85, Thermal Cycling 200, and Humidity Freeze 10 test series, it reveals the most significant parameter change that attributes to power degradation is V_{oc}, which means the variation of V_{oc} in the stress tests causes the largest variation on module power. As V_{oc} is a parameter strongly influenced by internal shunt of solar cell or bandgap of semiconductor material, the result indicates these features are mostly likely to be influenced by the stressing. For moisture corrosion tests, moisture penetrates into PV module rapidly (as illustrated by moisture

diffusion simulation at 85°C/85%R.H. condition) for a Glass-Backsheet structure. The ingress can attack dissimilar materials of solar cell as result of galvanic corrosion and such reaction may get intensified as the result of elevated temperature. It probably should be taken into consideration in module design to focus more on stabilizing V_{oc} against environmental stresses for better PV module durability.

Potential-induced degradation

As shown in previous chapters, potential-induced degradation (PID) causes the most severe degradation to certain PV technologies in the bias Damp Heat test. Bias polarity plays an important role as it determines the moving directions of ions in PV module. In negative bias condition, sodium ion Na^+ from front glass moves towards solar cell and the bias causes damage to CdTe thin-film module and CIGS thin-film module. This indicates such thin-film materials are more susceptible to the ion attack. For amorphous Si-based thin-film modules, the issue is much less severe. Thanks to its thick rubber sealing design along module edge for a-Si module, the electrical bias (positive or negative) causes no degradation to this module and in fact its performance was improved due to thermal annealing effect to a-Si based thin film.

The negative bias also significantly affects certain Si wafer modules (mono-Si and multi-Si, while back-contact mono-Si module or mono-Si/a-Si hetero module is immune to the issue. This serves as an evidence that Na^+ migrates from front glass and attacks the top surface of Si wafer where the junction is located. The attack of ions can result in degradation for the junction that affects carrier collection. For the back-contact mono-Si module, its P/N junction is at the back of wafer hence the ion migration doesn't influence its performance. For mono-Si/a-Si hetero module, it has a thin a-Si layer on mono-Si wafer that could plays as a shield to protect its semiconductor junction as a-Si seems to behave less sensitive to Na+ ion attack as discussed in previous paragraph.

In positive bias condition, most modules exhibit surface corrosion issue at the external surface of glass. The issue doesn't significantly affect module power although it influences light transmission. Only back-contact shows power degradation due to its surface charging issue unique to this PV technology.

To mitigate the effect of PID, frameless design that the CdTe and the BIPV module adopt and the thick rubber edge sealing design that a-Si module adopts should be taken into consideration in PV module application.

Moisture diffusion simulation

An important finding of the FEA simulation is it reveals the highly uneven moisture distribution at top surface of a Si wafer Glass-Backsheet PV module because moisture penetration is blocked by the wafer itself as Si is impermeable material to water. This is beneficial to the top surface of Si wafer as less chance of corrosion. From the moisture dose derived from the simulation at different locations of the Si wafer, the centre of the top Si wafer surface should experience the least moisture attack. The result gives a clear picture to understand how moisture diffusion progresses and where the most vulnerable locations are. The moisture dose in Damp Heat 85/85 test is found 3-5 times of that in Outdoor test of Singapore for the three regions of Si wafer (the centre of bottom surface, the edge of bottom surface, and the edge of top surface), while the ratio is about 5 orders higher at the centre of the top surface.

Thin-film module, unfortunately, doesn't have such feature in blocking moisture diffusion. Hence it needs other means against moisture diffusion, such as changing backsheet to back glass which is not uncommon for nowadays thin-film module.

The simulation also includes the exploration of the effects from backsheet thickness by comparing moisture concentration in Si wafer module with TPT backsheet. The PET thickness was modelled as 254 μm and 76 μm in the TPT backsheet. PET layer

in TPT backsheet plays an important role against moisture diffusion. The simulation shows that thin TPT backsheet allows moisture diffuse out of PV module more easily than thick TPT backsheet in moisture desorption process, however, it absorbs moisture faster than thick TPT in moisture absorption process. The overall moisture variation for the two cases however doesn't show obvious difference in field service of Singapore condition under the assumption that continuous sunny days apply. The result demonstrates the effect of backsheet on moisture desorption (e.g. at day time) and moisture absorption (e.g. at night time). The implication of the study seems the moisture absorbed is shown almost totally desorbed in day times and the TPT choice doesn't play an important role, as the module is more "breathable" with thin TPT backsheet that allows moisture entrapped diffusing out of PV module more easily. For different countries with different weather condition, e.g. a temperate country, the backsheet choice may influence moisture amount inside PV module thus influences performance.

The simulation also includes exploration on effects from encapsulant materials (ionomer vs EVA) and structural feature (metal string thickness) that shows interesting influence on moisture diffusion, which should be of help on PV module design optimization.

PV module characterization in Singapore weather condition

A series of characteristics tests reveals performance parameters ($NOCT_{sg}$, Temperature coefficient, Performance at $NOCT_{sg}$) for better estimation of PV module's performance in Singapore outdoor test condition. A study is performed on the instability issue of thin-film modules particularly for amorphous silicon-based modules through light soaking and thermal annealing. It reveals the thermal annealing effect of them that occurs at low annealing temperature (as low as 65°C and 85°C). The finding in this area supports the implementation of amorphous silicon-based

modules and/or other modules favouring hot weather for Singapore weather condition.

PV module outdoor performance and prediction for Singapore weather condition

Finally, the study combines various effects from degradation and characteristics of PV modules and delivers a module power prediction, and compares the predicted power output with the result of actual outdoor test in Singapore for each type of module. The CdTe module selected in this study appears to be a good choice in terms of module energy yield Wh/W_p for Singapore weather. However, it should be taken into consideration that this comment is based on limited test samples, limited test hours, and limited tests performed in this study. Further studies with larger sample size, increased test hours, and/or large-size outdoor test arrays should be performed to better distinguish their difference for tropical weather.

7.2 Future works

The work showed the different PV module behaviours in different tests. Further study should be continues on verifying the attributing factors from PV module structure and material on module performance such as NOCT, moisture ingress, biased Damp Heat test, etc. For example, one important finding of adding edge sealing rubber to increase insulation resistance between frame and glass deserves further experiment to establish a standard module design against potential-induced degradation. Also, further experiments could be performed to study the relationship between halogens from flux residue used in soldering strings with solar cells and the corrosions exhibited in the study such as “snail trail” effect in biased damp heat, because halogens are known to deteriorate corrosion resistance. This can be done by evaluating flux materials and cleaning techniques with special PV modules built in laboratories. Solutions against moisture ingress such as different encapsulant materials or varied string thickness

should be further verified through performance testing. Moisture induced degradation models on specific PV module types should be conducted to develop accelerated stressing model in large sample size for individual PV technologies to obtain statistically sound data for such model. The model will benefit durability study on product life and such experiments can be conducted with small-size solar module (e.g. single-cell module) built in laboratories under different moisture soaking conditions. Another important work should be keeping monitoring long-term performance of the modules in outdoor tests and verifying degradation rates and degradation phenomena with regard to the proposed power prediction model.

REFERENCES

1. Public Utilities Board of Singapore. Environmental Sustainability. http://www.pub.gov.sg/marina/Pages/Environmental-Sustainability.aspx

2. National Aeronautics and Space Administration. Helios Prototype aircraft. http://www.nasa.gov/centers/dryden/news/ResearchUpdate/Helios/

3. Wikipedia. http://en.wikipedia.org/wiki/File:Solar_cell.png

4. National Renewable Energy Laboratory. NREL efficiency map. http://www.nrel.gov/ncpv/

5. Suntech company website. http://www.suntech-power.com/

6. M.A. Quintana, D.L. King, F.M. Hosking, J.A. Kratochvil, R.W. Johnson, B.R. Hansen, N.G. Dhere, M.B. Pandit. "Diagnostic analysis of silicon photovoltaic modules after 20-year field exposure", *28th IEEE Photovoltaic Specialists Conference* 2000, pp.1420-1423

7. E.E. Van Dyk, A. Audouard, E.L. Meyer, C.D. Woolard. "Investigation of the degradation of a thin-film hydrogenated amorphous silicon photovoltaic module", *Solar Energy Materials & Solar Cells,* 91 (2007) 167–173

8. J.H. Wohlgemuth. "Long term photovoltaic module reliability", *NCPV and Solar Program Review Meeting* 2003; pp.179-182

9. M.S. Ibrahim, I. Abouhdima, M.B. Gantrari. "Performance of thirty years stand alone photovoltaic system", *24th European Photovoltaic Solar Energy Conference* 2009; pp.3995-3998

10. N.G. Dhere, V.V. Hadagal, K. Jansen. "Performance degradation analysis of high-voltage biased thin-film PV modules in hot and humid conditions", *31st IEEE Photovoltaic Specialists Conference* 2005; pp. 507-510.

11. Weatherwise Singapore, National Environmental Agency (NEA) of Singapore 2009; http://app2.nea.gov.sg/data/cmsresource/20090324939502642695.pdf

12. K.R. McIntosh, J.N. Cotsell, A.W. Norris, N.E. Powell, B.M. Ketola. "An optical comparison of silicone and EVA encapsulants under various spectra", *35th IEEE Photovoltaic Specialists Conference* 2010; pp. 269 -274

13. F. Jiang. "Investigation of solar energy for photovoltaic application in Singapore", *8th International Power Engineering Conference (IPEC 2007)* 2007; pp. 86-89

14. M. Nikolaeva-Dimitrova, R.P. Kenny, E.D. Dunlop. "Long term stability of a-Si:H thin film modules", *21st European Photovoltaic Solar Energy Conference* 2006; pp. 2565-2569

15. J.A. Del Cueto, B. Von Roedern. "Temperature-induced changes in the performance of amorphous silicon multi-junction modules in controlled light-soaking", *Progress in Photovoltaics: Research and applications* 1999; 7: 101-112

16. A. Luque, S. Hegedus, *Handbook of Photovoltaic Science and Engineering*, Wiley: UK, 2003.

17. D. C. Jordan, S. R., Kurtz. “Photovoltaic degradation rates - an analytical review,” *Progress in Photovoltaics: Research and Applications*, vol. 21, no. 1, pp. 12–29, 2013

18. J. H. Wohlgemuth, D. W. Cunningham, A. M. Nguyen, J. Miller. “Long term reliability of PV modules”, *2006 IEEE 4th World Conference on Photovoltaic Energy Conversion*, May 2006 Volume: 2, pp.2050-2053

19. C.R., Osterwald, T.J. McMahon, J.A. del Cueto. “Electrochemical corrosion of SnO_2:F transparent conducting layers in thin-film photovoltaic modules”, *Solar Energy Materials & Solar Cells* 79 (2003) 21–33

20. M.D. Kempe, G.J. Jorgensen, K.M. Terwilliger, T. J. McMahon, C.E. Kennedy, T. T. Borek. “Acetic acid production and glass transition concerns with ethylene-vinyl-acetate used in photovoltaic devices”, *Solar Energy Materials & Solar Cells* 91 (2007) 315–329

21. A.W. Czanderna, F.J. Pern. “Encapsulation of PV modules using ethylene vinyl acetate copolymer as a pottant: A critical review”, *Solar Energy Materials and Solar Cells*, 43 (1996) 101-181

22. F.J. Pern and A.W. Czanderna. “Characterization of ethylene vinyl acetate (EVA) encapsulant: Effects of thermal processing and weathering degradation on its discoloration”, *Solar Energy Materials and Solar Cells* 25 (1992) 3-23

23. G. TamizhMani. “Failure analysis of design qualification testing: 2007 VS.2005”, *33rd PVSC 2008*, pp.1-4

24. M.A. Quintana, D. L. King, T. J. McMahon and C. R. Osterwald. “Commonly observed degradation in field-aged photovoltaic modules”, *Photovoltaic Specialists Conference, 2002. Conference Record of the Twenty-Ninth IEEE*, pp.1436-1439

25. C.R. Osterwald, J. Adelstein, J.A. del Cueto, B. Kroposki, D. Trudell, and T. Moriarty, “Comparison of degradation rates of individual modules held at maximum power”, *Photovoltaic Energy Conversion, Conference Record of the 2006 IEEE 4th World Conference on (Volume:2)*, pp. 2085-2088

26. C.R. Osterwald, A. Anderberg, S. Rummel, and L. Ottoson. “Degradation analysis of weathered crystalline-silicon PV modules”, *Photovoltaic Specialists, IEEE Conference - PVSC, 2002*, pp.1392-1395

27. D. De Graaff, R. Lacerda, Z. Campeau. “Degradation mechanisms in Si module technologies observed in the field: Their analysis and statistics”, *NREL 2011 Photovoltaic Module Reliability Workshop*

28. A. Skoczek, T. Sample, and E.D. Dunlop. “The results of performance measure-ments of field-aged crystalline silicon photovoltaic modules”, *Prog. Photovolt: Res. Appl.* 2009; 17:227–240

29. P. Sanchez-Friera, M, Piliougine, J. Pelaez, J. Carretero and M. Sidrach de Cardona. “Analysis of degradation mechanisms of crystalline silicon PV modules after 12 years of operation in Southern Europe”, *Prog. Photovolt: Res. Appl.* 2011; 19:658–666

30. Y. Hishikawa. K. Morita, S. Sakamoto, T. Oshiro. “Field test results on the stability of 2,400 photovoltaic modules manufactured in 1990's”, *Photovoltaic Specialists Conference, 2002. Conference Record of the Twenty-Ninth IEEE*, pp.1687-1690

31. DuPont company website. Tedlar Polyvinyl Fluoride material, http://www.dupont.com/

32. M. De Bergalis, “Fluoropolymer films in the photovoltaic industry”, *Journal of Fluorine Chemistry* 125 (2004) 1255–1257

33. AGC solar company website. Float glass application. http://www.agc-solar.com/agc-solar-products.html

34. M.D. Kempe, T. Moricone, M. Kilkenny. “Effects of cerium removal from glass on photovoltaic module performance and stability”, *Proc. SPIE 7412, Reliability of Photovoltaic Cells, Modules, Components, and Systems II, 74120Q (2 September 2009)*

35. M. Murphy, A. Lifton. “The impact of soldering materials and process on cSi module reliability”, *Web seminar of Alphametal PV technologies*, 2012

36. Hsin-Hsin Hsieh, Wen-Kuei Lee, Tao-Chih Chang, Chi-Shiung Hsi. “Photo-voltaic modules of crystalline solar cells using a new type assembly structure”, *Microsystems Packaging Assembly and Circuits Technology Conference (IMPACT)*, 2010 5th International, pp.1–4

37. B. Su. “Electrical, thermomechanical and reliability modelling of electrically conductive adhesives”, *PhD thesis, Georgia Institute of Technology*, 2006

38. F. Song, S.W. Ricky Lee. “Corrosion of Sn-Ag-Cu lead-free solders and the corresponding effects on board level solder joint reliability”, *2006 Electronic Components and Technology Conference*, pp.891-898

39. P. Waters. “The effects of moisture on thin film delamination and adhesion”, *Master thesis, College of engineering university of south Florida*, 2005

40. A. Realini. “Mean time before failure of photovoltaic modules”, *Final report BBW 99.0579*, 2003

41. A.J. Carr. “A detailed performance comparison of PV modules of different technologies and the implications for PV system design methods”, *PhD thesis, Murdoch University of Western Australia*, 2005

42. N. G. Dhere. “Reliability of PV modules and balance-of-system components”, *Photovoltaic Specialists Conference, 2005. Conference Record of the Thirty-first IEEE*, pp.1570–1576

43. K. Whitfield, A. Salomon, S. Yang, I. Suez. “Damp Heat versus field reliability for crystalline silicon”, *Photovoltaic Specialists Conference, 2012. Conference Record of the Thirty-eight, IEEE*, 001864-001870

44. G. R. Mon, G. Whitla, R. Ross, Jr., M. Neff. “The role of electrical insulation in electrochemical degradation of terrestrial photovoltaic modules”, *IEEE Trans-actions on Electrical Insulation* Vol. EI-20 No.6, 1985, pp.989-996

45. ASM handbook. Volume 13B. *Corrosion: Materials*. 2005

46. G.R. Mod, L.C. Wen, R. Ross, Jr. "Water-module interaction studies", *Photovoltaic Specialists Conference, 1988., Conference Record of the Twentieth IEEE,* pp.1098–1102

47. M.D. Kempe. "Modelling of rates of moisture ingress into photovoltaic modules", *Solar Energy Materials & Solar Cells* 90 (2006) 2720–2738

48. S. N. Dhoot. "Sorption and transport of gases and organic vapours in poly(ethylene terephthalate)", *PhD thesis, The University of Texas at Austin*, 2004

49. DuPont company website. PV5300 and Elvax materials. http://www.dupont.com/

50. Y. Meydbray, K. Wilson, E. Brambila, A. Terao, S. Daroczi. "Solder joint degradation in high efficiency all back contact solar cells", *Proceedings of the 22th European Photovoltaic Solar Energy Conference, Milan, Italy, September. 2007:* pp.3-7

51. J. McPherson, G. Bishel, J. Ondrusek. "VLSI corrosion models: a comparison of acceleration factors", *Proceedings of Third Intern. Symp. on Corrosion and Reliability of Electronic Materials and Devices, Electrochem. Soc*., V. 94-29, pp. 270-276 (1994).

52. H. Abe, D. Chul, T. Yamamoto, T. Yagihashi, Y. Endo, H. Saito. "Cu wire and Pd-Cu wire package reliability and molding compounds", *Electronic Components and Technology Conference (ECTC), 2012 IEEE 62nd*, pp.1117-1123

53. T. Uno, T. Yamada. "improving humidity bond reliability of copper bonding wires", *2010 Electronic Components and Technology Conference*, pp.1725-1732

54. T. Takemoto, T. Funaki. "Role of electrode potential difference between lead-free solder and copper base metal in wetting", *Material Transactions,* V43, No.8 (2002), pp.1784-1790

55. J.E. Shelby, *Introduction to glass science and technology*, 2nd ed., UK: 2005

56. P. Hacke, M. Kempe, K. Terwilliger, S. Glick, N. Call, S. Johnston, S. Kurtz, I. Bennett, M. Kloos. "Characterization of multicrystalline silicon modules with system bias voltage applied in Damp Heat", *25th European Photovoltaic Solar Energy Conference and Exhibition*, 2010, pp.3760-3765

57. P. Hacke, K. Terwilliger, S. Glick, D. Trudell, N. Bosco, S. Johnston,. S. Kurtz. "Test-to-Failure of crystalline silicon modules", *5th IEEE Photovoltaic Specialists Conference*, 2010, 000,244-000250

58. V.v. Hadagali, "High voltage bias testing and degradation analysis of photovoltaic modules", *Master Thesis, University of Central Florida*, 2005

59. International Electrotechnical Commission, IEC 62804, "Test methods for detection of potential-induced degradation of crystalline silicon photovoltaic (PV) modules"

60. C. R. Osterwald and T. J. McMahon. "History of accelerated and qualification

testing of terrestrial photovoltaic modules: A literature review", *Prog. Photovolt: Res. Appl*. 2009; 17:11–33

61. D. Peck, "A comprehensive model for humidity correlation", *IEEE-Reliability physics symposium proceedings*, pp. 44 (1986)

62. C.F. Dunn, J.W. McPherson, "Temperature cycling acceleration factors in VLSI applications," *IEEE-Reliability physics symposium proceedings*, pp. 252 (1990)

63. S. Manson, "*Thermal stress and low-cycle fatigue*," McGraw-Hill, New York, (1966).

64. O. Hallberg. "Encapsulated modules and time to fail model as a function of the environment and package properties", *IEEE/ Proceedings of the IRPS,* 1982. pp.27–33

65. Joint Electron Device Engineering Council, JEP122G, "Failure mechanisms and models for semiconductor devices"

66. O. Hallberg, D. Peck. "Recent humidity accelerations, a base for testing standards", *Quality and Reliability Engineering International*, vol. 7, no. 3, 1991, pp.169-80.

67. V.A. Kuznetsova, R.S. Gaston, S.J. Bury, S.R. Strand. "Photovoltaic reliability model development and validation", *Photovoltaic Specialists Conference (PVSC), 2009 34th IEEE,* pp.432–436

68. T. Dierauf, A. Growitz, S. Kurtz, J. Cruz, E. Riley, C. Hansen. "Weather corrected performance ratio", Technical Report, NREL/TP-5200-57991, April 2013

69. K. Whitfield, A. Salomon, "Modelling based on Damp Heat testing", *Solaria*, 2012. http://www1.eere.energy.gov/solar/pdfs/pvmrw12_tuespm_solaria_whitfield.pdf

70. International Electrotechnical Commission, IEC61215, "Crystalline silicon terrestrial photovoltaic (PV) modules – Design qualification and type approval"

71. International Electrotechnical Commission, IEC61646, "Thin-film terrestrial photovoltaic (PV) modules – Design qualification and type approval"

72. Z.P. Xiong, A.A.O. Tay. "Modelling of viscoelastic effects on interfacial delamination in IC packages", *50th Electronic Components and Technology conference*, 2000. pp.1326-1331

73. T.Y. Lin, A. A.O. Tay. "Influence of temperature, humidity and defect location on delamination in plastics packages", *IEEE Transactions on Components and Packaging Technologies*, Volume:22 , Issue: 4, pp.512 –518

74. X.J. Fan, S.W.R. Lee, Q. Han. "Experimental investigations and model study of moisture behaviors in polymeric materials", *Microelectronics Reliability* 49 (2009) 861–871

75. P. Hülsmann, M. Heck, M. Köhl. “Simulation of Water Vapor Ingress into PV-Modules under Different Climatic Conditions,” Journal of Materials, vol. 2013, http://dx.doi.org/10.1155/2013/102691

76. N. Kim, C. Han. “Experimental characterization and simulation of water vapor diffusion through various encapsulants used in PV modules”, *Solar Energy Materials & Solar Cells,* 116, (2013) 68–75

77. J. Crank, *The mathematics of diffusion*, 1979

78. ABAQUS theory manual. http://www.maths.cam.ac.uk/computing/software/abaqus_docs/docs/v6.12/books/stm/default.htm

79. Z.P. Xiong, A.A.O. Tay, “Finite element analysis on moisture diffusion in crystalline silicon PV modules”, Draft paper for publication.

80. D.L. Staebler, C.R. Wronski. “Reversible conductivity changes in discharge-produced amorphous Si”, *Appl. Phys. Lett.* 31 (1977) 292.

81. R. Swanson. “The surface polarization effect in high-efficiency silicon solar cells”, *Proceedings of the 15th International Photovoltaic Science & Engineering Conference*, Shanghai: China; 2005, pp.410-411.

82. Z.P. Xiong, T. M. Walsh, A.G. Aberle. “PV module durability testing under high voltage biased Damp Heat conditions”, *Energy Procedia* 8 (2011) 384–389

83. S. Meyer, S. Richter, S. Timmel, M. Glaser, M. Werner, S. Swatek. “Snail Trails: Root Cause Analysis and Test Procedures “, Energy Procedia 03/2013; 38:498. DOI: 10.1016/j.egypro.2013.07.309

84. Fraunhofer CSP presents results of Potential-Induced Degradation (PID), 2012, http://www.en.csp.fraunhofer.de/press-and-events/details/id/857/

85. Solaredge company website. “Application note: Monitoring portal performance ratio calculation”. http://www.solaredge.com/files/pdfs/monitoring_performance_ratio_calculation.pdf

86. T. M. Walsh, Z.P. Xiong, K. Y. Sheng, A. A.O. Tay, A.G. Aberle. “Singapore modules – optimized PV modules for the tropics”, *Energy Procedia* 15 (2012) pp.388-395